Department of Physics
Umeå University

EP-DT-EO
February 8, 2016

LHCb Upstream Tracker box

Thermal studies and conceptual design

Master's Thesis in Engineering Physics, 30hp

Student: Oskar Mårtensson
E-mail: osma0009@student.umu.se

Supervisor: Joao Carlos Batista Lopes
E-mail: Joao.Carlos.Batista.Lopes@cern.ch

Examiner: Michael Bradley
E-mail: michael.bradley@physics.umu.se

Abstract

The LHC (Large Hadron Collider) will have a long shut down in the years of 2019 and 2020, referred to as LS2. During this stop the LHC injector complex will be upgraded to increase the luminosities, which will be the first step of the high luminosity LHC program (which will be realized during LS3 that takes place in 2024-2026). The LHCb experiment, whose main purpose is to study the *CP*-violation, will during this long stop be upgraded in order to withstand a higher radiation dose, and to be able to read out the detector at a rate of 40MHz,compared to 1MHz at present. This change will improve the trigger efficiency significantly. One of the LHCb sub-detectors the Trigger Tracker (TT), will be replaced by a new sub-detector called UT. This report presents the early stage design (preparation for mock-up building) of the box that will be isolating the new UT detector from the surroundings and to ensure optimal detector operation. Methods to fulfill requirements such as light and gas tightness, Faraday-cage behavior and condensation free temperatures, without breaking the fragile beryllium beam pipe, are established.

Sammanfattning

LHC (Large Hadron Collider) kommer under åren 2019-2020 att ha ett längre driftstopp. Under detta driftstopp så kommer LHC's injektionsanordningar att uppgraderas för att kunna sätta fler protoner i circulation i LHC, och därmed öka antalet partikelkollisioner per tidsenhet. Denna uppgradering kommer att vara första steget i "High Luminocity LHC"-programmet som kommer att realiseras år 2024-2026. LHCb-experimentet, vars främsta syfte är att studera *CP*-brott, kommer också att uppgraderas under stoppet 2019-2020. Framför allt så ska avläsningsfrekvensen ökas från dagens 1MHz till 40MHz, och experimentet ska förberedas för de högre strålningsdoser som kommer att bli aktuella efter stoppet 2024-2026. En av LHCb's deldetektorer, TT detektorn, kommer att bytas ut mot en ny deldetektor som kallas UT. Den här rapporten presenterar den förberedande designen av den låda som ska isolera UT från dess omgivning och försäkra optimala förhållanden för detektorn. Kraven på den isolerande lådan och tillvägagångssätt för att uppfylla dessa krav presenteras.

Nomenclature

Acronyms

LHCb	-Large Hadron Collider beauty
ATLAS	-A Torodial LHC Apparatus
CMS	-Compact Muon Solenoid
ALICE	-A Large Ion Collider Experiment
LS	-Long stop
TT	-Trigger Tracker
UT	-Upstream Tracker
RICH	-Ring-imaging Cherenkov detector
ECAL	-Electromagnetic Calorimeter
HCAL	-Hadron Calorimeter
FEA	-Finite element analysis
***CP*-violation**	-Charge Parity violation
TDR	-Technical Design Report
PUR	-Polyurethane
LEP	-Large Electron–Positron collider
IP	-Interaction Point

Parameters

A	-Area, $[m^2]$
E	-Emitted power, $[W]$
E_0	-Initial elasticity modulus, $[Pa]$
H	-Hardness, $[ShoreA]$
I	-Current, $[A]$
L	-Characteristic length, $[m]$
R_e	-Electrical resistance, $[\Omega]$
R_t	-Thermal resistance, $[K/W]$
ΔT	-Temperature gradient, $[°C]$ or $[K]$
T_s	-Surface temperature, $[°C]$ or $[K]$
T_∞	-Ambient temperature, $[°C]$ or $[K]$
U	-Voltage, $[V]$
Nu_L	-Nusselt number
Ra_L	-Rayleigh number
Gr_L	-Grashof number
Pr	-Prandtl number
h_c	-Convection heat transfer coefficient, $[W/m^2 * K]$
h_r	-Radiation heat transfer coefficient, $[W/m^2 * K]$
h_{comb}	-Combined heat transfer coefficient, $[W/m^2 * K]$
k	-Thermal conductivity, $[W/m * K]$
q	-Heat flux $[W]$
ν	-Kinematic viscosity, $[m^2/s]$
α	-Thermal diffusivity, $[m^2/s]$
β	-Volumetric thermal expansion coefficient, $[1/K]$
μ	-Viscosity, $[kg/s * m]$
λ	-Wavelength, [m]
ϵ	-Emissivity
c_p	-Specific heat at constant pressure, $[J/kg * K]$

Constants

g	-Gravitational acceleration,$[m/s^2]$
c	-Speed of light $[m/s]$
h	-Planck's constant $[eV * s]$
σ	-Stefan-Boltzmann constant $[W/m^2K^4]$

Acknowledgments

First of all, I would like to thank my supervisor Joao Carlos Batista Lopes, who has been helping me with all kind of stuffs during the whole year that I have spent on CERN. Everything from how to buy bus tickets, to how to use software's that I have never used before. He has introduced me to a lot of useful methods and techniques that i would probably not have tried if it were not for him, and for this I am truly grateful.

I would like to thank Francois Boyer, Olivier Jamet and Burkhard Schmidt for all their help and all the trust they have put in me during this project. I would also like to thank the rest of the EP-DT-EO group for making my time at CERN very pleasant and educational. I would like to thank Michael Bradley at Umeå University for the constructive comments he has given me on this project. Last but not least, I would like to thank my student colleague Kasper Hörnqvist for never turning my questions down and repeatedly providing me with useful insights.

Contents

Oskar Mårtensson
osma0009@student.umu.se

1 Context

The European Organization for Nuclear Research, CERN (*Conseil Européen pour la Recherche Nucléaire*, in french) is a European research organization, founded in 1954, that operates the largest particle physics laboratory in the world. The organization has 21 member states. However, CERN cooperates with physicists, engineers and universities from far more countries than just the member states. The main purpose of CERN is to study high-energy physics in order to better understand the laws of physics and why our universe have become what it is today. The main site of CERN is located on the Swiss-French border outside the city of Geneva, and that is the place from where this project is executed.[1]

1.1 The Large Hadron Collider

The Large Hadron Collider (LHC) is the worlds largest and most powerful particle collider. It was built between 1998 and 2008 and is the result of a collaboration between over 10 000 people from over 100 countries. LHC is a circular particle accelerator with a 27km circumference. It was built in the old tunnels made for the particle accelerator LEP, which was dismantled to make room for the newer LHC. In the LHC, protons are accelerated to speeds close to the speed of light and then smashed in to each other. There are several interaction points along the LHC, and each has its own set of detectors to record the collisions for further analysis. The LHC has multiple areas of use, for example investigation of supersymmetric theories and the nature of dark matter.

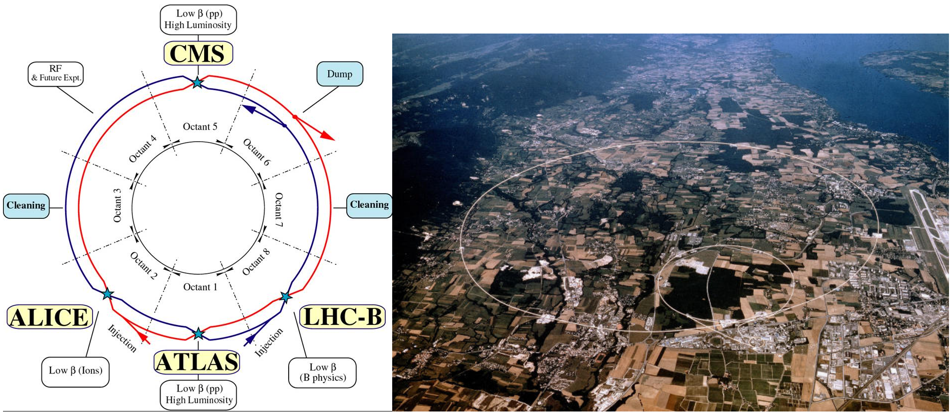

Figure 1.1: Left: Sketch over the LHC with beam interaction points marked out. Right: photograph over the Geneva region with LHC underground path marked out.

1.2 The LHCb experiment

The LHCb experiment is carried out in a collaboration between 66 different institutes and involves about 700 scientists [2]. The main purpose of LHCb is to investigate composite particles containing b-quarks (also called *beauty* quarks or *bottom* quarks), or c-quarks (also called *charm* quarks) and their decay. Compared to general purpose detectors like CMS or ATLAS, LHCb looks quite different. Unlike the general purpose detectors ATLAS and CMS, which are hermetic, LHCb uses a cone shape to take advantage of the fact that the probability distribution for B-meson production has a peak at low angles (angle between beam pipe and particle tracks).

The experiment aims to answer the question; Why is there still a lot of matter left after the creation of universe, but no antimatter? A more complete description of so called B-physics and it's benefits can be found in Section 1.2.1.

1.2.1 Physics motivation

Matter was born in the early universe and consisted out of a sort of plasma consisting of freely moving quarks and leptons. As the universe expanded and got colder, the more massive particles got converted by the weak interaction (the particles decay into lighter particle and emits a W or Z boson) into the lightest "generation" of matter, which is the only matter we can see stable on the Earth today [3]. In the high energy collisions in the LHC, the heavier generations of matter that existed in the early universe, can be reproduced and studied to a greater extent than the conditions on Earth normally allows.

One of the big questions that LHCb tries to answer is the origin of the matter- antimatter asymmetries in the universe , which physicists refer to as the *CP*-violation (violation of the postulated *CP*-symmetry). The *CP*-symmetry is the product of **C**harge conjugation symmetry and **P**arity symmetry. This means that a systems behavior should not change if all electrical charges are inverted (charge conjugation) and all spatial coordinates are inverted (parity) at the same time. Particle transformations through the weak force have however been shown to violate this postulated symmetry in some cases. Investigation of these asymmetries is the key to understand why the universe today is so dominated by matter with respect to antimatter, as well as it might shed light on other phenomena that cannot be explained by the standard model.

CP-violation was first observed in 1957 in the particles called K-mesons (also called "kaons"). A meson is a particle composed by one quark and one anti quark, held together by gluons (strong interaction force carrying particles). After the discovery of *CP*-violation in the K-meson system, many theorists predicted that the same violation should be observed in other systems. The natural next step is to study B-mesons, since they contain the heavier b-quark from the third generation of matter (the lighter s-quark, or its antiquark, can be found in all K-mesons).

The b-quarks role in the standard model is shown in Figure 1.2. The study of B-mesons was one of the main purposes for building LHCb, and it has been confirmed that the B-mesons do indeed show *CP*-violation.[4][5] B-mesons are copiously produced in the LHC, in which protons are accelerated to an energy up to 7TeV, thus about 7000 times their rest mass. Just like Einstein's rules of relativity becomes more pronounced at higher speeds, the unknown rules and equations that governs our fundamental particles are expected to be more pronounced at higher energy densities (such as in the early universe).

Another reason to increase the energies of the colliding particles is the ability to probe smaller distances. Since photons are limited to probe only distances larger than their own wavelength, given by de Broglie's relation

$$\lambda = hc/E \quad , \tag{1}$$

smaller distances can be probed when higher energies are used. Thus by increasing the energies we are allowed to look "inside" things we before only could watch from the outside, or maybe not at all.

By increasing the luminosity, more collisions will be produced and there will be more particles to study. Increasing the luminosity will therefore increase statistical accuracy and rare decays will occur more frequently. Thus there is a pursuit of higher energy and higher luminosity in the particle beams, in order to be able to understand the physical laws we have yet to understand.

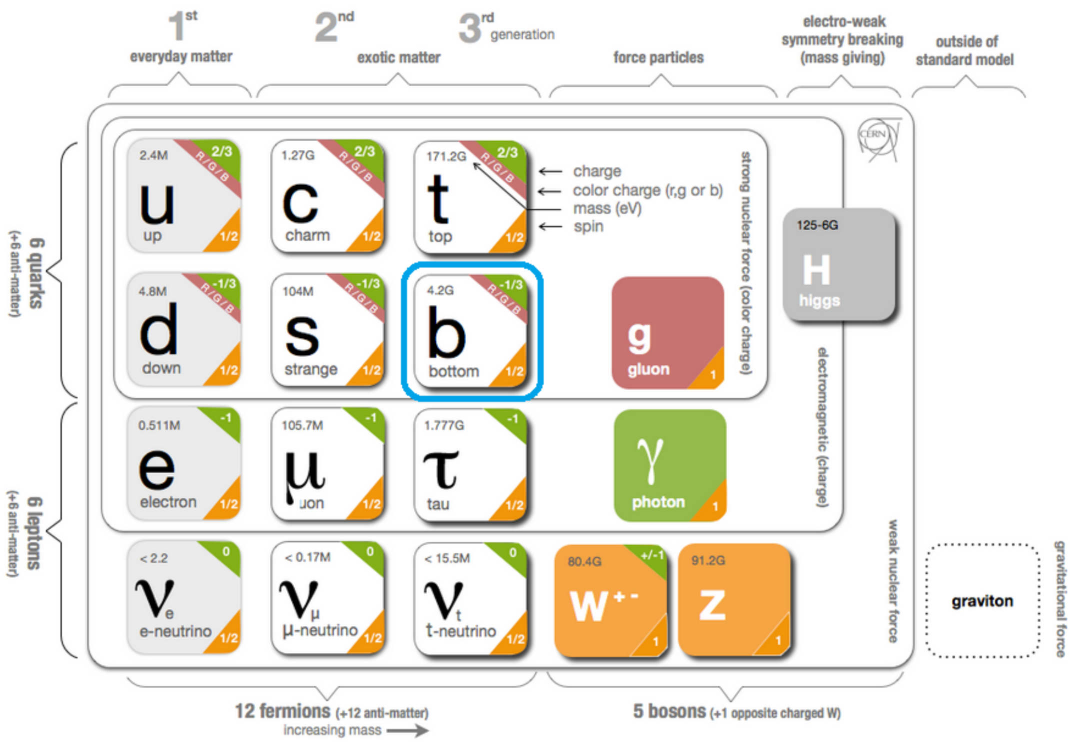

Figure 1.2: A graphic presentation of the standard model. The b-quark marked in blue.

1.2.2 The LHCb Upstream Tracker (UT)

The LHCb-detector is to be upgraded in 2019-2020, in order to improve the read out rate and to make the detector ready to operate at about 5 times higher luminosities. Many subdetectors are going to be either upgraded or replaced due to the new requirements and improved technologies available. One subdetector system that is going to be replaced is the Trigger Tracker (TT), which will be replaced by the new Upstream Tracker (UT). They both serve the same purpose, which is to reconstruct charged particle tracks with high spatial resolution. The TT was designed to withstand an integrated luminosity of approximately $10fb^{-1}$ ($1fb^{-1}$ is equal to approximately 100 trillion proton-proton collisions), which is not sufficient for the post-upgrade LHC. The new UT have been designed to withstand an integrated luminosity of at least $50fb^{-1}$. Also, exchanging the old TT for the new UT will provide a trigger readout at 40MHz, compared to the old readout at 1MHz [6]. The position of the TT in LHCb is shown in Figure 1.3. A computer generated 3D-model of the LHCb-detector can be seen in Figure 1.4

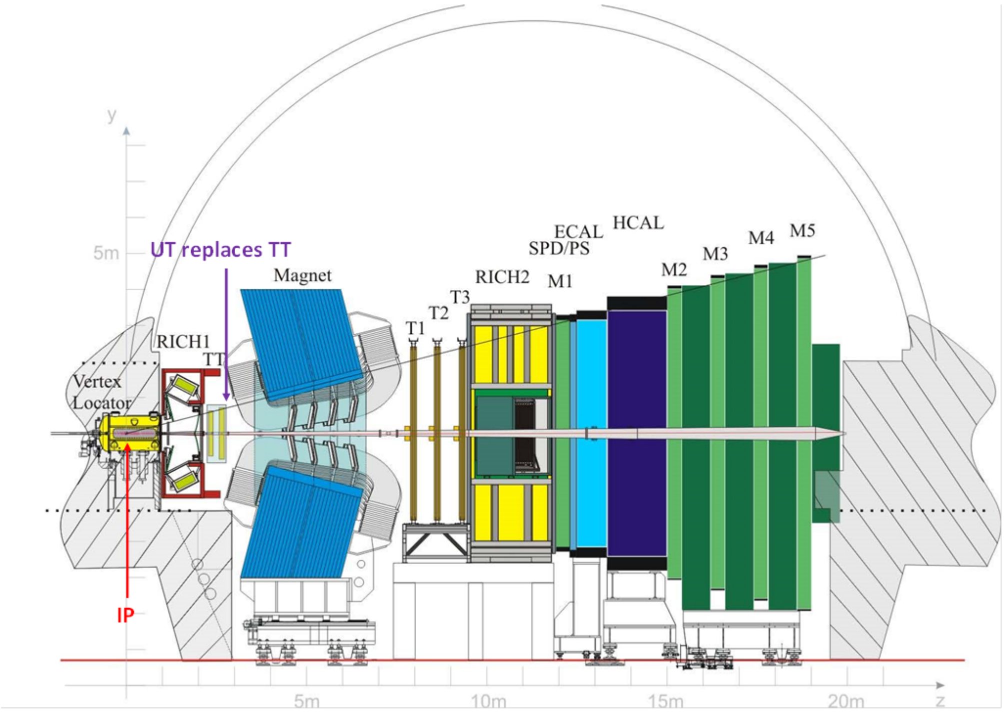

Figure 1.3: The LHCb-detector as it looks today, with TT marked out by a purple arrow. [7]

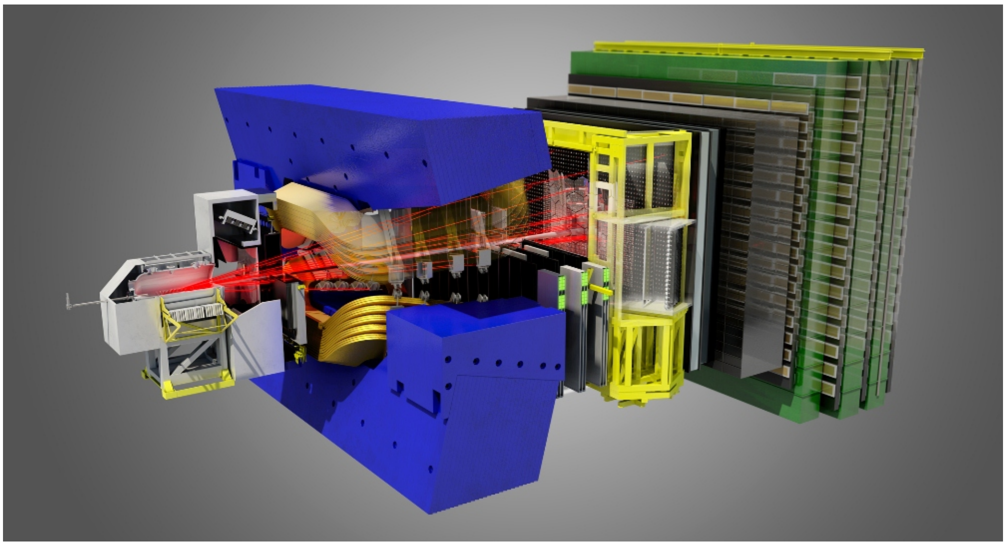

Figure 1.4: Computer generated 3D-model over the LHCb-detector.

1.2.2.1 UT working principle

The UT sensors are silicon sensors (more precisely; single sided silicon micro-strip sensors) located approximately 2.5m downstream from LHCb's interaction point, (upstream of LHCb dipole magnet). The silicon sensors are solid state detectors. When a charged particle with high energy travels through a n-type silicon plate it will ionize some of the atoms and create electron-hole pairs. Due to an electric field that is applied over the electrodes, the holes and electrons will drift away from each other. The holes will eventually reach the p-doped implant. This will create a hole overflow in the material, and thus create a small current. This current will then be seen as a signal that can be translated into coordinates for the particle track. This working principle is illustrated in Figure 1.5.

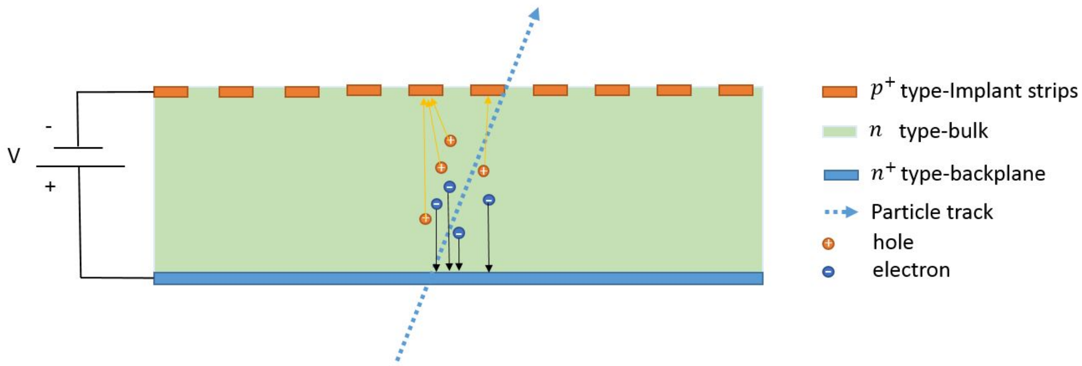

Figure 1.5: The working principle of a single sided silicon micro strip detector.

In the UT, the silicon sensors are mounted on staves, together with cables and the other electronics that are necessary in order to make a readout from the sensors. The staves are then assembled in to four planes. The orientation and dimensions of the planes are shown in Figure 1.7. Figure 1.6 shows the stave construction.

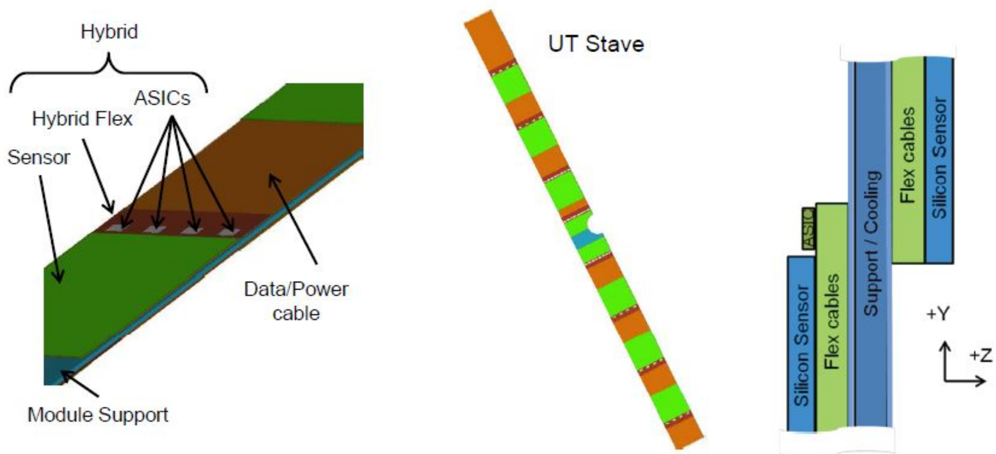

Figure 1.6: The UT staves [7]

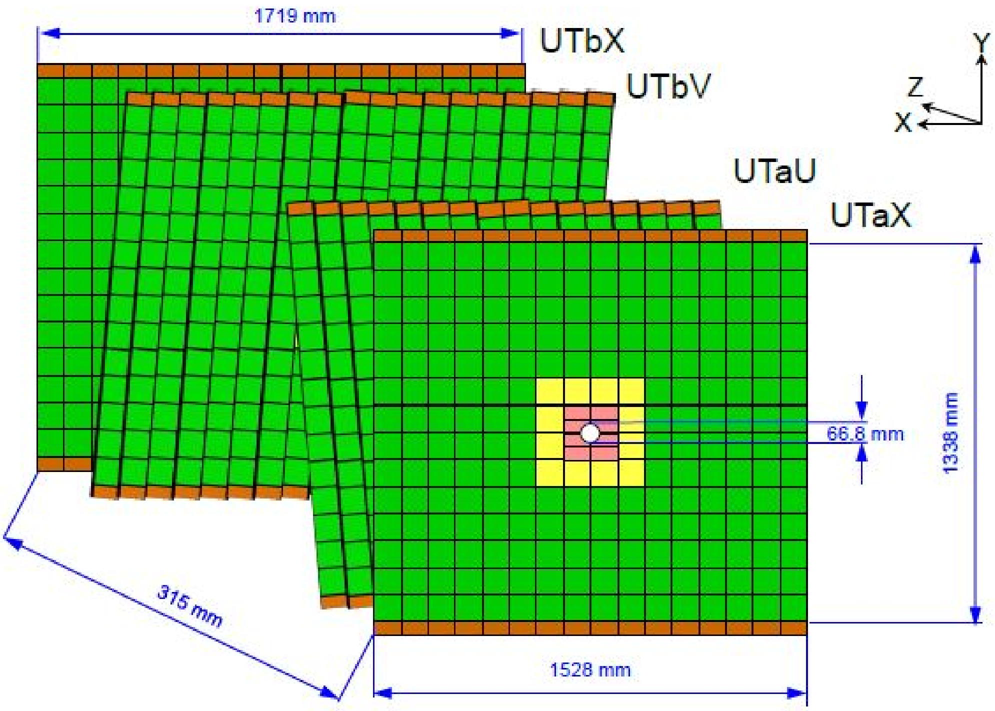

Figure 1.7: The UT geometry looking downstream [7].

1.2.2.2 UT-box requirements

It is of great importance to isolate the detector from its surroundings in order to ensure adequate environment conditions. Light (photons) would produce signals in the detector, and thus the detector has to be operated in the dark. This is achieved by enclosing the detector in a box (from here on called the UT-box). The development of the UT-box will be the main focus in this thesis. The main requirements on the UT-box are the following;

1. **The force transmitted from the UT-box to the LHCb beam pipe has to be limited.**
   The LHCb beam pipe is made of Beryllium, since it is almost transparent to the particles that should be studied. The use of a more dense metal could lead to undesired showering of particles coming from the interaction point. Beryllium is very fragile and will break if high pressure is applied. This is a critical requirement since a high pressure can cause the LHCb beam pipe to rupture and in that case, the LHC would stop. Not more than a few Newtons of force are allowed to be applied when the box is closed.

2. **The UT-box should be light tight.**
   Photons will yield a signal from the UT-detector even though they are not to be detected by the UT.

3. **The UT-box should act as a Faraday-cage.**
   External electromagnetic fields can produce noise and spoil the signals generated by particles of interest. Thus the UT-box should act as a Faraday-cage in order to prevent this from happening.

4. **The UT-box should provide good thermal insulation.**
   The ambient temperature in the LHCb cavern is about $20°C$. On the other hand, the silicon sensors have to be kept at a temperature $\leq -5°C$ in order to operate properly. The UT-staves will be cooled using a CO_2 cooling system. This cooling system will have a capacity of 5kW, of which 500W are reserved for heat transfer through the UT-box. The rest is mostly needed for the heat that the detector electronics generate. However, if the UT-box is not well thermally insulated and let more heat flow through than the cooling system is able to transport away, the temperature will rise and cause the sensors to fail after irradiation.

5. **The UT-box should be light.**
   The UT-box should be made of light materials with low radiation length. Radiation length is a material property related to the energy loss of high energy, electromagnetic-interacting particles, when propagating through the material.

6. **The UT-box should be radiation resistant.**
   The properties of the UT-box are not allowed to change due to the radiation exposure. The UT-box have to withstand a minimum dose of $5 \times 10^7 rad$.

7. **The UT-box should be gas tight.**
   The UT-box will be continuously flushed with either dry air or dry N_2 gas in order to prevent moisture condensation on the detector itself and on the beam pipe. There will be a slight over pressure in the UT-box so that the dry gas will leak out, instead of humid gas leaking in through holes and gaps in the UT-box. Small leaks are expected but they have to be limited.

8. **The detector has to be accessible.**
   To simplify future upgrades and reparations of the UT, it should be possible to easily remove the UT-box from the beam pipe, and to reinstall it without damaging anything.

2 Design of the UT-box

In this section, the design and the concepts implemented to ensure that the UT-box requirements are fulfilled, are presented.

2.1 UT-Box geometry

The dimensions and the position of the UT-box are presented in Figure 2.1 and Figure 2.2. In order to make the UT-detector accessible, the UT-box is constructed to be able to be split in half. The UT-box will be mounted on rails so that alignment of the UT-box is ensured when closing it. Figure 2.3 shows one half of the split UT-box, and the frame that will be attached to the rails. The rails can be seen in Figure 2.2. In Figure 2.4, the whole UT-box without frame, and without detector planes inside, can be seen.

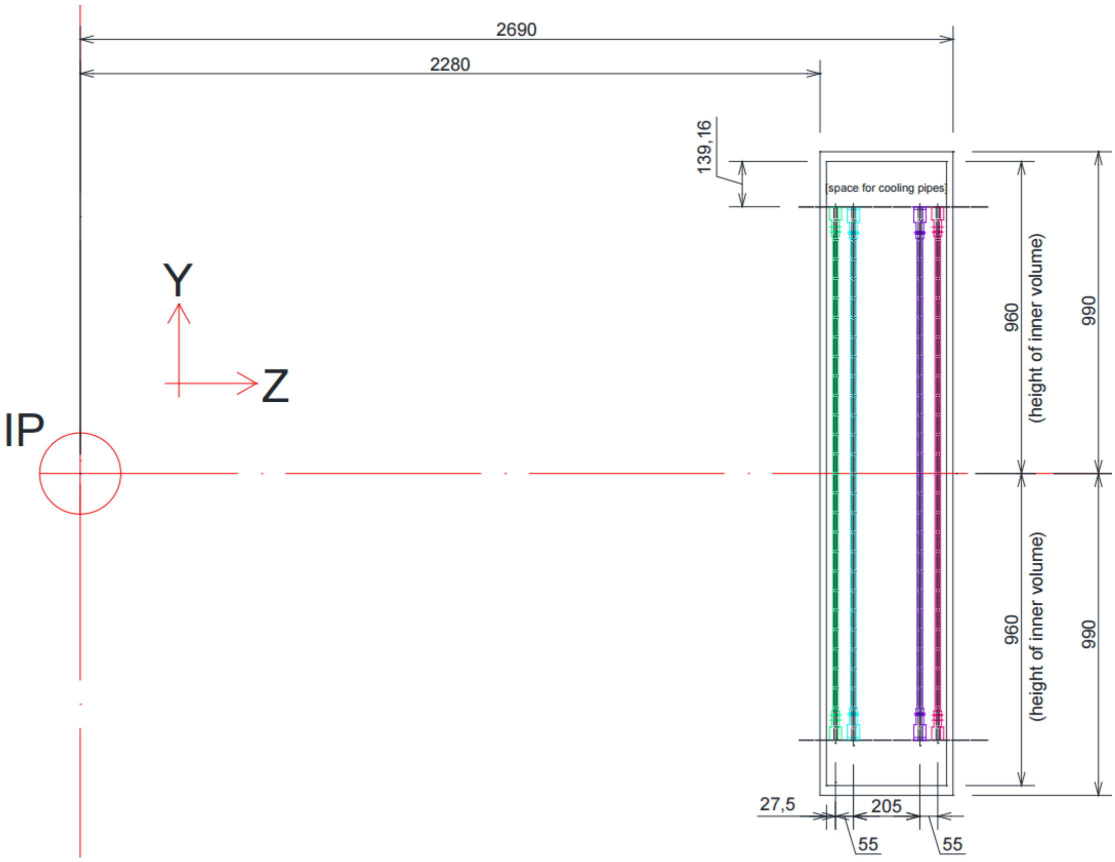

Figure 2.1: Side view of the UT-box, dimensions in [mm], [8].

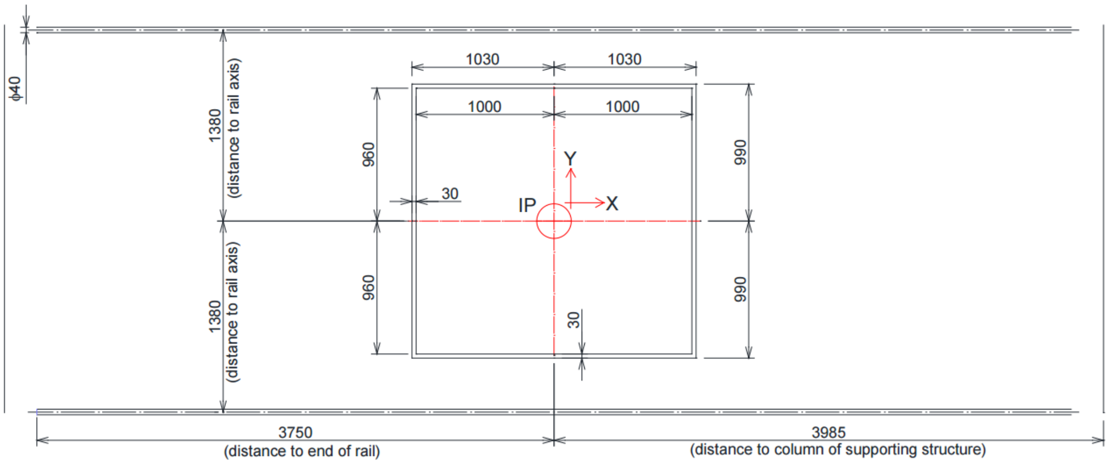

Figure 2.2: Front view of the UT-box and rails, dimensions in $[mm]$, [8].

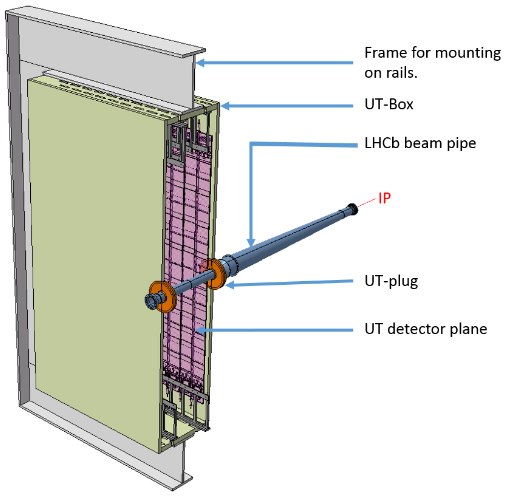

Figure 2.3: Half UT-box, with rail mountings attached.

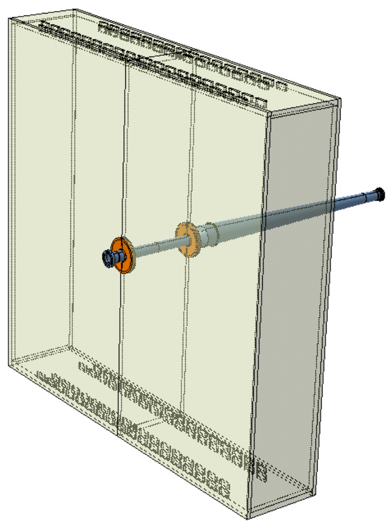

Figure 2.4: Transparent view of empty UT-box.

2.1.1 Interface to the beam pipe

In order to reduce the force applied on the beam pipe to a minimum, but still ensure tightness, the area close to the beam pipe is made out of an elastomer. The elastomer can easily deform when compressed, and thus reduces the force transmitted to the beam pipe. This concept is illustrated in Figure 2.5. The elastomer part closest to the beam pipe will from here on be called the UT-plug. section 4 investigates this requirement in depth.

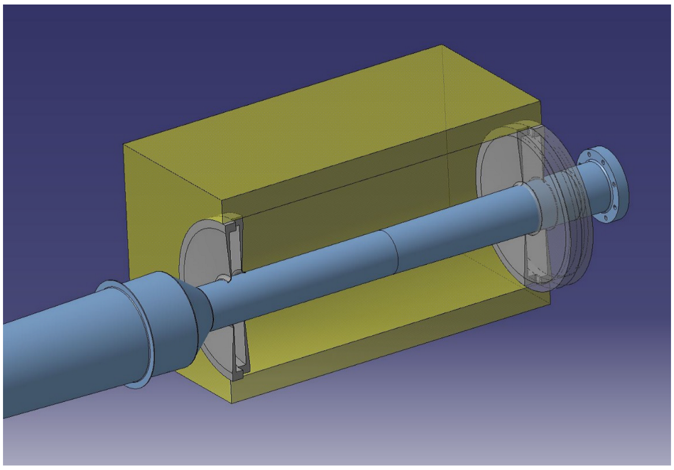

Figure 2.5: Concept picture of the UT-plug interfacing the LHCb beam pipe. The box dimensions are arbitrary in this picture

2.1.2 Gas tightness

To reduce the risk of air getting in to the UT-box, the UT-box will be flushed with either dry air or dry N_2 gas at a slight over pressure, as mentioned before. To "lock in" the dry gas, the UT-plug will have a small arc-shape closest to the beam pipe. This will cause the slight over pressure to push the UT-plug towards the pipe and therefore achieve a better sealing. This concept can be seen in Figure 2.5 and Figure 3.1 among others. The arc shape closest to the beam pipe will also serve to redirect some of the force applied in the direction perpendicular to the beam pipe to be parallel to the beam pipe.

2.1.3 Light tightness

The critical part in the question of light tightness will be the area where the UT-box is split, especially around the beam pipe and therefore the UT-plug. To ensure light tightness of the UT-plug, two important concepts have been implemented. The first measure is to put a disc of an opaque material inside a cavity in the UT-plug. The photons cannot travel through the disc and instead have to travel around it, thus minimizing the risk of undesired photons interacting with the detector. This concept is illustrated in Figure 2.6.

The second measure implemented in order to ensure light tightness is the angular displacement of the plugs split line on its inside compared to its outside. The risk of photons getting inside the UT-box, in case of inadequate closing, is significantly reduced by these measures. This concept is illustrated in Figure 2.7.

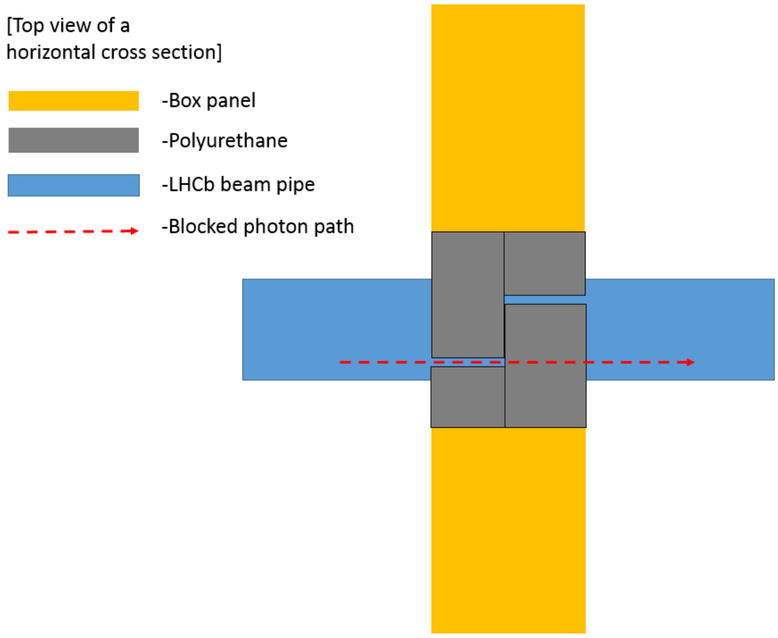

Figure 2.7: Cross section view (top view) of the plugs split section and its angular displacement on the outside compared to the inside.

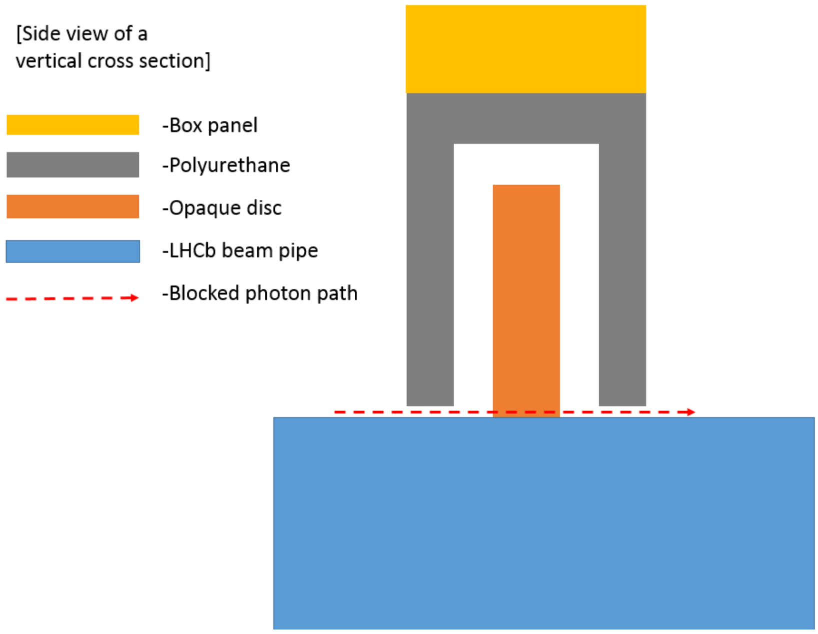

Figure 2.6: Photon blocking disc placed inside the UT-plug cavity.

2.2 Material selection

2.2.1 Radiation hardness

The critical point in terms of radiation hardness of the UT-box is the interface between the box and the LHCb beam pipe, the UT-plug. It is important that the properties of the elastomer in the UT-plug does not alter with radiation exposure. The UT-plug will have to withstand a gamma dose of 5×10^7 rad (equivalent to 5×10^5 Gy). Two elastomers have been shown to fulfill the radiation hardness requirements, Ethylene-propylene and Polyurethane. This is shown in Figure 2.8. Of those two elastomers, Polyurethane was chosen due to the slightly higher radiation dose required for moderate to severe damage, and due to previous experiences with the material. Polyurethane has been used for similar purposes at positions close to the beam pipe before and have been proven to perform well. In this report, each dimension of the plug is investigated from a thermal point of view, and the rigidity of the polyurethane is evaluated. This is important in order to be able to manufacture a plug that satisfies the requirements.

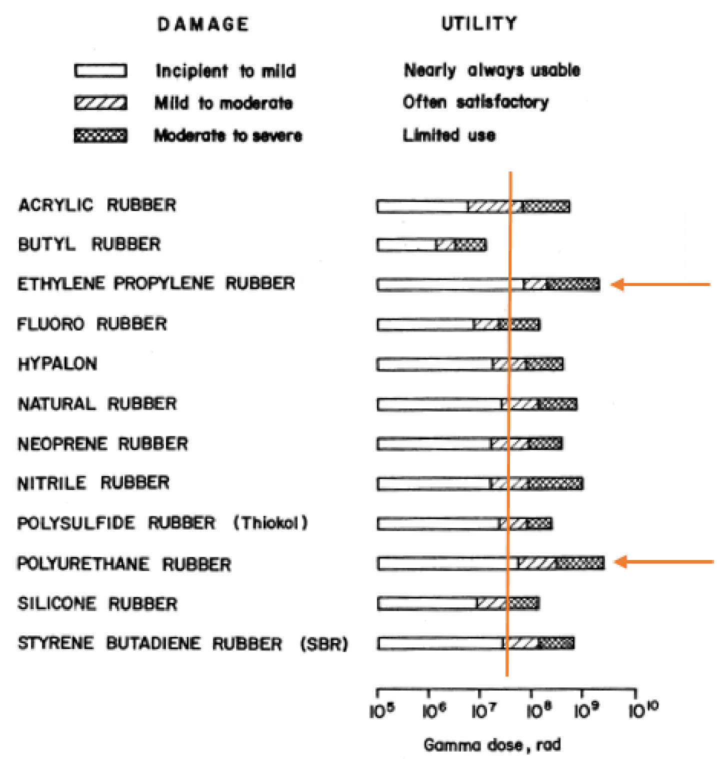

Figure 2.8: Radiation hardness for some polymers [9].

2.2.2 Thermal properties

The panels of the UT-box will be made out of a sandwich-structured composite. The sandwich-structured composite is a concept commonly used to achieve high bending stiffness with low density. Such a sandwich is composed by a thick lightweight core with a thin but stiff skin attached to each side. A low density is desired since it both increases the radiation length, and minimizes the stresses in the UT-box material. In order to minimize the heat flux through the UT-box walls, it has been decided to use Airex R82.60 [10] as core. Airex is a good thermal insulator with a thermal conductivity of $0.036W/(mK)$, and is very light with a density of $60kg/m^3$. The radiation length of Airex is about $0.25\%X_0$ for 2cm. Carbon fiber [11], are used for the skins, which provide the mechanical stability required for the UT-box.

2.2.3 Electrical shielding

In order to make the UT-box acting as a Faraday cage, one layer of a thin copper net (Dexmet 2CU6-100FA [12]), will be embedded in the carbon fiber skins of the UT-box panels. The copper net in all panels are connected together to make the Faraday cage. This concept have been tested and validated. The copper net is shown in Figure 2.9, a complete technical report on the panel production can be found in Appendix D. The diameter of the holes in this copper net is 2.54mm, and thus electromagnetic radiation with a wavelength superior to this will to get blocked. 2.54mm wavelength is in the short end of the microwave-region.

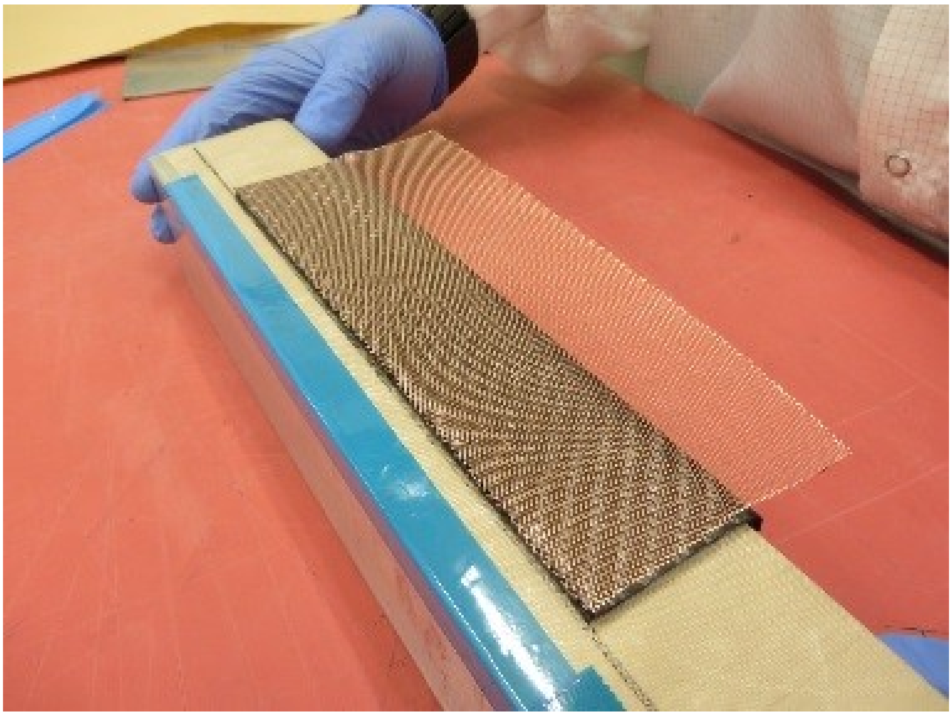

Figure 2.9: Copper net to assure electrical shielding.

3 Thermal assessment

The thermal analysis of the UT-box will include both analytical and numerical calculations. The panels of the UT-box (the walls, roof and floor) are symmetrical in all directions except their normal directions. Thus the analysis can be reduced to one dimension and solved analytically.
The UT-plug on the other hand is not as symmetrical, and is not expected to insulate thermally as well as the panels. The UT-plug is therefore a critical area in terms of temperature. Because of this, a FEA (Finite Element Analysis) were conducted for the thermal aspects of the UT-plug. The finite element method is a numerical method to find approximate solutions to boundary value problems for partial differential equations. The problem domain is divided into smaller sub-domains called finite elements. The problem is then solved by minimizing an associated error function through variational methods.

Condensation shall be avoided in order to minimize the performance requirements of the detectors internal cooling system, and so that water does not start to accumulate in the experiment. The dew point in the experimental cavern is estimated to be at 12°C, thus a temperature superior to 12°C is desired all around the UT-box, including the UT-plug region.

3.1 Heat transfer theory

In this section I will explain the most important concept behind the calculations in my thermal analysis. A direct consequence of the second law of thermodynamics is that it is impossible to transfer heat from a cold body to a warmer body without inserting additional energy. Heat can however, and will, flow spontaneously from a warm body to a colder one.

Second law of thermodynamics: *If no energy enters or leaves a closed system, the potential energy of the systems state will always be less than, or equal to that of the initial state.*

Heat can be transferred from one body or system to another in different ways, and in this section I will explain the different heat transfer modes that can occur, and how they relate to each other in a so-called "thermal circuit". The system will be in steady state and no time dependent analysis is therefore conducted.

3.1.1 Conduction

Heat transfer through conduction can be viewed as energy migrating from more energetic particles to less energetic particles through collisions between the particles. A well known empirical law that describes this kind of heat transfer is *Fourier's law of conduction*, which is stated in it's differential form in as

$$\vec{q''} = -k\nabla T \quad , \tag{2}$$

where $\vec{q''}$ is the heat flux density ($\vec{q''} \equiv \vec{q}/A$, where $\vec{q}$ is the heat flux and A is the cross sectional area perpendicular to $\vec{q}$), T is the temperature, and k is the *thermal conductivity.*

The one dimensional version of the same law is

$$q''_x = -k\frac{dT}{dx} \quad . \tag{3}$$

For all linear temperature distribution (in all solids at steady state), Equation 3 can be rewritten as

$$q''_x = -k\frac{\Delta T}{l} \quad , \tag{4}$$

where ΔT is the temperature difference between two points and l is the distance between the same two points.

3.1.2 Convection

Heat transfer caused by macroscopic movements of a fluid (advection) in combination with diffusion, is called heat transfer through convection. The heat transferred by convection is thus very dependent on the flow of the fluid involved. Since fluid dynamics is to great extent governed by the Navier-Stokes equations, which does not have a known general solution, practically all relations used to determine the *convection heat transfer coefficient* h_c is empirical. There are three modes of convective heat transfer. There is free convection due to buoyancy-driven fluid flow, forced convection due to external flow and convection with phase change (condensation or boiling). Typical h_c-values for each mode are shown in Table 3.1.

Process	Phase	Typical h_c $[W/(m^2 * K)]$
Free convection	Gas	2-25
	Liquid	50-1000
Forced convection	Gas	25-250
	Liquid	100-20000
Convection with phase change	both	2500-100000

Table 3.1: Typical heat transfer coefficient for each convective heat transfer mode[13]

The most common way to calculate h_c is to first calculate a parameter called the *Nusselt number*

$$Nu_L = \frac{\text{Convective heat transfer}}{\text{Conductive heat transfer}} = \frac{L \cdot h_c}{k} \quad , \tag{5}$$

and from there calculate h_c through

$$h_c = \frac{k \cdot Nu_L}{L} \quad , \tag{6}$$

in which L is the characteristic length. The Nusselt number is the dimensionless ratio between heat transfer through convection, and heat transfer through conduction. There are many empirical relations for this number, which applies for different conditions. Since it is hard to determine an exact value for Nu_L and h, it is common to instead calculate the average of those values over the whole contact surface between the fluid and the solid. In many of the empirical relations to calculate Nu_L, another dimensionless parameter is required, namely the *Rayleigh number*. The Rayleigh number is the product of the *Grashof number* and the *Prandtl number*, as described by

$$Ra_L = Gr_L \cdot Pr = \frac{g\beta(T_s - T_\infty)L^3}{\nu\alpha} \quad . \tag{7}$$

In Equation 7, g is the gravitational acceleration, T_s is the surface temperature of the solid, T_∞ is the ambient temperature, β is the volumetric thermal expansion coefficient of the fluid, α is the thermal diffusivity and ν is the kinematic viscosity.
The Grashof number

$$Gr_L = \frac{g\beta(T_s - T_\infty)L^3}{\nu^2} \tag{8}$$

can be interpreted as a measure of the ratio between buoyancy forces and viscous forces in the fluid, and the Prandtl number

$$Pr = \frac{c_p\mu}{k} = \frac{\nu}{\alpha} \tag{9}$$

as the ratio between momentum and thermal diffusivities. By calculating those dimensionless numbers, one can deduce the average h_{cond} for many simple geometries.

3.1.3 Radiation

Thermal radiation is heat transported by photons that is emitted by all bodies of a non/zero temperature. Thus, unlike heat transfer through convection and conduction, this heat transfer mode does not require a material medium to be transported in. There is an upper limit to the magnitude of the emitted power from a surface of temperature T_s. This upper limit is described by the *Stefan-Boltzmann law*

$$E_b = \sigma T_s^4 \quad . \tag{10}$$

The constant σ is the Stefan–Boltzmann constant. A body emitting the maximal possible heat, yielded by Equation 10 is called a blackbody. In reality there is not a lot of real blackbodies. To make Equation 10 apply to more realistic bodies, it is multiplied by a factor ϵ. In the following equation, ϵ is a material property called *emissivity* which has a value between 0 and 1, corresponding to how much of the maximal emissive power that is really emitted.

$$E = \epsilon \sigma T_s^4 \tag{11}$$

The absolute majority of all real bodies are not only able to emit thermal radiation, but are also able to absorb thermal radiation from it's surrounding. Let G designate the total incident thermal radiation (i.e. *irradiation*), and let γ designate the fraction of incident thermal radiation that is absorbed by the body (i.e. *absorptivity*). The net heat flux density is then given by

$$q''_{rad} = \frac{q_{rad}}{A} = \epsilon \sigma T_s^4 - \gamma G \quad . \tag{12}$$

Kirchoff's law of thermal radiation states that $\gamma = \epsilon$ for all materials in thermal equilibrium (steady state). From this,

$$q''_{rad} = \epsilon \sigma (T_s^4 - T_\infty^4) \tag{13}$$

can be derived, and it applies to all cases with a large isothermal surrounding.

For the sake of putting up a thermal circuit, it is convenient to state the net heat flux as

$$q_{rad} = h_r A (T_s - T_\infty) \quad . \tag{14}$$

By applying $a^2 - b^2 = (a-b)(a+b)$ on Equation 12 two times, and combining the result with Equation 14, the following expression for the *radiation heat transfer coefficient* can be derived

$$h_r = \epsilon \sigma (T_s + T_\infty)(T_s^2 + T_\infty^2) \quad . \tag{15}$$

3.1.4 Thermal circuit concept

The reciprocal of thermal conductance is called thermal resistance. This property is similar to electric resistance in the manner that it directs heat flow in a way similar to how electric resistance directs electric current. As an example, the relation between U, I and R_e described by Ohm's law

$$U = I \cdot R_e \quad , \tag{16}$$

is also a valid relation if the variables are replaced by $\Delta T, q$ and R_t, as in

$$\Delta T = q \cdot R_t \quad . \tag{17}$$

A one dimensional temperature analysis through a solid of n layers (with perfect thermal contact) can be viewed as n thermal resistors connected in series (where $R_t = \frac{L}{A \cdot k}$), and the total resistance can then be yielded by

$$R_{t_{tot}} = \sum_{i=1}^{n} R_{t_i} = \sum_{i=1}^{n} \frac{L}{A \cdot k_i} \quad . \tag{18}$$

In case there is radiation or convection involved, then k_i should be replaced by h_{conv} or h_{rad} respectively. If both convection and radiation occurs, then k_i should be replaced by the *combined heat transfer coefficient* stated in [14],

$$h_{comb} = h_r + h_c \quad . \tag{19}$$

It should be noted that the h-coefficients are constructed to be independent of L (i.e. $L = 1$ for all h) since it describes the behavior of a surface rather than that of a volume (which k does for conduction).

3.2 Analytical calculations

To assist in future calculations similar to the ones that I have made, the calculations were saved as Mathcad files. I have made a few different tools, but to make this report concise, I will only present the tools that have been directly necessary to conduct the FEA. I have put the tools as appendices, but a short description of every tool is presented in this section.

UT-box thermal analysis (Appendix A)
This tool assists in analytical calculations regarding temperature distributions in a box consisting of no more than three layers, with constant inner and surrounding temperature. This tool also provides the convection heat transfer coefficients (h) used in the thermal FEA.
Since h depends on the difference between the surface temperature and the ambient temperature, which is dependent on the heat flux, which in turn is dependent of h, an iterative method is used to solve h. An initial estimation of the surface temperatures is made. This initial estimation then gives a one dimensional circuit, from which a heat flux magnitude can be derived. This heat flux magnitude will then be used to recalculate the surface temperatures which were initially estimated. If the difference is large, a new estimation, based on the achieved results, is made. This process is then iterated until the temperatures match. The achieved surface temperatures and convection coefficients are stated in Table 3.2. The calculated outside surface temperatures of the UT-box shows that condensation will not occur on the UT-box panels. However, those calculations does not show

that there wont be condensation on the UT-plug, and thus a thermal FEA is conducted for the region closest to the beam pipe. Table 3.2 also shows that the calculated heat flux (a total of about 319W) is below the internal cooling systems limit at 500W.

Wall	$T_{in}[°C]$	$T_{out}[°C]$	$h_{in}[W/(m^2 * K)]$	$h_{out}[W/(m^2 * K)]$	Q $[W]$
Vertical	0.1	15.7	1.080	1.018	266.6
Top	-0.9	15.6	0.894	0.841	24.7
Bottom	0.2	16.3	2.796	3.025	27.5

Table 3.2: Summary of most important results from Appendix A.

Cavity convection analysis (Appendix B)
This tool serves to check if convection can be neglected in an air volume enclosed by two parallel plates of different temperatures.

Heat transfer comparison between two vertical plates (Appendix C)
This is a tool to compare the magnitudes of heat transfer through radiation, conduction and through natural convection, between two equal parallel plates with air in between. This can justify the neglecting of a heat transfer mode, if it is shown to be of insignificant magnitude compared to the other modes, and thereby simplify calculations.

3.3 Numerical calculations (FEA) on the UT-plug

This section presents a thermal FEA (parametric study) made on the polyurethane interface between the LHCb beam pipe and the UT-box, the UT-plug. The study is conducted in the *ANSYS 16.1* software package.

The purpose of this study is to determine a geometry for the UT-plug that ensures that no condensation occurs on the surfaces which are in contact with air. Table 3.3, Table 3.4 and Table 3.6 provide a list of parameters which describes the geometric and material properties of the UT-plug. Values that were considered as constants in the computation are shown in Table 3.3. The analyzed geometries of the UT-plug were selected based on geometric constraints, UT-operating requirements and material limitations. The parameters are varied one at the time in order to understand the link between the temperature in the outer face of the UT-plug and each specific parameter. The mounting of the interface in the UT-box is illustrated in Figure 2.5. Figure 3.1 shows a sketch of the UT-plug cross-section and illustrates the parameters that were considered in the iterative FEA thermal analysis.

3.3.1 Boundary conditions and model parameters

Property	Value	Unit
Airex conductivity (K3)	0.036	$W/(m*K)$
Polymer emissivity	0.95	
Outside temperature	20	°C
Inside temperature	-5	°C
Outside convection coefficient	1.018	$W/(m^2*K)$
Inside convection coefficient	1.080	$W/(m^2*K)$
Mesh element size	0.001	
Element type	All solid	

Table 3.3: Non-altered model properties. In-depth calculations of the convection coefficients can be found in Appendix A.

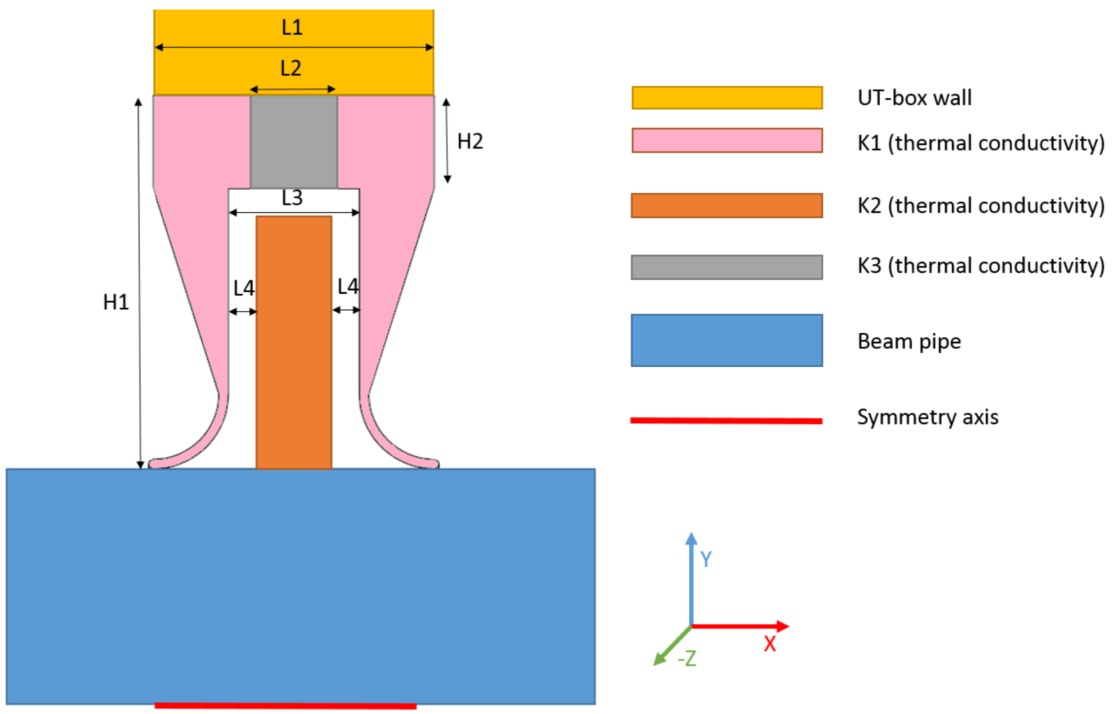

Figure 3.1: Parameters visualized.

The following assumptions and simplifications have been made:

Symmetry planes: XY,XZ

Surface contacts:
Assumed perfect contact between the materials and the air in contact with solids.

Perfect insulated surfaces:
Surfaces in face-to-face contact with either the LHCb beam pipe or the wall of the UT-box.

Convection in cavity:
According to analytical calculations, convection in the cavity can be neglected as long as L4<6.8mm. The calculations performed can be seen in Appendix B.

Radiation in cavity:
Taking into account the temperature difference between the cavity's surfaces (worst case scenario) it can be concluded that the heat transfer by radiation can be neglected with respect to the heat transfer by conduction (see detailed calculation in Appendix C). Figure 3.2 shows that the highest temperature difference is 4.2 °C which corresponds to a heat transfer of $1.0W/m^2$. This values of heat transfer is insignificant with respect to the value computed by conduction, $157W/m^2$. This is a typical behavior for all configurations.

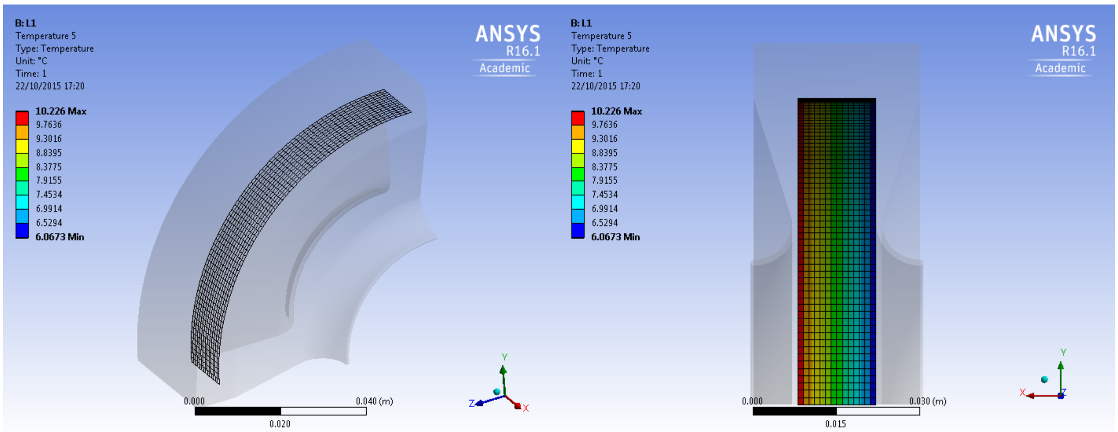

Figure 3.2: Temperatures without radiation in the cavity.

3.3.2 Results

A variety of configurations were used. For each configuration, a thermal assessment was performed in which some parameters were kept constant whilst other parameters were varied. In this report the two configurations that are most important for the final conclusions are presented. The first configuration does not include an Airex divider in between the polyurethane parts, whilst the second does.

3.3.2.1 Homogeneous polyurethane plug

Figure 3.3 shows a typical temperature distribution on the UT-plug (a) and more specifically on its outer surface (b), for the standard configuration without Airex, whose parameter values are shown inTable 3.4. Figure 3.3 (b) shows that the highest temperature on the outer surface is located at the inner radius and the lowest temperature is located at the outer radius. Figure 3.4 to Figure 3.11 show plots of the temperature extremes on the UT-plug's outer surface. The blue line shows the minimum temperature of the outer surface, and the red line shows the maximum temperature of the outer surface. Figure 3.4 shows the temperatures dependency with the parameter H1.

Parameter	Standard value	Tested range	Unit	Figure
H1	40	30-70	mm	Figure 3.4
H2	10	5-15	mm	Figure 3.5
L1	20	20-40	mm	Figure 3.6
L2	0	0-20	mm	Figure 3.7
L3	14	10-18	mm	Figure 3.8
L4	2	1-4	mm	Figure 3.9
K1	0.4	0.05-0.7	W/(m*K)	Figure 3.10
K2	0.036	0.03-0.18	W/(m*K)	Figure 3.11

Table 3.4: Standard values and tested range for all parameters, for the non-Airex configuration.

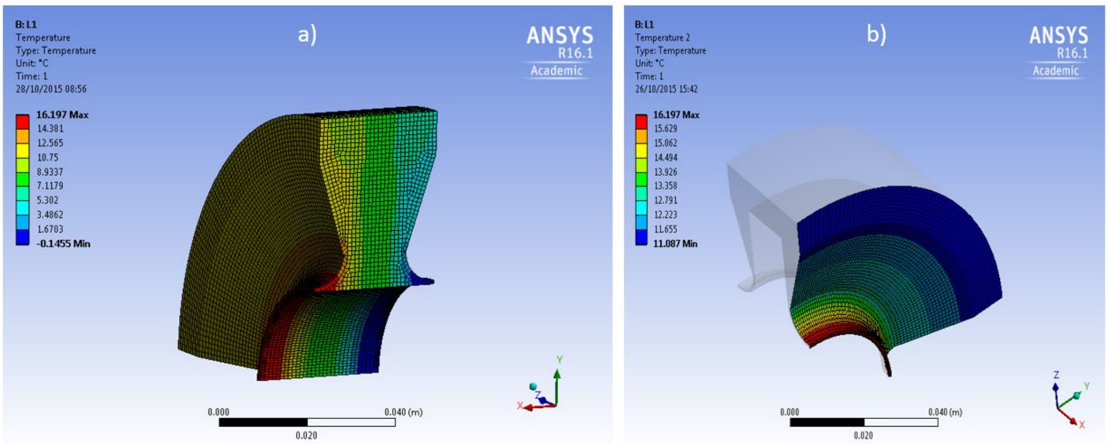

Figure 3.3: Typical temperature distribution on all bodies (a) and outer surface (b), for the non-Airex standard configuration.

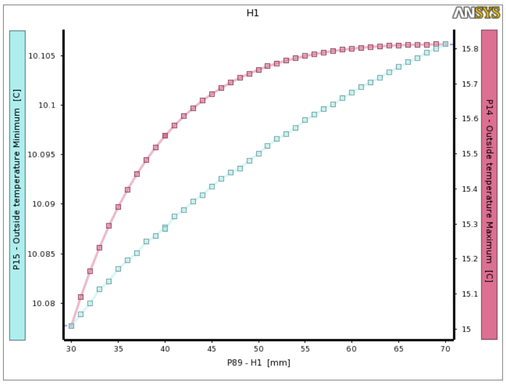

Figure 3.4: Maximum and minimum temperatures on the outer surface vs H1, for the non-Airex standard configuration.

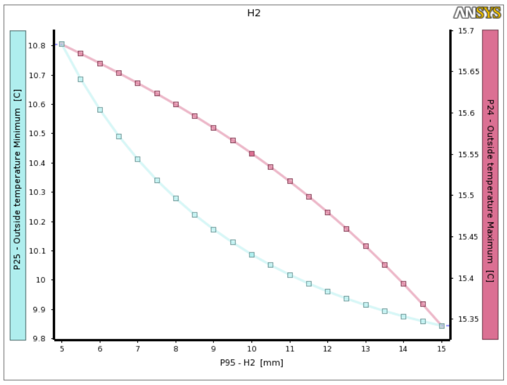

Figure 3.5: Maximum and minimum temperatures on the outer surface vs H2, for the non-Airex standard configuration.

Based on the results plotted in Figure 3.4, it can be concluded that H1 should be maximized in order to increase the minimum temperature of the outer surface. The range of the minimum outside temperature however, is very small for H1 and thus H1 is regarded insignificant for the thermal aspects. Figure 3.5 suggests that H2 should be minimized and Figure 3.6 suggests that L1 should be maximized.

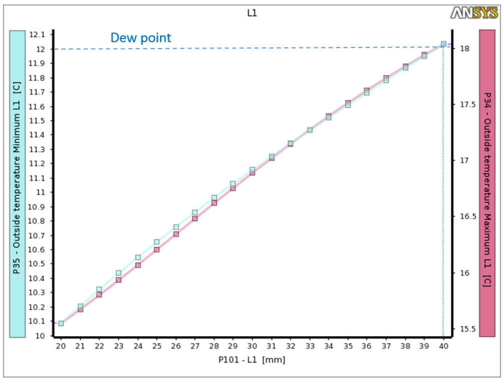

Figure 3.6: Maximum and minimum temperatures on the outer surface vs L1, for the non-Airex standard configuration.

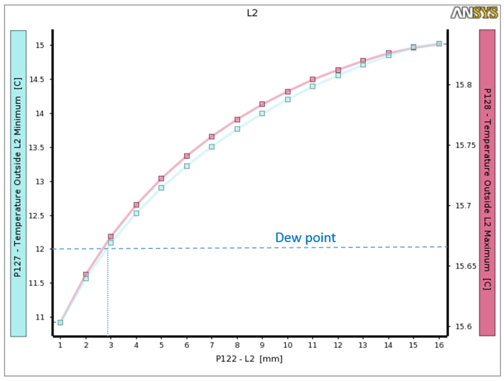

Figure 3.7: Maximum and minimum temperatures on the outer surface vs L2, for the non-Airex standard configuration.

Figure 3.7 suggest that introducing an Airex piece between two polymer parts, could increase the outer temperature. According to the figure, a 3mm thick Airex piece can be sufficient to achieve an outer temperature greater than 12°C. The thicker the Airex piece, the better.

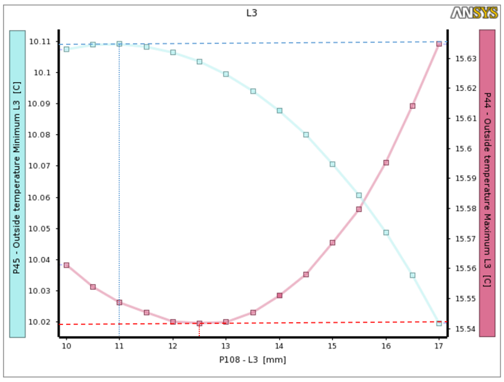

Figure 3.8: Maximum and minimum temperatures on the outer surface vs L3, for the non-Airex standard configuration.

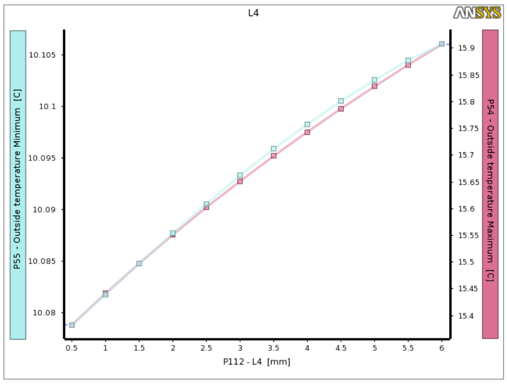

Figure 3.9: Maximum and minimum temperatures on the outer surface vs L4, for the non-Airex standard configuration.

Figure 3.8 shows that the minimum outside temperature has a maxima when L3 is about 11mm. The relationship between L4 and outer temperatures is shown in Figure 3.9. The dependency is not very strong, for the minimum temperature. However, all outside temperatures increases as L4 increases. Thus L4 should be maximized.

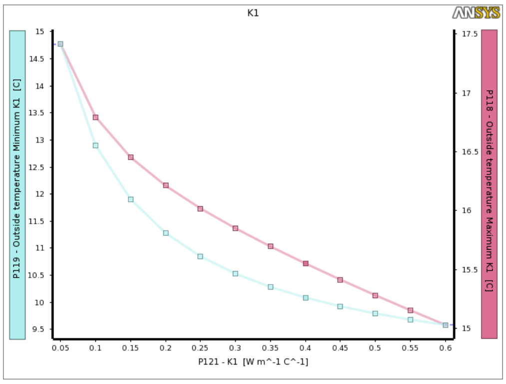

Figure 3.10: Maximum and minimum temperatures on the outer surface vs K1, for the non-Airex standard configuration.

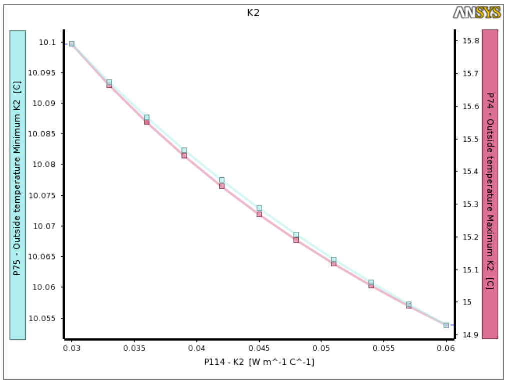

Figure 3.11: Maximum and minimum temperatures on the outer surface vs K2, for the non-Airex standard configuration.

The dependence of the thermal conductivity of the polymer is shown in Figure 3.10 and the dependence of the thermal conductivity of the disc inside the cavity is shown in Figure 3.11. The temperature range is greater in Figure 3.10 than Figure 3.11, thus it is evident that the thermal conductivity of the polymer has a bigger impact on the outer surface temperatures, than the thermal conductivity of the disc. The thermal error for the standard configuration without Airex is shown in Figure 3.12. The thermal error in *ANSYS 16.1* is the percentage error in the energy norm, which is calculated through a method described in [15], by using discontinuities in the heat flux field. The magnitude of the error indicates that the computed results are good to at least the second decimal.

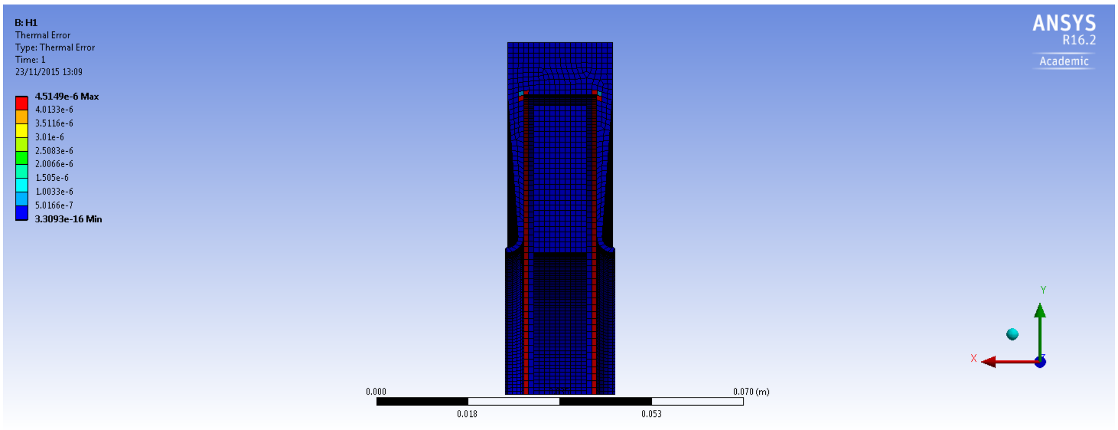

Figure 3.12: Thermal error for the standard configuration without Airex.

A summary of the conclusion on each parameter and the range of the minimum temperature related to it is presented in Table 3.5. By looking at Table 3.5 it can be concluded that there are three parameters that can be altered to achieve a minimum outside temperature superior to 12°C. However, K1 will be difficult to regulate since the material used needs to fulfill other requirements such as radiation hardness. L1 will most probably be limited to a maximum of 20mm due to mechanical properties of the UT-box. This leaves L2, the width of the dividing Airex, as the easiest way to ensure an outside temperature superior to 12°C. The average heat flux through the outer surface for this standard configuration is calculated to 117$[W/m^2]$.

Parameter	Should be	Minimum outside temperature range $[°C]$
K1	Minimized	14.77 - 9.58 = 5.19
L2	Maximized	15.02 - 11.00 = 4.02
L1	Maximized	12.03 - 10.10 = 1.93
H2	Minimized	10.81 - 9.85 = 0.96
L3	Minimized, max value about 11mm	10.11 - 10.02 = 0.09
K2	Minimized	10.10 - 10.05 = 0.05
H1	Maximized	10.11 - 10.08 = 0.03
L4	Maximized	10.11 - 10.08 = 0.03

Table 3.5: Summary of suggested approaches for each parameter in the standard configuration without Airex, ordered by relevance.

3.3.2.2 Heterogeneous plug

According to Figure 3.7, a 3mm Airex piece can be sufficient to ensure that no condensation occurs on the outside. To further investigate the behavior of a plug divided by an Airex piece, a new standard configuration was set up. This configuration is presented in Table 3.6. L2 is set to 6mm and is not altered since it is already evident that thicker is better, and 6mm is regarded to be close to the upper limit of the thickness when regarding mechanical problems that might occur. Most critical is the attachment of the polyurethane to the

Airex. The attachment might not be rigid enough if the Airex is too wide, since this implies thinner polyurethane parts.

Parameter	Standard value	Tested range	Unit	Figure
H1	65	50-70	mm	Figure 3.13
H2	10	5-15	mm	Figure 3.14
L1	20	20-40	mm	Figure 3.15
L2	6	not altered	mm	–
L3	12	8-16	mm	Figure 3.16
L4	2	0.5-5	mm	Figure 3.17
K1	0.4	0.05-0.7	W/(m*K)	Figure 3.18
K2	0.036	0.03-0.06	W/(m*K)	Figure 3.19
K3	0.036	0.036-0.1	W/(m*K)	Figure 3.20

Table 3.6: Standard values and tested range for all parameters, for the configuration with Airex.

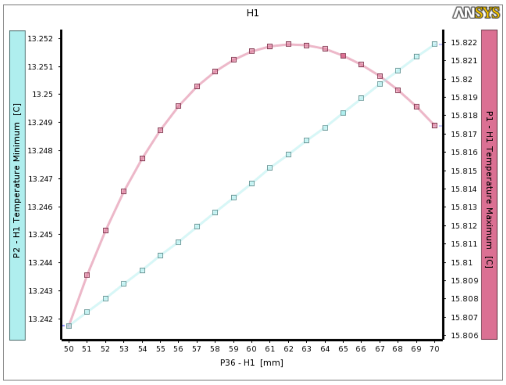

Figure 3.13: Maximum and minimum temperatures on the outer surface vs H1, for the standard configuration with an Airex divider.

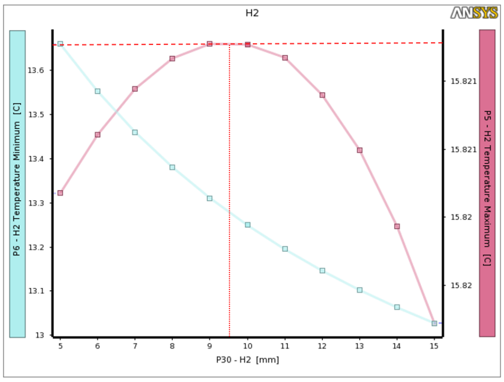

Figure 3.14: Maximum and minimum temperatures on the outer surface vs H2, for the standard configuration with an Airex divider.

The behavior of the minimum outside temperature in Figure 3.13 and Figure 3.14 is similar to the behavior in Figure 3.4 and Figure 3.5 respectively, with the difference that H2 now have maxima for the maximum temperature at about 9.5mm. However, the minimum temperature is decreasing with increasing H2 throughout the whole computed range. Thus H2 should be minimized. In Figure 3.15, L1 is plotted against the outside temperature extremes and in Figure 3.16, L3 is.

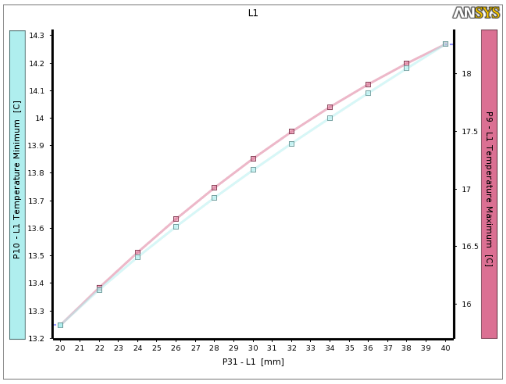

Figure 3.15: Maximum and minimum temperatures on the outer surface vs L1, for the standard configuration with an Airex divider.

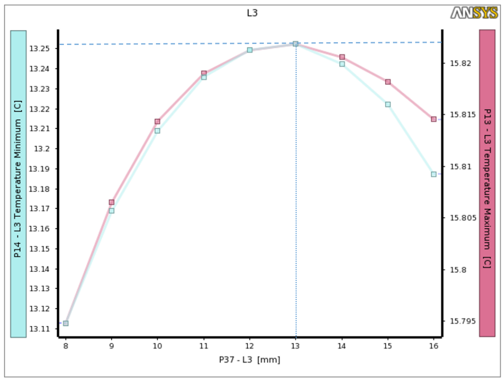

Figure 3.16: Maximum and minimum temperatures on the outer surface vs L3, for the standard configuration with an Airex divider.

The minimum temperature range in Figure 3.6 is almost half of the range presented in Figure 3.15. Thus the L1 dependence is smaller for the Airex configuration compared to the non-Airex configuration. In Figure 3.16 it is shown that both the outside maximum and minimum temperatures have a maxima at about 13mm. Thus this value should be targeted for L3.

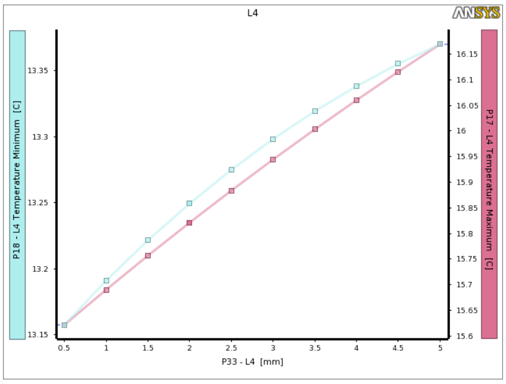

Figure 3.17: Maximum and minimum temperatures on the outer surface vs L4, for the standard configuration with an Airex divider.

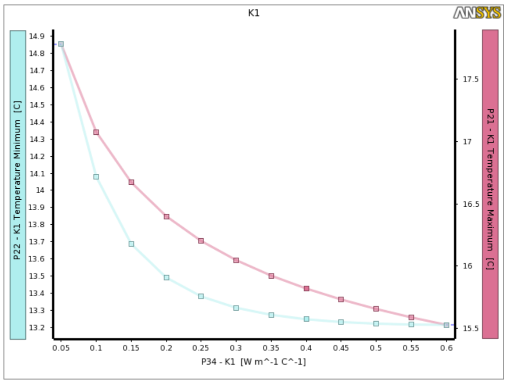

Figure 3.18: Maximum and minimum temperatures on the outer surface vs K1, for the standard configuration with an Airex divider.

The L4 dependence shown in Figure 3.17 is similar to the one shown in Figure 3.9, but with a larger range. Thus L4 should still be maximized. Figure 3.18 shows the new dependence of K1 and Figure 3.19 the dependence of K2. As expected, the thermal conductivity of the polymer still has a bigger impact on the outside temperatures than the thermal conductivity of the disc in the cavity.

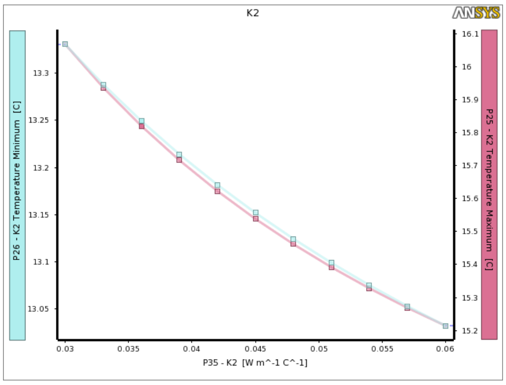

Figure 3.19: Maximum and minimum temperatures on the outer surface vs K2, for the standard configuration with an Airex divider.

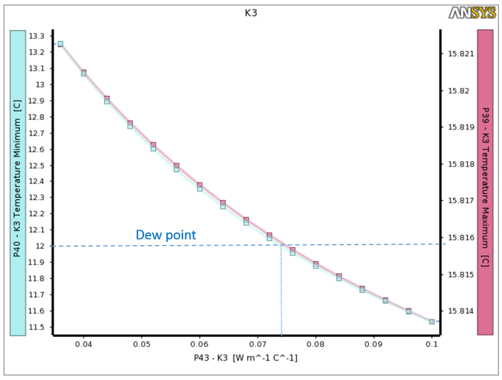

Figure 3.20: Maximum and minimum temperatures on the outer surface vs K3, for the standard configuration with an Airex divider.

In case it is not possible to put Airex between the polymer parts, K3 have also been investigated in this standard configuration. Figure 3.20 suggest that Airex could be replaced by a material with a thermal conductivity below approximately 0.075 $W/(m * K)$, without causing condensation. A typical thermal error for the standard configuration is shown in Figure 3.21. The error is similar to the one presented in Figure 3.12 and the results are also here rounded to a two decimal digit. The average heat flux through the outer surface for this standard configuration is calculated to $96[W/m^2]$.

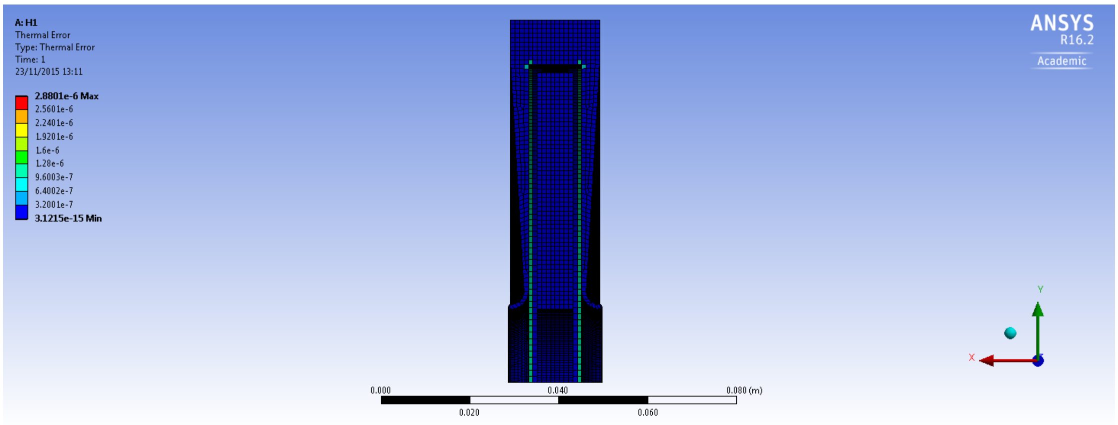

Figure 3.21: Thermal error for the standard configuration with Airex.

3.3.3 Conclusions

In Figure 3.22 and Figure 3.23 a comparison between the temperature distributions corresponding to the two standard configurations are presented. The configuration without Airex will according to this analysis cause condensation, whilst the configuration with Airex will not. Figure 3.22 shows all bodies and Figure 3.23 shows the outer surface of the plug.

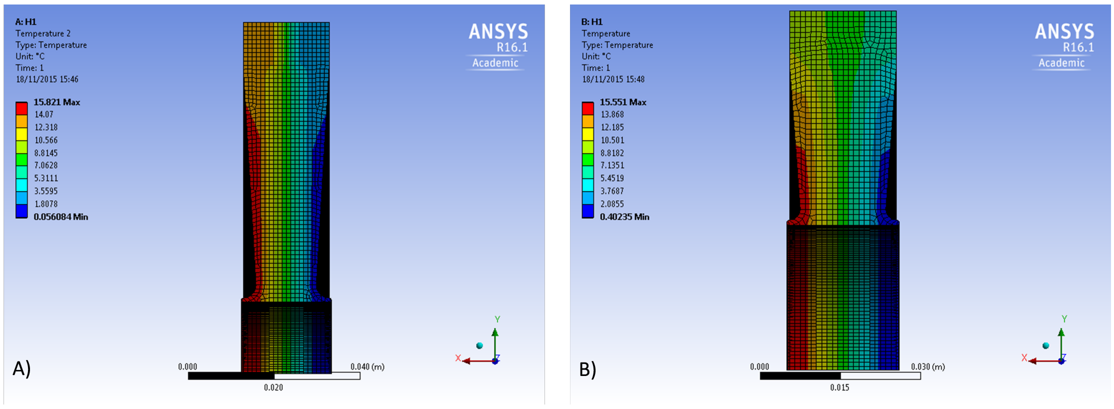

Figure 3.22: Temperature distribution on all bodies for the standard configuration with Airex (A), and without Airex (B)

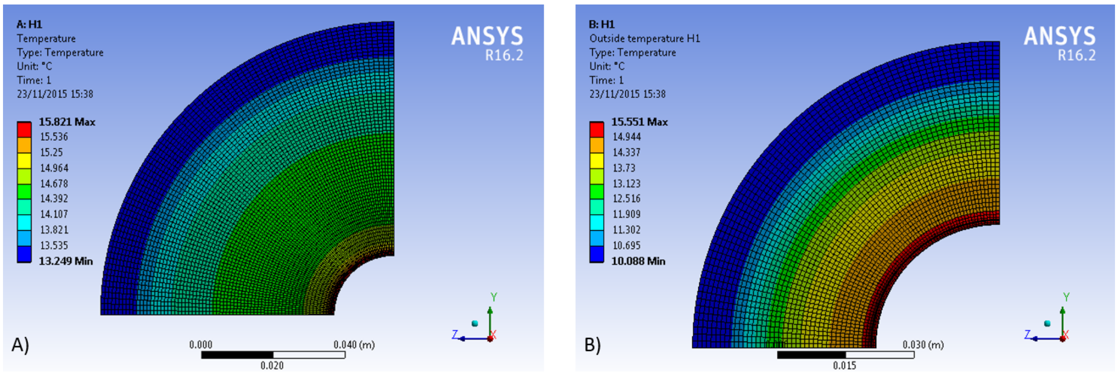

Figure 3.23: Temperature distribution on the outer surface for the standard configuration with Airex (A), and without Airex (B)

A summary of the conclusion on each parameter and the range of the minimum temperature related to it, are presented in Table 3.5 (without Airex) and Table 3.7 (with Airex).

Parameter	Should be	Minimum outside temperature range [$°C$]
K3	Minimized	15.82 - 11.54 = 4.28
K1	Minimized	14.85 - 13.22 = 1.63
L1	Maximized	14.27 - 13.26 = 1.01
H2	Minimized	13.66 - 13.03 = 0.63
K2	Minimized	13.33 - 13.03 = 0.30
L4	Maximized	13.37 - 13.16 = 0.21
L3	Maximized, max value about 13mm	13.25 - 13.11 = 0.14
H1	Maximized	13.25 - 13.24 = 0.01

Table 3.7: Summary of suggested approaches for each parameter in the standard configuration with Airex, ordered by relevance.

It can be seen in Table 3.7 that the top 3 relevant parameters for the outside temperature are K3, K1 and L1, of which none is easy to regulate due to mechanical and radiation requirements. The fourth most relevant parameter only have a minimum outside temperature range of 0.631°C. Thus one can conclude that an Airex piece (or any other material with a thermal conductivity of less than $0.075W/(m*K)$), in between the polymer parts will be the easiest way to avoid condensation on the outside without making the plug very thick. The calculated heat fluxes suggest that the total heat flux through the plug and the rest of the UT-box, will not exceed the 500W of cooling that the cooling plant can provide. The results are visualized in Figure 3.24

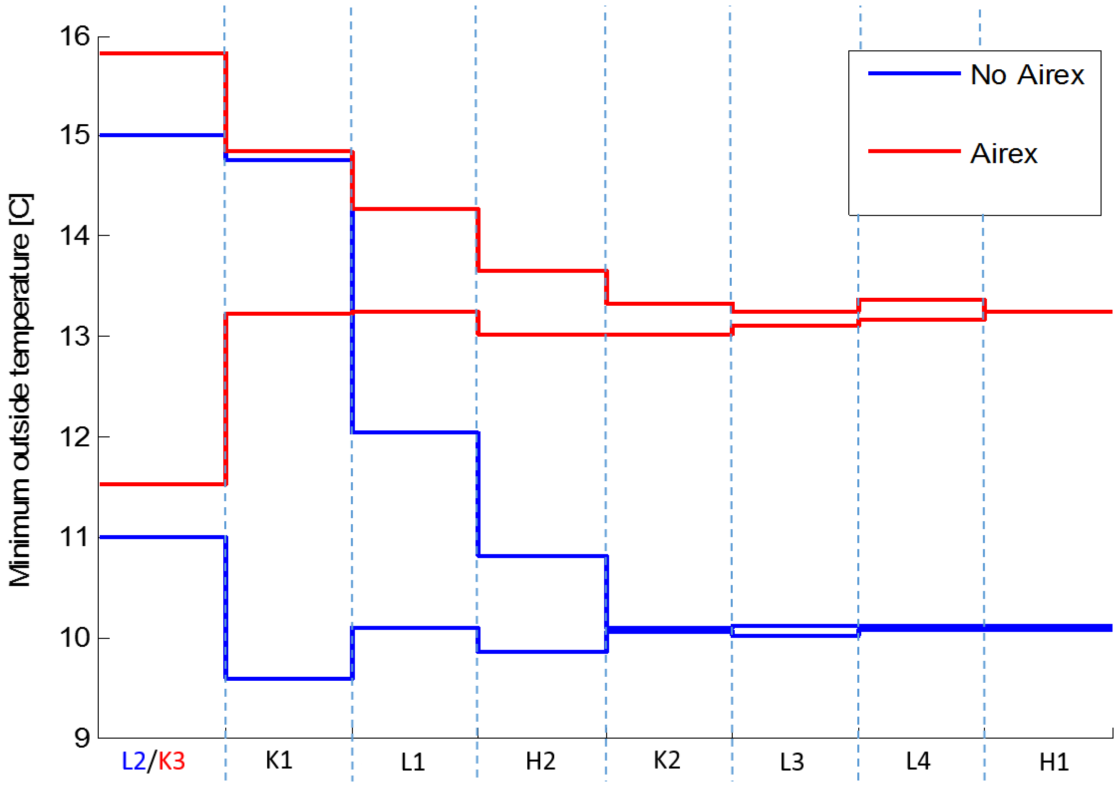

Figure 3.24: Visualization of the resulting temperature extremes presented in Table 3.7 and Table 3.5. Configuration with Airex in red and configuration without Airex in blue.

3.3.4 Decided dimensions

Taking into account the results of this thermal analysis, mechanical analysis and geometric constraints, dimensions for the UT-plug were set as indicated in the figures below. The plug will be manufactured in three separate parts, of which two are identical polyurethane parts. The polyurethane part is shown in Figure 3.25 and the central Airex part in Figure 3.26. The assembly of the suggested parts are shown in Figure 3.27. The polyurethane parts were manufactured according to the process described in Appendix F

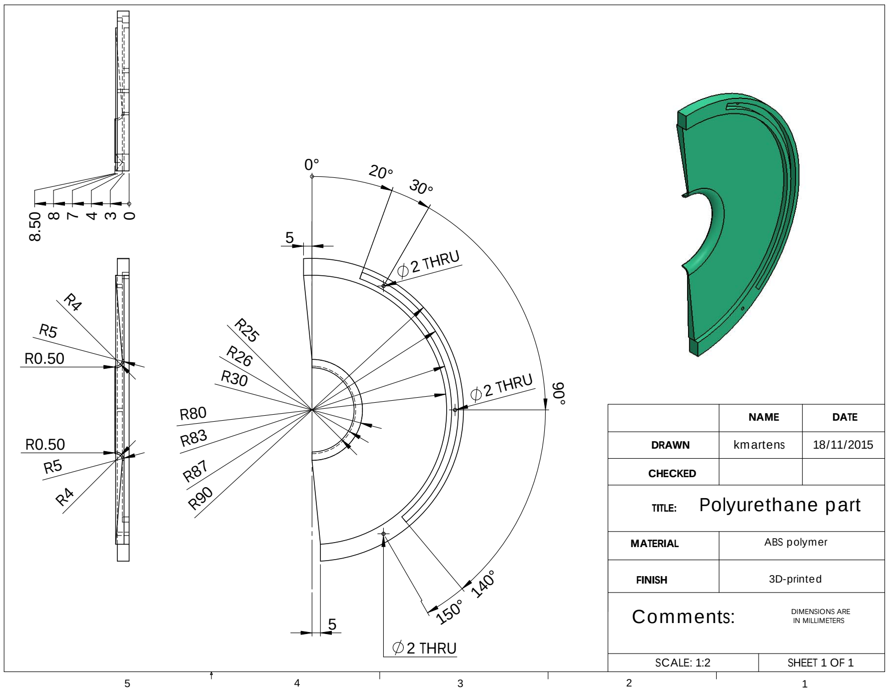

Figure 3.25: Drawing of the Polymer part.

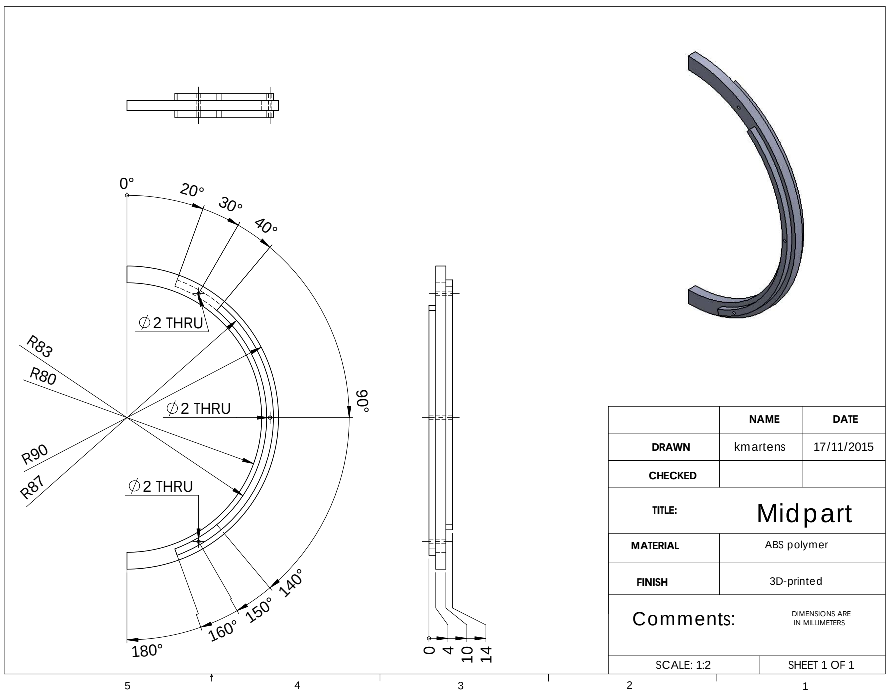

Figure 3.26: Drawing of the middle part.

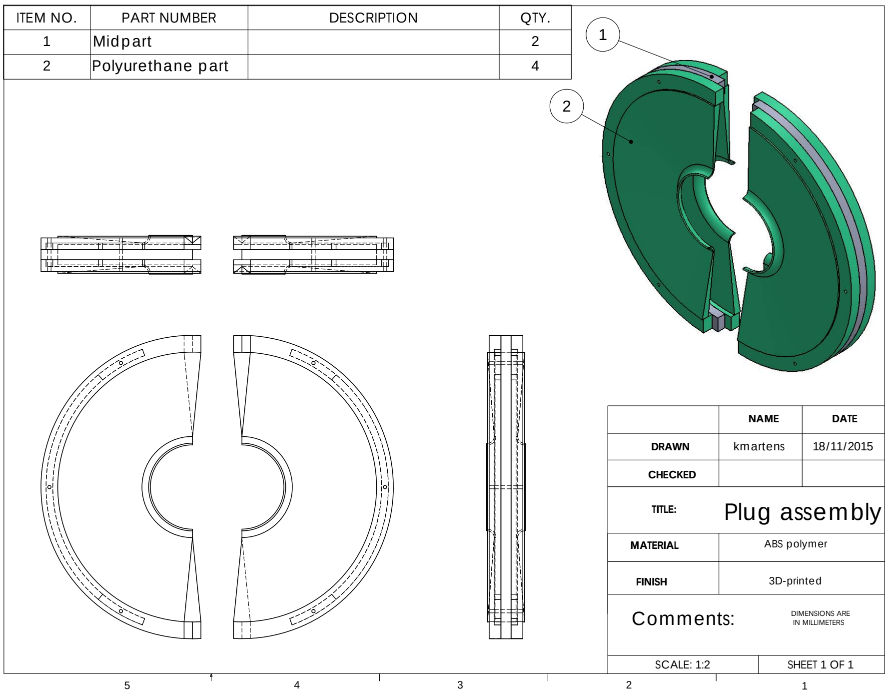

Figure 3.27: Drawing of the assembly of the polymer part and the middle part into a complete plug

4 Force evaluation

To assure that the fragile beryllium beam pipe will not break from the pressure applied by the plug, a mechanical simulation and rigidity measurements were performed on the plug.

4.1 Simulation

The plug simulated have the geometries stated in Section 3.3.4.

4.1.1 Model

To decrease the execution time for the mechanical simulation, only half of one side of the plug is simulated. The results should thus be doubled in order to achieve the total force applied by one half plug. The value of the friction coefficient between the beryllium pipe and the polyurethane plug is not known but estimated to be somewhere in the region 0.1-0.8 [17].

The displacement of the plug will not be more than 2mm in case of adequate closing. However, in case the plug accidentally get displaced more, a displacement larger than 2mm should be investigated. Thus a 4mm displacement towards the beam pipe is applied. The displacement is ramped up.

The Mooney-Rivlin model was the model used in this simulation with the parameters stated in Table 4.1. The initial elasticity modulus was based on the material hardness and calculated through

$$E_0 = 6894.76 \cdot (11.427 \cdot H - 0.4445 \cdot H^2 + 0.0071 \cdot H^3) \ , \tag{20}$$

where H is the hardness. The Poisson ratio were calculated to 0.501, which means that there is no global volume change under loads.

Property	Value			Unit
Material hardness	40	60	80	Shore A
Initial elasticity modulus	$1.38 \cdot 10^6$	$4.27 \cdot 10^6$	$1.18 \cdot 10^7$	Pa
Initial shear modulus	$4.60 \cdot 10^5$	$1.42 \cdot 10^6$	$3.92 \cdot 10^6$	Pa
Mooney coefficients	$C_{10} = 1.84 \cdot 10^5$	$C_{10} = 5.69 \cdot 10^5$	$C_{10} = 1.57 \cdot 10^6$	Pa
	$C_{01} = 4.60 \cdot 10^4$	$C_{01} = 1.42 \cdot 10^5$	$C_{01} = 3.91 \cdot 10^5$	Pa

Table 4.1: Material properties used in the mechanical simulations.

The geometry and the boundary conditions are shown in Figure 4.1 and the results are shown in Figure 4.2-Figure 4.5. Figure 4.2 shows the force dependence on the friction coefficient, with 4mm displacement and *Shore A 40* as hardness. Figure 4.3 shows the force dependence on displacement, with 0.45 as friction coefficient and *Shore A 40* as hardness.

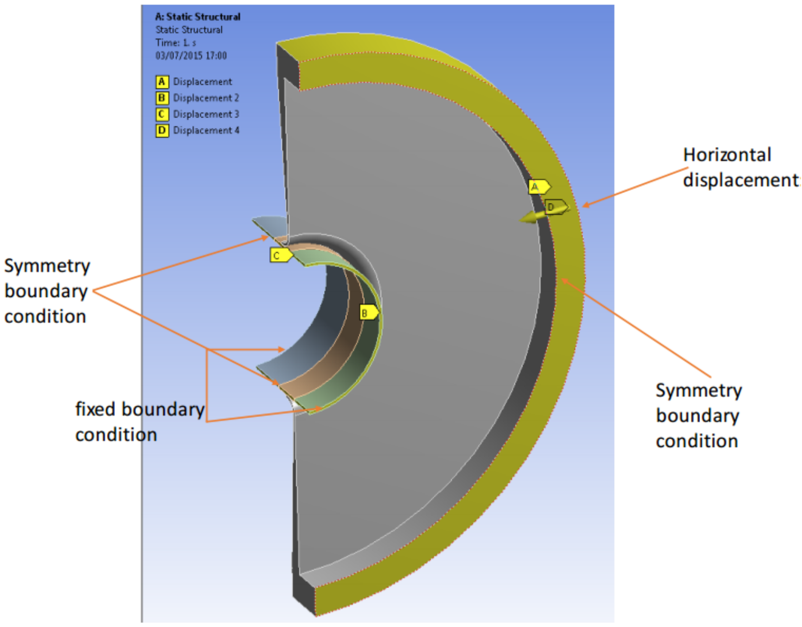

Figure 4.1: Geometry and boundary conditions for the mechanical simulation. The reaction force are probed on the beige pipe section.

4.1.2 Results

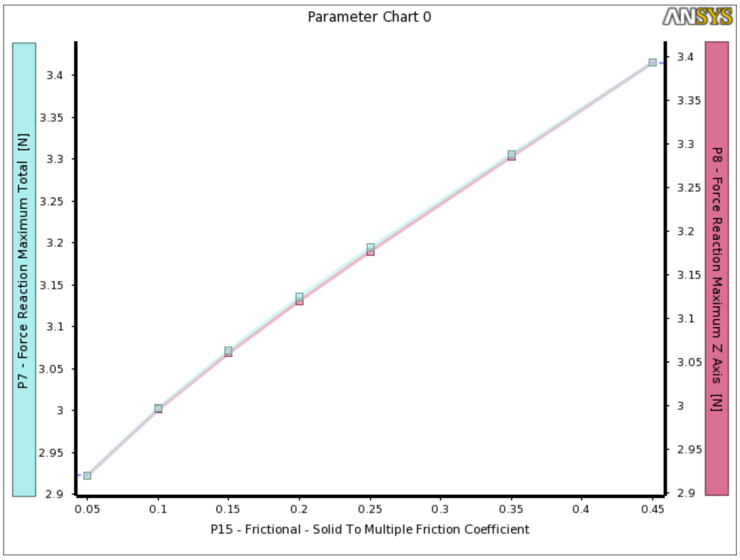

Figure 4.2: Simulation results for *Shore A 40*. Reaction force plotted against friction coefficient. Blue line and scale shows the total reaction force, the red line and scale shows the reaction force in the Z-direction (perpendicular to the beam pipe).

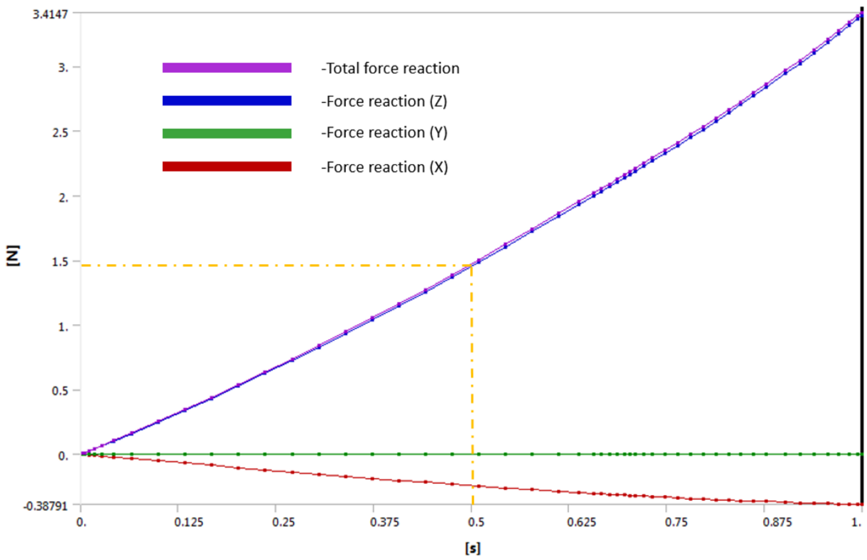

Figure 4.3: Simulation results for *Shore A 40* with 0.45 as friction coefficient. Reaction force plotted against time (since displacement of 4mm are ramped up over 1s). Time can be converted to displacement by multiplying the time value by 4mm.

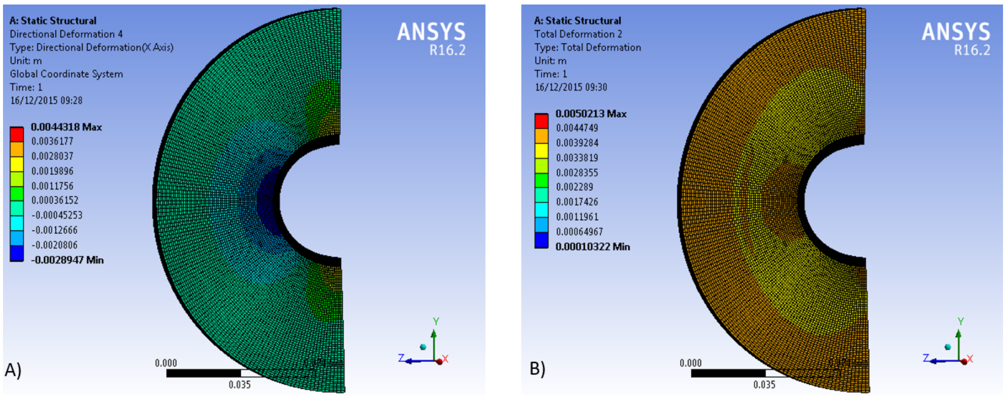

Figure 4.4: Calculated deformation on the UT-plug for *Shore A 40*. Deformation in X-direction (*A*), and total deformation (*B*).

Figure 4.3 suggests that the force applied on the beam pipe is about 3N at 2mm displacement (force have to be doubled since only one side is simulated) for *Shore A 40*. This magnitude of the force is acceptable. In Figure 4.4 (*A*). it can be seen that the deformation in the X-direction (parallel to the beam pipe) is below 4.5mm. The total deformation is shown in Figure 4.4 (*B*), and is calculated to be about 5mm. Figure 4.5 suggest that there is a strong hardness dependence and that the total reaction force could be as high as 58.2N at 4mm displacement for a plug with the hardness *Shore A 80*.

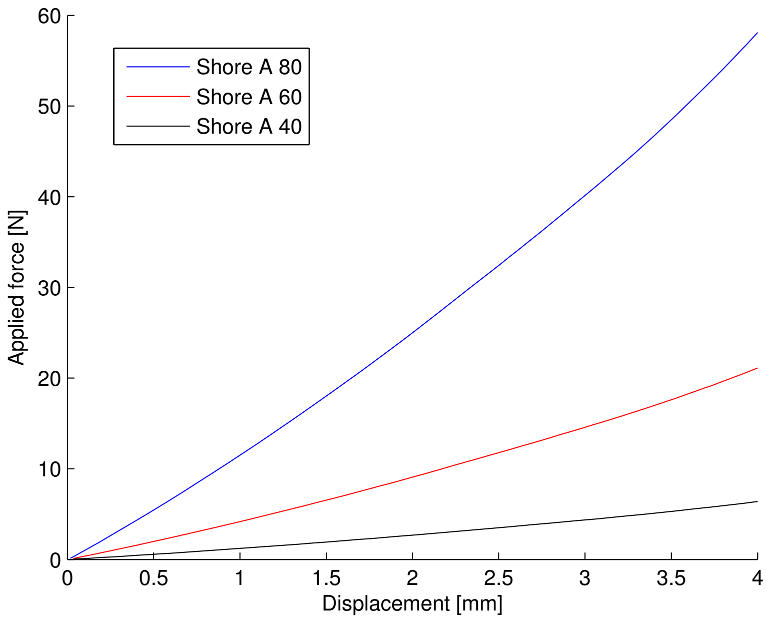

Figure 4.5: Simulation results for all hardness's. The total reaction force (i.e. for both plug halves) plotted against displacement.

4.2 Testing

4.2.1 Setup

To perform the compression tests, the tensile testing machine *Tinius Olsen H5KT* [18] were used. This machine measures both displacement and applied force. The results are analyzed in MATLAB R2014a.

To be able to use this tensile testing machine for a compression test, a sample holder has been manufactured. The sample holder has been manufactured in two separate parts. One part that holds the actual sample (Figure 4.6), and second part that is used to attach the holder to the tensile testing machine (Figure 4.7). The part shown in Figure 4.7 can thus be replaced in the future in order to use the holder in another machine or setup. Figure 4.8 shows the assembly of the two holder parts. Both holder parts were 3D-printed. The test was performed by attaching the sample holder to the compression machine and compress it against an acrylic pipe. The acrylic beam pipe was used to simulate the LHCb beam pipe. The diameter of the acrylic beam pipe is 25mm.

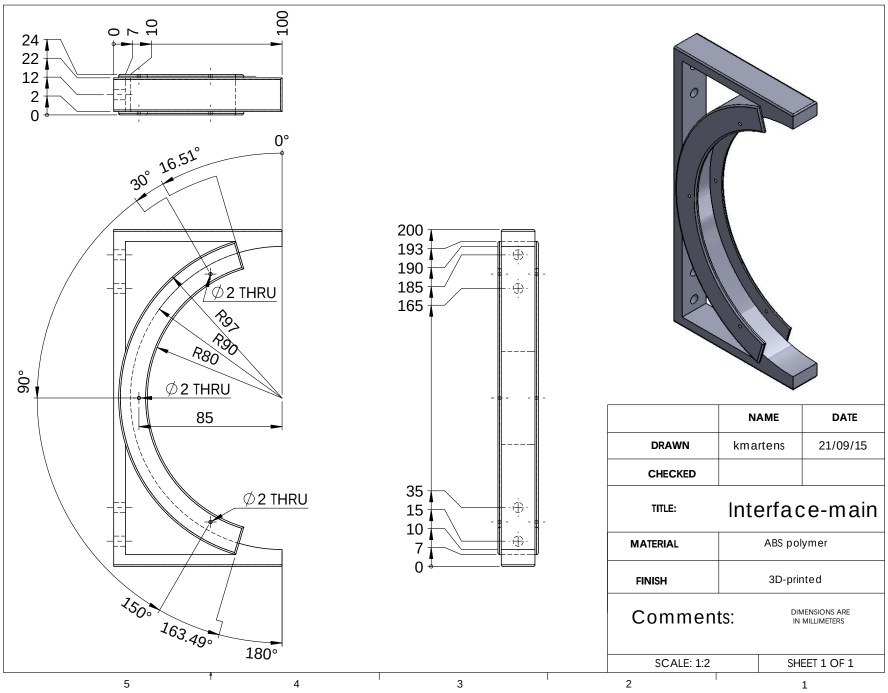

Figure 4.6: Drawing of the main part of the sample holder.

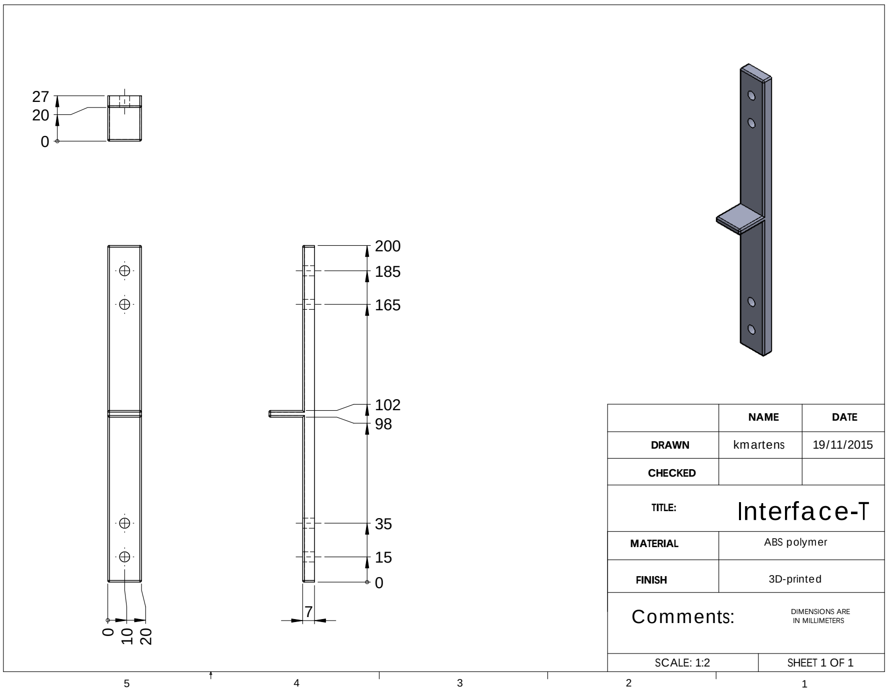

Figure 4.7: Drawing of the back piece to the sample holder.

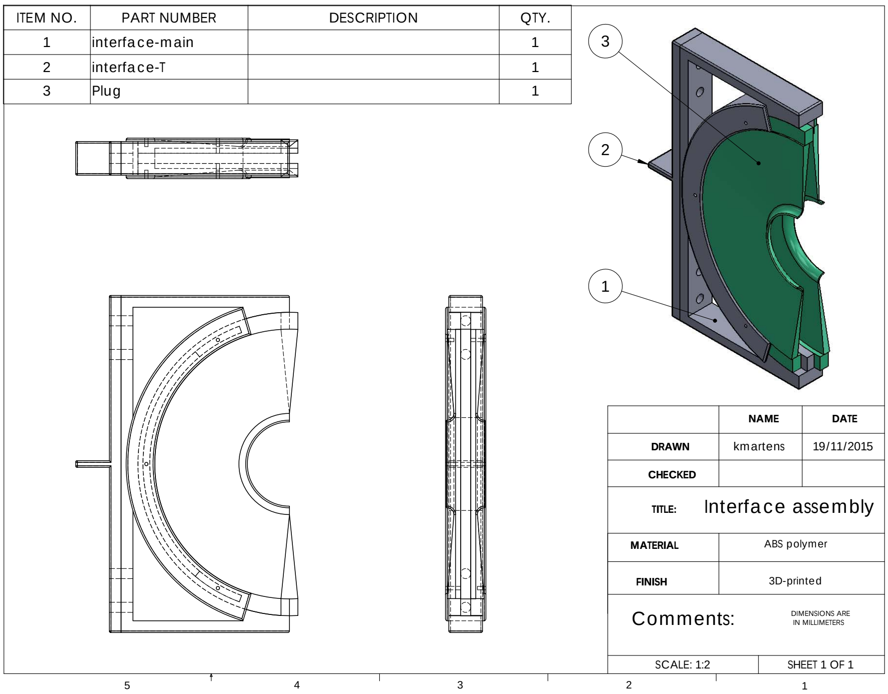

Figure 4.8: Drawing of the assembled sample holder.

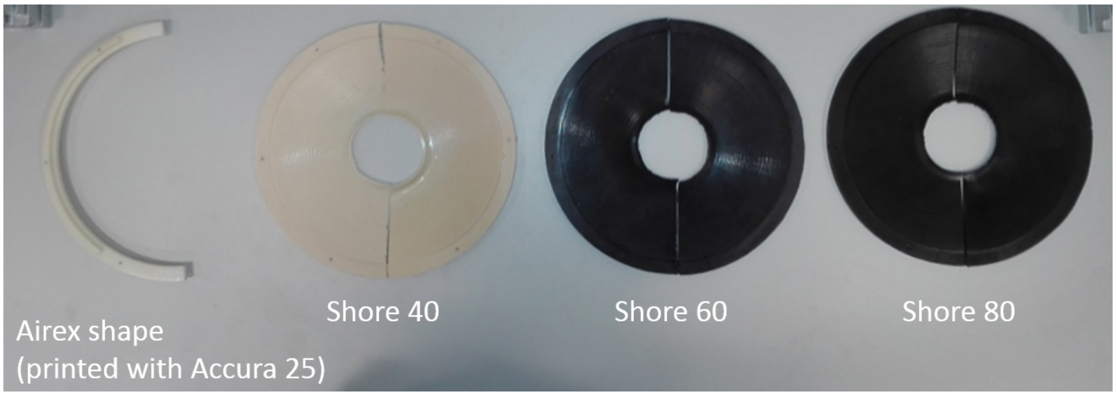

Figure 4.9: Plug parts used in compression test.

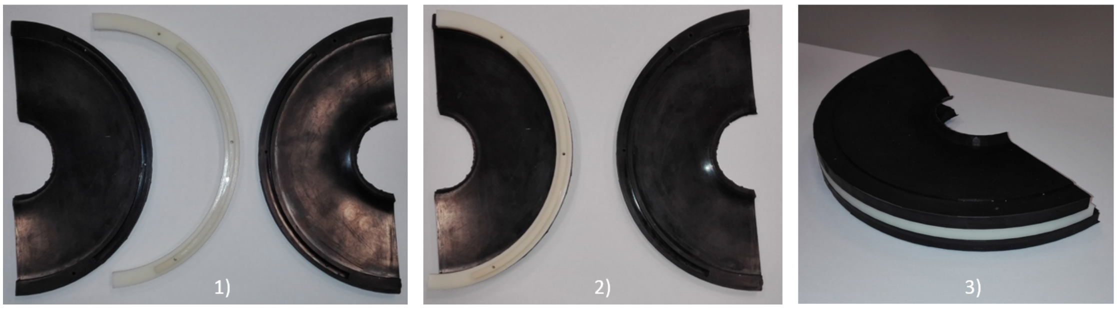

Figure 4.10: Plug assembly process

The tested plugs are shown in Figure 4.9 and the assembly process is shown in Figure 4.10. The assembled setup, during a compression test, is shown in Figure 4.11.

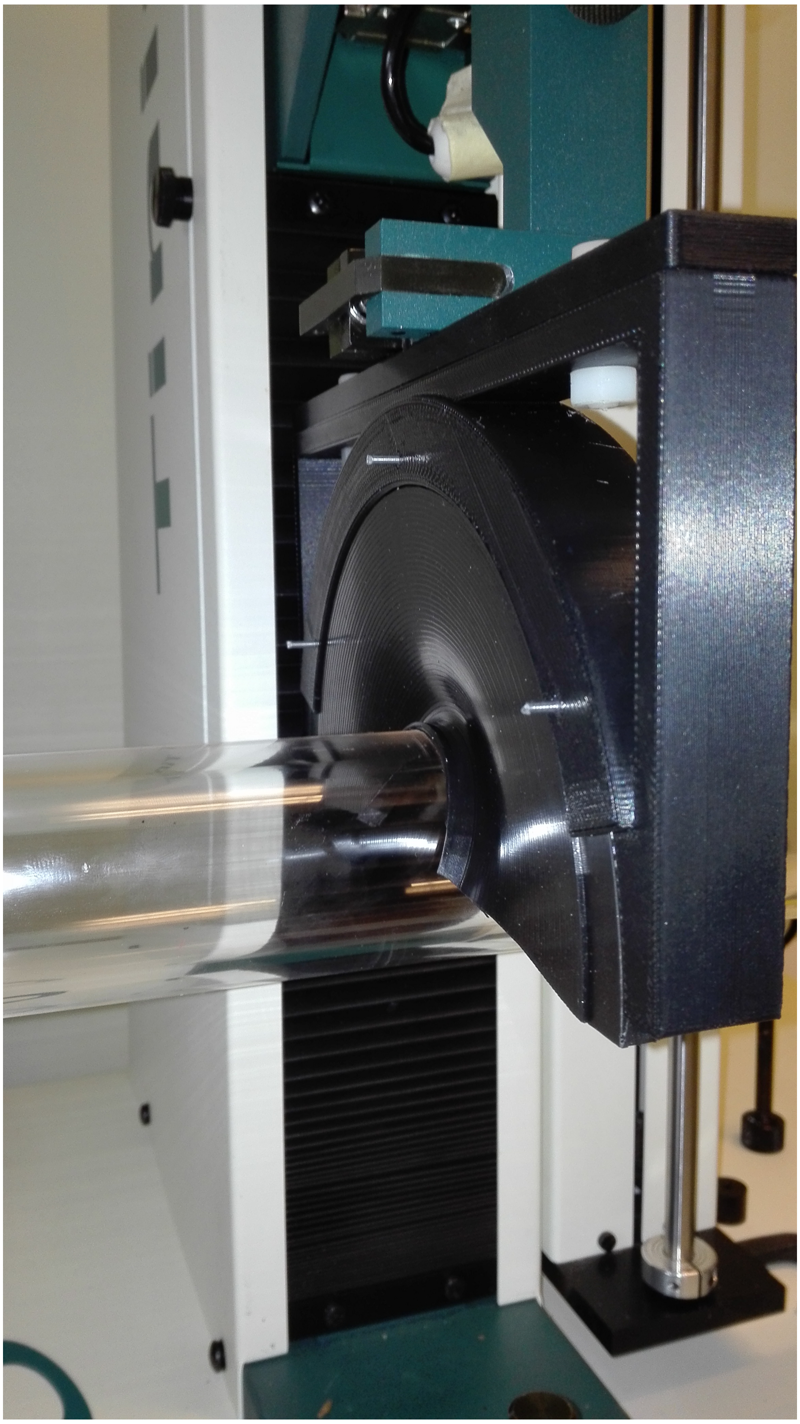

Figure 4.11: A compression test being performed

4.2.2 Results

Each plug were tested 10 times. The measurements are started at the smallest visible distance above the beam pipe. This means that there is a negative force applied (since the machine then have to hold the sample up). To make sure that the compression tests starts at the same position relative to the beam pipe, for all measurements, the data before the first registered positive force are erased, and the measured displacement at this point is subtracted from the displacement values. The results from the compression test are shown in Figure 4.12. Figure 4.13 shows the order in which the tests on the *Shore A 80* plug were performed.

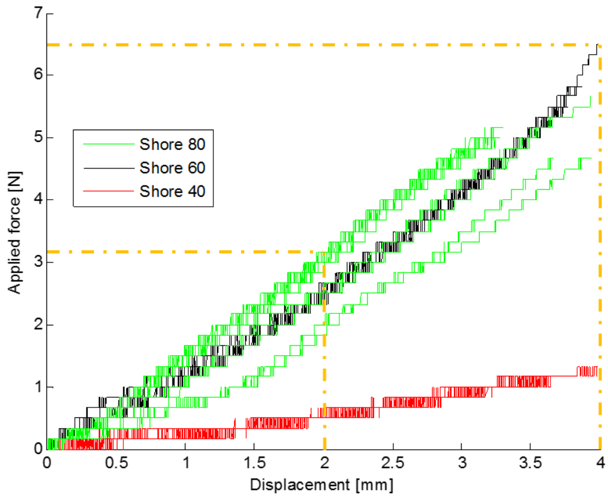

Figure 4.12: Compression test results.

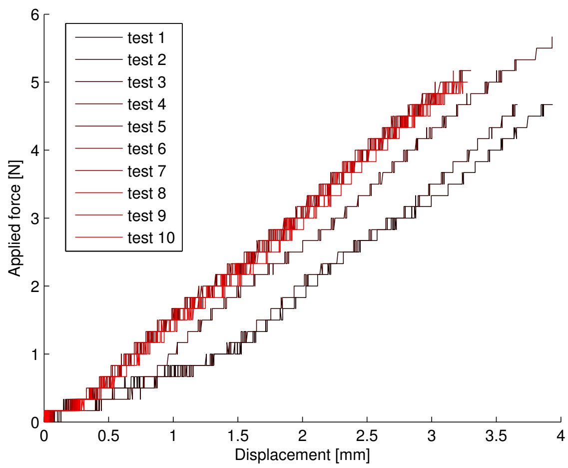

Figure 4.13: Numbered compression test results for the *Shore A 80* plug.

4.3 Conclusion

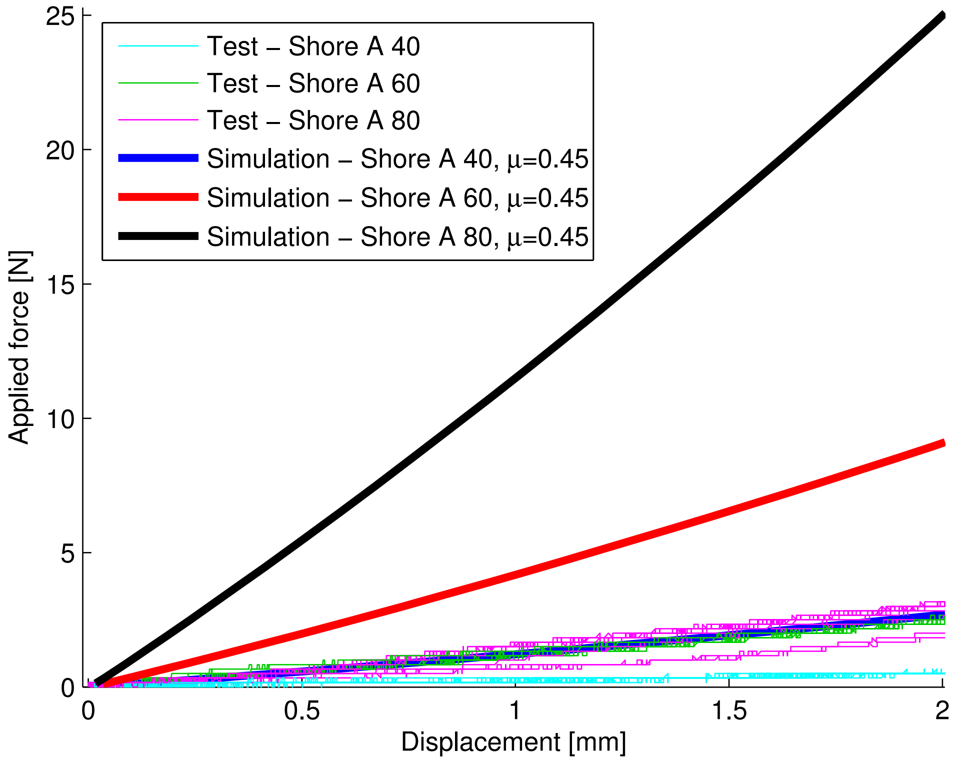

Figure 4.14: All calculated and measured forces plotted against the displacement

Figure 4.14 shows that there is a large difference between calculated and measured forces. This could be a consequence of inadequate estimations of the material properties, or it might be the case that the Mooney-Rivlin model is not suited for polyurethane of such shape. The Mooney-Rivlin model is one of the most basic models for hyper-elastic materials and is known to overestimate the reaction force, but a deviation of this magnitude was not expected. However, it should be noted that the *Shore A 60* test is similar to the *Shore A 40* calculations.
Figure 4.12 shows that the largest measured force at a 2mm displacement is about 3N, which is acceptable. The spread of the shore 80 measurements suggest that hardness of the plug implies a greater dependence on previous compressions.

The fact that some of the measured forces for the *Shore A 80* plug is lower than for the *Shore A 60* plug indicates that the shore number is not to be trusted completely. Other geometries than the one stated in Section 3.3.4 have been tested and the maximum force that have been measured at 2mm displacement is about 6.5N. The maximum force measured for 4mm compression is about 17N. This underpins the conclusion that the shore numbers should not be trusted completely and suggests that forces of this magnitude should still be considered possible, and that the calculations for *Shore A 80* should be considered the worst case scenario.

In order to be concise in the manufacturing process of the UT-plugs, and to assure that the force applied on the beam pipe will not brake it, a mixing ratio of the Polyurethane ingredients, and a curing cycle should be defined and carefully tested.

There seems to be a correlation between H1 and the applied force, but since the geometries tested does not have all other dimensions in common, it cannot be confirmed. An increased H1 seem to imply an increased force (and it increases the mass), thus it could be desired to minimize H1. Manufacturing difficulties puts a limit on how small H1 could be. It should be investigated how small H1 could be without causing problems in the manufacturing process.

The observed displacement in the beam pipe direction are of similar shape to the displacement shown in Figure 4.4. A linear regression has been made on all simulation- and test results. The reaction force F at a x mm displacement can thus be approximated through

$$F(x) = x * P(1) + P(2) \tag{21}$$

where the coefficients $P(1)$ and $P(2)$ are fetched from Table 4.2. Table 4.3 shows the calculated and measured forces for some displacements.

	Simulation			Test		
Hardness [Shore A]	40	60	80	40	60	80
P(1)	1.57	5.28	14.51	0.31	1.44	1.52
P(2)	-0.27	-0.96	-2.44	-0.16	-0.11	-0.46

Table 4.2: Linear regression coefficients for the simulation- and test results.

	Simulation			Test		
Hardness [Shore A]	40	60	80	40	60	80
Displacement [mm]	Force [N]					
0.5	0.6	2.0	5.4	0.2-0.3	0.5-0.8	0.3-0.7
1	1.3	4.2	11.2	0.2-0.4	1.2	0.6-1.7
1.5	2.1	6.4	18	0.3-0.5	1.7-1.8	1.0-2.4
2	2.9	9.0	24.8	0.5-0.7	2.3-2.7	1.8-3.2
2.5	3.8	11.8	32.4	0.6-0.8	3.2-3.5	2.6-4.2
3	4.7	14.6	40.4	0.8-1.0	4.0-4.2	3.2-4.8
3.5	5.7	17.5	48.4	1.0-1.2	4.8-5.2	3.8-5.0
4	6.8	21.1	58.2	1.2-1.3	6.3-6.5	4.5-5.7

Table 4.3: Simulation and measurement results for some displacements.

5 Conclusions

The aim of this thesis is to establish concepts and methods so that the requirements of the UT-box can be fulfilled. The most important conclusions, and therefore the main results of this thesis, are stated below.

- **A heterogeneous UT-plug has been calculated to perform better thermally than a homogeneous polyurethane plug.**
  Through analytical and numerical calculations it has become evident that the heterogeneous plug is the best approach to avoid condensation on the UT-plug.

- **It has been confirmed that condensation will not occur on the outside of the panels.**

- **The Carbon-Airex composite panel concept has been validated.**
  The sandwich structured composites, that will make the UT-walls, have been confirmed to be stable. Stable in the way that the carbon fiber skins and the Airex core are properly attached to each other by the cocuring process.

- **The copper net concept to ensure Faraday-cage behavior has been validated.**
  The electrical conductance in a copper net embedded in the carbon fiber skins has been measured and proven to be good.

- **A possible method for panel connection has been validated.**
  The method to attach a 90 °angle piece in the joints between the panels, in order to connect the copper nets together has been validated.

- **Radiation resistance of the UT-plug has been assured.**

- **A UT-plug manufacturing method has been validated.**
  The UT-plug can be manufactured by 3D-printing a mold (high resolution is required). The method have however shown difficulties in production of small plugs.

- **A mixing ratio and curing cycle for the Polyurethane in the UT-plug have to be defined.**
  In order to ensure that all UT-plugs have the same material properties, and to eliminate the risk of rupture in the beam pipe, a mixing ratio and a curing cycle for the polyurethane part have to be defined and tested.

Those conclusions will serve as a basis for the construction of a mock-up of the UT-box. The mock-up will serve to test how everything works out when put together and to determine which areas might require special attention or further development. If the mock-up do not show the need to change any method or concept, they will be implemented in the LHCb upgrade taking place in 2019-2020.

References

[1] Oskar Mårtensson, *Cooling system design for the Micromegas detector*, October 2015
Available at:
https://edms.cern.ch/document/1538222
07/12/2015,09:39

[2] http://home.web.cern.ch/about/experiments/lhcb
21/09/2015,13:24

[3] Frank Close, *Particle physics- A very short introduction*, 2012, Oxford University Press

[4] John Ellis, *Why does CP violation matter to the universe*, September 1999
Available at:
http://cerncourier.com/cws/article/cern/28092
11/10/2015,18:56

[5] Alfio Lazzaro, *CP Violation in B mesons*, March 2007
Available at:
http://www.slac.stanford.edu/cgi-wrap/getdoc/slac-pub-12440.pdf
11/10/2015,20:44

[6] Jason Andrews, *Upgrade of the Upstream Tracker at LHCb*, April 2015
Available at:
https://cds.cern.ch/record/2013250/files/LHCb-TALK-2015-081.pdf
29/10/2015,09:35

[7] LHCb collaborations *LHCb tracker upgrade TDR*, February 2014
Available at:
https://cds.cern.ch/record/1647400/files/LHCB-TDR-015.pdf
21/09/2015,13:36

[8] Joao Carlos Batista Lopes and Oskar Mårtensson, *UT BOX STRUCTURAL AND THERMAL ASSESSMENT*, April 2015
Available at:
https://edms.cern.ch/document/1507417
11/12/2015,10:41

[9] M.H. Van de Voorde and C.Restat, *Selection guide to organic materials for nuclear engineering*, May 1972
Available at:
https://cds.cern.ch/record/186329/files/CERN-72-07.pdf
07/12/2015,09:39

[10] http://www.sicomin.com/datasheets/product-pdf1037.pdf
11/12/2015,11:18, (Data sheet for Airex R82)

[11] http://www.aerospares.hu/files/loctite/SynSkin_HC_9837_1.pdf
19/01/2016,13:00, (Data sheet for carbon fiber)

[12] http://www.dexmet.com/1_pdf/Lightning%20Strike%20Brochure.pdf
01/12/2015,14:15, (Data sheet for copper net)

[13] Theodore L. Bergman, Adrienne S. Lavine, Frank P. Incropera & David P. Dewitt, *Fundamentals of heat and mass transfer* 6th Edition, 2007, R.R. Donnelley

[14] ASHRAE, *ASHRAE Handbook - Fundamentals*, 2015
Available at:
`http://shop.iccsafe.org/media/wysiwyg/material/8950P203-sample.pdf`
04/12/2015,14:31

[15] H. C. Huang and R. W. Lewis, *Adaptive Analysis for Heat Flow Problems Using Error Estimation Techniques.*, April 1989.
Proc. Sixth Int. Conf. for Numerical Methods in Thermal Problems, U.K. July 1989, Pineridge Press, SWansea (1989)

[16] Yunus A. Cengel, *Introduction to Thermodynamics and Heat Transfer*, 2nd Edition, 2008, McGraw-Hill Publishing Company

[17] `http://www.gallaghercorp.com/images/kinetic-coefficient-graphs.gif`
14/12/2015,16:02

[18] `http://www.tiniusolsen.com/pdf/B140D.pdf`
01/12/2015,14:15, (Data sheet for tensile tester)

A : UT-box thermal analysis

CALCULATION REPORT

PH/DT-EO
EDMS NUMBER: 1511711

Prepared by: Kurt Oskar Edvin Martensson

Checked by: Joao Carlos Batista Lopes

Purpose: To assist in analytical calculations regarding temperature distributions in a box consisting of no more than three layers, with constant inner and surrounding temperature. The box contains nitrogen and is surrounded by air.

1. Problem description

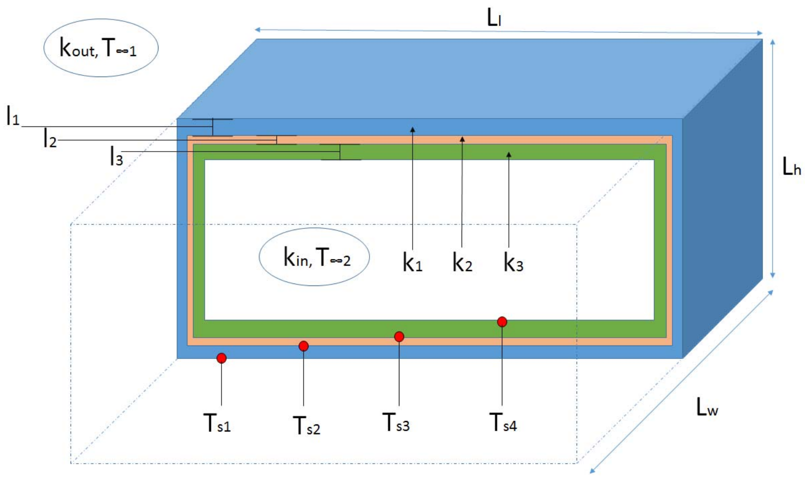

Simplifications made:
- Stand alone box
- Neglected thermal resistance at interfaces
- Gray and diffusive surfaces
- No reflection of radiation emitted from box (Thus correspond to a "coldest case")

Assumptions made:
- Steady state
- Ambient surrounding

1

CALCULATION REPORT

PH/DT-EO
EDMS NUMBER: 1511711

2. Input

2.1 Temperatures

$T_{\infty 1} := 20\ °C$ [Temperature of surrounding]

$T_{\infty 2} := -5\ °C$ [Temperature inside the box]

2.2 Geometry

$L_h := 1.9\ m$ [Height of box]

$L_w := 2.08\ m$ [Width of box]

$L_l := 0.43\ m$ [Length of box]

$l_1 := 2\ mm$ [Thickness of outermost layer]

$l_2 := 20\ mm$ [Thickness of middle layer]

$l_3 := 2\ mm$ [Thickness of innermost layer]

2.3 Thermal conductivity

$k_1 := 1.5\ \frac{W}{m \cdot K}$ [Conductivity of outermost layer]

$k_2 := 0.036\ \frac{W}{m \cdot K}$ [Conductivity of middle layer]

$k_3 := 1.5\ \frac{W}{m \cdot K}$ [Conductivity of innermost layer]

2.4 Others

$g := g = 9.807\ \frac{m}{s^2}$ [Acceleration due to gravity]

$\sigma = \left(5.67 \cdot 10^{-8}\right) \frac{kg}{s^3 \cdot K^4}$ [Boltzmann constant]

$\varepsilon_1 := 0.98$ [Emissivity of of outermost layer]

$\varepsilon_2 := 0.98$ [Emissivity of of innermost layer]

CALCULATION REPORT

PH/DT-EO
EDMS NUMBER: 1511711

3. Heat transfer in vertical walls

3.1 Film temperatures

In order to calculate the convection heat transfer coefficient, the properties of the fluid should be determined at the so called "film temperature", i.e. the mean of surface temperature and the temperature of the fluid "at infinity". To be able to calculate this, one have to use an estimated value for the temperatures of the surfaces, since they are unknown. If this initial guess turns out to be far away from the result acheived, it should be updated to the result acheived. This process should then be iterated until the result is close enough to the estimations.

3.1 Film temperatures on vertical walls

$T_{s1.v.ini} := 15.7\ °C$ [Estimated outer surface temperature]

$T_{s4.v.ini} := 0.1\ °C$ [Estimated inner surface temperature]

$$T_{f.out.v} := \frac{\left(T_{\infty 1} + T_{s1.v.ini}\right)}{2} = 291\ K$$

$$T_{f.in.v} := \frac{\left(T_{\infty 2} + T_{s4.v.ini}\right)}{2} = 270.7\ K$$

[Film temperatures at which the fluid properties should be evaluated] {Eq 7.2}[1]

CALCULATION REPORT

PH/DT-EO
EDMS NUMBER: 1511711

3.2 Fluid properties (Linearly interpolated from table A.4 [1] in Appendix 1.)

$$Pr_{out.v} := \left(\frac{T_{f.out.v}}{K} - 250\right) \cdot \frac{(0.720 - 0.707)}{50} + 0.707 = 0.718$$

$$Pr_{in.v} := \left(\frac{T_{f.in.v}}{K} - 250\right) \cdot \frac{(0.727 - 0.716)}{50} + 0.716 = 0.721$$

[Prandtl number of air on outside
and nitrogen inside]

$$\nu_{out.v} := \left(\left(\frac{T_{f.out.v}}{K} - 250\right) \cdot \frac{(15.89 - 11.44)}{50} + 11.44\right) \cdot 10^{-6}\ \frac{m^2}{s} = \left(1.509 \cdot 10^{-5}\right)\ \frac{m^2}{s}$$

$$\nu_{in.v} := \left(\left(\frac{T_{f.in.v}}{K} - 250\right) \cdot \frac{(15.86 - 11.48)}{50} + 11.48\right) \cdot 10^{-6} \left(\frac{m^2}{s}\right) = \left(1.329 \cdot 10^{-5}\right)\ \frac{m^2}{s}$$

[kinematic viscosity of air on
outside and nitrogen inside]

$$\alpha_{out.v} := \left(\left(\frac{T_{f.out.v}}{K} - 250\right) \cdot \frac{(22.5 - 15.9)}{50} + 15.9\right) \cdot 10^{-6} \left(\frac{m^2}{s}\right) = \left(2.131 \cdot 10^{-5}\right)\ \frac{m^2}{s}$$

$$\alpha_{in.v} := \left(\left(\frac{T_{f.in.v}}{K} - 250\right) \cdot \frac{(22.1 - 15.8)}{50} + 15.8\right) \cdot 10^{-6} \left(\frac{m^2}{s}\right) = \left(1.841 \cdot 10^{-5}\right)\ \frac{m^2}{s}$$

[thermal diffusivity of air on
outside and nitrogen inside]

$$k_{out.v} := \left(\left(\left(\frac{T_{f.out.v}}{K} - 250\right) \cdot \frac{(26.3 - 22.3)}{50} + 22.3\right) \cdot 10^{-3}\right) \frac{W}{m \cdot K} = 0.026\ \frac{W}{m \cdot K}$$

$$k_{in.v} := \left(\left(\left(\frac{T_{f.in.v}}{K} - 250\right) \cdot \frac{(25.9 - 22.2)}{50} + 22.2\right) \cdot 10^{-3}\right) \frac{W}{m \cdot K} = 0.024\ \frac{W}{m \cdot K}$$

[thermal conductivity of air on
outside and nitrogen inside]

CALCULATION REPORT

PH/DT-EO
EDMS NUMBER: 1511711

3.3. Heat transfer on the inside

3.3.1 Convection on the inside

$l_{tot} := l_1 + l_2 + l_3 = 0.024\ m$ [Total thickness of the wall]

$\beta_{in.v} := \frac{1}{T_{f.in.v}} = 0.004\ \frac{1}{K}$ [Volumetric thermal expansion coefficient on the intside] {Eq 9.9}[1]

$$Ra_{in.v} := \frac{g \cdot \beta_{in.v} \cdot (T_{s4.v.ini} - T_{\infty 2}) \cdot (\max(L_h, L_w) - 2 \cdot l_{tot})^3}{\nu_{in.v} \cdot \alpha_{in.v}} = 6.335 \cdot 10^9$$

[Rayleigh number on the inside] {Eq 9.25}[1]

$$Nu_{in.v} := \begin{cases} 0.68 + \dfrac{\left(0.67 \cdot Ra_{in.v}^{0.25}\right)}{\left(1 + \left(\dfrac{0.492}{Pr_{in.v}}\right)^{\frac{9}{16}}\right)^{\frac{4}{9}}} & \text{if } Ra_{in.v} < 10^9 \\ 0.825 + \dfrac{\left(0.387 \cdot Ra_{in.v}^{0.25}\right)}{\left(1 + \left(\dfrac{0.492}{Pr_{in.v}}\right)^{\frac{9}{16}}\right)^{\frac{8}{27}}} & \text{else} \end{cases} = 92.451$$

[Nusselt number on the inside]

{Eq 9.27}[1]

{Eq 9.26}[1]

$$h_{conv.in.v} := \frac{k_{in.v} \cdot Nu_{in.v}}{\max(L_h, L_w, L_l) - 2 \cdot l_{tot}} = 1.08\ \frac{W}{m^2 \cdot K}$$

[Convection heat transfer coefficient on the inside] {Eq 9.24}[1]

3.3.2 Radiation on the inside

$$h_{rad.in.v} := \varepsilon_2 \cdot \sigma \cdot \left((T_{s4.v.ini} + T_{\infty 2}) \cdot (T_{s4.v.ini}^2 + T_{\infty 2}^2)\right) = 4.41\ \frac{1}{W} \cdot \frac{W}{m^2 \cdot K} \cdot W$$

[Radiation heat transfer coefficient on the inside] {Eq 1.9}[1]

3.3.3 Combined radiation and convection on the inside

$$h_{comb.in.v} := h_{rad.in.v} + h_{conv.in.v} = 5.489\ \frac{kg}{s^3 \cdot K}$$

[2]

CALCULATION REPORT

PH/DT-EO
EDMS NUMBER: 1511711

3.4. Heat transfer on the outside

3.4.1 Convection on the outside

$$\beta_{out.v} := \frac{1}{T_{f.out.v}} = 0.003\ \frac{1}{K}$$

[Volumetric thermal expansion coefficient on the outside] {Eq 9.9}[1]

$$Ra_{out.v} := \frac{g \cdot \beta_{out.v} \cdot (T_{\infty 1} - T_{s1.v.ini}) \cdot \max(L_h, L_w)^3}{\nu_{out.v} \cdot \alpha_{out.v}} = 4.055 \cdot 10^9$$

[Rayleigh number on the outside] {Eq 9.25}[1]

$$Nu_{out.v} := \left\| \begin{array}{l} \text{if } Ra_{out.v} < 10^9 \\ \quad \left\| 0.68 + \dfrac{\left(0.67 \cdot Ra_{out.v}^{0.25}\right)}{\left(1 + \left(\dfrac{0.492}{Pr_{out.v}}\right)^{\frac{9}{16}}\right)^{\frac{4}{9}}} \right. \\ \text{else} \\ \quad \left\| 0.825 + \dfrac{\left(0.387 \cdot Ra_{out.v}^{0.25}\right)}{\left(1 + \left(\dfrac{0.492}{Pr_{out.v}}\right)^{\frac{9}{16}}\right)^{\frac{8}{27}}} \right. \end{array} \right| = 82.757$$

[Nusselt number on the outside]

{Eq 9.27}[1]

{Eq 9.26}[1]

$$h_{conv.out.v} := \frac{k_{out.v} \cdot Nu_{out.v}}{\max(L_h, L_w, L_l)} = 1.018\ \frac{W}{m^2 \cdot K}$$

[Convection heat transfer coefficient on the outside] {Eq 9.24}[1]

3.4.2 Radiation on the outside

$$h_{rad.out.v} := \varepsilon_1 \cdot \sigma \cdot (T_{s1.v.ini} + T_{\infty 1}) \cdot \left(T_{s1.v.ini}^{\ 2} + T_{\infty 1}^{\ 2}\right) = 5.478\ \frac{1}{m^2 \cdot K} \cdot W$$

[Radiation heat transfer coefficient on the outside] {Eq 1.9}[1]

3.4.3 Combined radiation and convection on the inside

$$h_{comb.out.v} := h_{conv.out.v} + h_{rad.out.v} = 6.496\ \frac{kg}{s^3 \cdot K}$$

[2]

CALCULATION REPORT

PH/DT-EO
EDMS NUMBER: 1511711

3.5 Results on vertical walls

$$R''_{tot.v} := \frac{1}{h_{comb.out.v}} + \frac{l_1}{k_1} + \frac{l_2}{k_2} + \frac{l_3}{k_3} + \frac{1}{h_{comb.in.v}} = 0.894\ \frac{s^3 \cdot K}{kg}$$

[Thermal resistance over the vertical walls] {Eq 3.6, 3.9, 3.13& 3.19}[1]

$$q''_v := \frac{(T_{\infty 1} - T_{\infty 2})}{R''_{tot.v}} = 27.953\ \frac{kg}{s^3}$$

[Heat flux through vertical walls] {Eq 3.19}[1]

$$T_{s1.v} := T_{\infty 1} - q''_v \cdot \left(\frac{1}{h_{comb.out.v}}\right) = 288.847\ K$$

$$T_{s2.v} := T_{s1.v} - \frac{q''_v \cdot l_1}{k_1} = 288.809\ K$$

$$T_{s3.v} := T_{s2.v} - \frac{q''_v \cdot l_2}{k_2} = 273.28\ K$$

$$T_{s4.v} := T_{s3.v} - \frac{q''_v \cdot l_3}{k_3} = 273.242\ K$$

[Temperatures of different surfaces/interfaces of the vertical walls] {Eq 1.2 & 1.3a}[1]

$$T_{inside.v} := T_{s4.v} - q''_v \cdot \left(\frac{1}{h_{comb.in.v}}\right) = 268.15\ K$$

$$q_{v1} := q''_v \cdot L_h \cdot L_l = 22.838\ W$$
$$q_{v2} := q''_v \cdot L_h \cdot L_w = 110.472\ W$$

[Heat flow through the each kind of the vertical walls of the box]

$$q_v := 2 \cdot (q_{v1} + q_{v2}) = 266.62\ W$$

[Total heat flow through the vertical walls of the box]

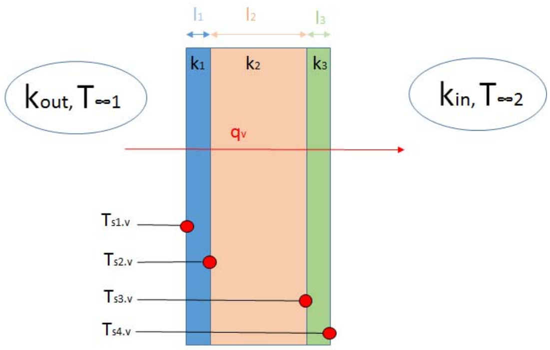

CALCULATION REPORT

PH/DT-EO
EDMS NUMBER: 1511711

4. Heat transfer through the top

4.1 Film temperatures on top

$T_{s1.t.ini} := 15.63\ °C$ [Estimated outer surface temperature]

$T_{s4.t.ini} := 0.21\ °C$ [Estimated inner surface temperature]

$$T_{f.out.t} := \frac{(T_{\infty 1} + T_{s1.t.ini})}{2} = 290.965\ K$$

$$T_{f.in.t} := \frac{(T_{\infty 2} + T_{s4.t.ini})}{2} = 270.755\ K$$

[Film temperatures at which the fluid properties should be evaluated] {Eq 7.2}[1]

4.2 Fluid properties

(Linearly interpolated from table A.4 [1] in Appendix 1.)

$$\nu_{out.t} := \left(\left(\frac{T_{f.out.t}}{K} - 250\right) \cdot \frac{(15.89 - 11.44)}{50} + 11.44\right) \cdot 10^{-6}\ \frac{m^2}{s} = \left(1.509 \cdot 10^{-5}\right)\ \frac{m^2}{s}$$

$$\nu_{in.t} := \left(\left(\frac{T_{f.in.t}}{K} - 250\right) \cdot \frac{(15.86 - 11.48)}{50} + 11.48\right) \cdot 10^{-6}\ \left(\frac{m^2}{s}\right) = \left(1.33 \cdot 10^{-5}\right)\ \frac{m^2}{s}$$

[kinematic viscosity of air on outside and nitrogen inside]

$$\alpha_{out.t} := \left(\left(\frac{T_{f.out.t}}{K} - 250\right) \cdot \frac{(22.5 - 15.9)}{50} + 15.9\right) \cdot 10^{-6}\ \left(\frac{m^2}{s}\right) = \left(2.131 \cdot 10^{-5}\right)\ \frac{m^2}{s}$$

$$\alpha_{in.t} := \left(\left(\frac{T_{f.in.t}}{K} - 250\right) \cdot \frac{(22.1 - 15.8)}{50} + 15.8\right) \cdot 10^{-6}\ \left(\frac{m^2}{s}\right) = \left(1.842 \cdot 10^{-5}\right)\ \frac{m^2}{s}$$

[thermal diffusivity of air on outside and nitrogen inside]

$$k_{out.t} := \left(\left(\left(\frac{T_{f.out.t}}{K} - 250\right) \cdot \frac{(26.3 - 22.3)}{50} + 22.3\right) \cdot 10^{-3}\right)\ \frac{W}{m \cdot K} = 0.026\ \frac{W}{m \cdot K}$$

$$k_{in.t} := \left(\left(\left(\frac{T_{f.in.t}}{K} - 250\right) \cdot \frac{(25.9 - 22.2)}{50} + 22.2\right) \cdot 10^{-3}\right)\ \frac{W}{m \cdot K} = 0.024\ \frac{W}{m \cdot K}$$

[thermal conductivity of air on outside and nitrogen inside]

CALCULATION REPORT

PH/DT-EO
EDMS NUMBER: 1511711

4.3 Heat transfer on the outside

4.3.1 Convection on the outside

The outside of the "roof" of the box is considered as the upper surface of a cold plate, since it is definitely not warmer than surrounding temperature $T_{\infty 1}$.

$$\beta_{out.t} := \frac{1}{T_{f.out.t}} = 0.003 \ \frac{1}{K}$$

[Volumetric thermal expansion coefficient on the outside] **{Eq 9.9}**[1]

$$Ra_{out.t} := \frac{g \cdot \beta_{out.t} \cdot \left(T_{\infty 1} - T_{s1.t.ini}\right) \cdot \max\left(L_h, L_w\right)^3}{\nu_{out.t} \cdot \alpha_{out.t}} = 4.123 \cdot 10^9$$

[Rayleigh number on the outside] **{Eq 9.25}**[1]

$$Nu_{out.top} := 0.27 \cdot Ra_{out.t}^{\ 0.25}$$

[Nusselt number on the outside] **{Eq 9.32}**[1]

$$h_{conv.out.t} := \frac{k_{out.t} \cdot Nu_{out.top}}{\max\left(L_h, L_w, L_l\right)} = 0.841 \ \frac{W}{m^2 \cdot K}$$

[Convection heat transfer coefficient on the outside] **{Eq 9.24}**[1]

4.3.2 Radiation on the outside

$$h_{rad.out.t} := \varepsilon_1 \cdot \sigma \cdot \left(T_{s1.t.ini} + T_{\infty 1}\right) \cdot \left(T_{s1.t.ini}^{\ 2} + T_{\infty 1}^{\ 2}\right) = 5.476 \ \frac{1}{m^2 \cdot K} \cdot W$$

[Radiation heat transfer coefficient on the outside] **{Eq 1.9}**[1]

4.3.3 Combined radiation and convection on the inside

$$h_{comb.out.t} := h_{conv.out.t} + h_{rad.out.t} = 6.317 \ \frac{kg}{s^3 \cdot K}$$

[2]

CALCULATION REPORT

PH/DT-EO
EDMS NUMBER: 1511711

4.4 Heat transfer on the inside

4.4.1 Convection on the inside

The inside of the "roof" of the box is considered as the lower surface of a hot plate, since it is definitely not colder than $T_{\infty 2}$.

$$\beta_{in.t} := \frac{1}{T_{f.in.t}} = 0.004 \ \frac{1}{K}$$

[Volumetric thermal expansion coefficient on the intside] {Eq 9.9}[1]

$$Ra_{in.t} := \frac{g \cdot \beta_{in.t} \cdot \left(T_{s4.t.ini} - T_{\infty 2}\right) \cdot \left(\max\left(L_h, L_w\right) - 2 \cdot l_{tot}\right)^3}{\nu_{in.t} \cdot \alpha_{in.t}} = 6.465 \cdot 10^9$$

[Rayleigh number on the inside] {Eq 9.25}[1]

$$Nu_{in.top} := 0.27 \cdot Ra_{in.t}^{\ 0.25} = 76.562$$

[Nusselt number on the inside] {Eq 9.32}[1]

$$h_{conv.in.t} := \frac{k_{in.t} \cdot Nu_{in.top}}{\max\left(L_h, L_w, L_l\right) - 2 \cdot l_{tot}} = 0.894 \ \frac{W}{m^2 \cdot K}$$

[Convection heat transfer coefficient on the inside] {Eq 9.24}[1]

4.4.2 Radiation on the inside

$$h_{rad.in.t} := \varepsilon_2 \cdot \sigma \cdot \left(T_{s4.t.ini} + T_{\infty 2}\right) \cdot \left(T_{s4.t.ini}^{\ 2} + T_{\infty 2}^{\ 2}\right) = 4.412 \ \frac{1}{m^2 \cdot K} \cdot W$$

[Radiation heat transfer coefficient on the inside] {Eq 1.9}[1]

4.4.3 Combined radiation and convection on the inside

$$h_{comb.in.t} := h_{conv.in.t} + h_{rad.in.t} = 5.307 \ \frac{kg}{s^3 \cdot K}$$

[2]

CALCULATION REPORT

PH/DT-EO
EDMS NUMBER: 1511711

4.5 Results at the top

[Thermal resistance over the "roof" of the box]
{Eq 3.6, 3.9, 3.13 & 3.19}[1]

$$R''_{tot.top} := \frac{1}{h_{comb.out.t}} + \frac{l_1}{k_1} + \frac{l_2}{k_2} + \frac{l_3}{k_3} + \frac{1}{h_{comb.in.t}} = 0.905\ \frac{s^3 \cdot K}{kg}$$

$$q''_{top} := \frac{(T_{\infty 1} - T_{\infty 2})}{R''_{tot.top}} = 27.625\ \frac{kg}{s^3}$$

[Heat flux through the "roof" of the box]
{Eq 3.19}[1]

$$q_{top} := q''_{top} \cdot L_w \cdot L_l = 24.708\ W$$

[Heat flow through the "roof" of the box]

$$T_{s1.top} := T_{\infty 1} - q''_{top} \cdot \left(\frac{1}{h_{comb.out.t}}\right) = 288.777\ K$$

$$T_{s2.top} := T_{s1.top} - \frac{q''_{top} \cdot l_1}{k_1} = 288.74\ K$$

$$T_{s3.top} := T_{s2.top} - \frac{q''_{top} \cdot l_2}{k_2} = 273.393\ K$$

$$T_{s4.top} := T_{s3.top} - \frac{q''_{top} \cdot l_3}{k_3} = 273.356\ K$$

[Temperatures of different surfaces/interfaces of the "roof"]
{Eq 1.2 & 1.3a}[1]

$$T_{inside.top} := T_{s4.top} - q''_{top} \cdot \left(\frac{1}{h_{comb.in.t}}\right) = 268.15\ K$$

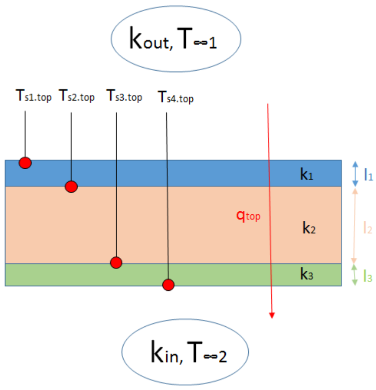

11

CALCULATION REPORT

PH/DT-EO
EDMS NUMBER: 1511711

5. Heat transfer through the bottom

5.1 Film temperatures on bottom

$T_{s1.b.ini} := 16.3\ °C$ [Estimated outer surface temperature]

$T_{s4.b.ini} := -0.85\ °C$ [Estimated inner surface temperature]

$$T_{f.out.b} := \frac{(T_{\infty 1} + T_{s1.b.ini})}{2} = 291.3\ K$$

$$T_{f.in.b} := \frac{(T_{\infty 2} + T_{s4.b.ini})}{2} = 270.225\ K$$

[Film temperatures at which the fluid properties should be evaluated] {Eq 7.2}[1]

5.2 Fluid properties

(Linearly interpolated from table A.4 [1] in Appendix 1.)

$$\nu_{out.b} := \left(\left(\frac{T_{f.out.b}}{K} - 250\right) \cdot \frac{(15.89 - 11.44)}{50} + 11.44\right) \cdot 10^{-6}\ \frac{m^2}{s} = \left(1.512 \cdot 10^{-5}\right)\ \frac{m^2}{s}$$

$$\nu_{in.b} := \left(\left(\frac{T_{f.in.b}}{K} - 250\right) \cdot \frac{(15.86 - 11.48)}{50} + 11.48\right) \cdot 10^{-6}\ \left(\frac{m^2}{s}\right) = \left(1.325 \cdot 10^{-5}\right)\ \frac{m^2}{s}$$

[kinematic viscosity of air on outside and nitrogen inside]

$$\alpha_{out.b} := \left(\left(\frac{T_{f.out.b}}{K} - 250\right) \cdot \frac{(22.5 - 15.9)}{50} + 15.9\right) \cdot 10^{-6}\ \left(\frac{m^2}{s}\right) = \left(2.135 \cdot 10^{-5}\right)\ \frac{m^2}{s}$$

$$\alpha_{in.b} := \left(\left(\frac{T_{f.in.b}}{K} - 250\right) \cdot \frac{(22.1 - 15.8)}{50} + 15.8\right) \cdot 10^{-6}\ \left(\frac{m^2}{s}\right) = \left(1.835 \cdot 10^{-5}\right)\ \frac{m^2}{s}$$

[thermal diffusivity of air on outside and nitrogen inside]

$$k_{out.b} := \left(\left(\left(\frac{T_{f.out.b}}{K} - 250\right) \cdot \frac{(26.3 - 22.3)}{50} + 22.3\right) \cdot 10^{-3}\right)\ \frac{W}{m \cdot K} = 0.026\ \frac{W}{m \cdot K}$$

$$k_{in.b} := \left(\left(\left(\frac{T_{f.in.b}}{K} - 250\right) \cdot \frac{(25.9 - 22.2)}{50} + 22.2\right) \cdot 10^{-3}\right)\ \frac{W}{m \cdot K} = 0.024\ \frac{W}{m \cdot K}$$

[thermal conductivity of air on outside and nitrogen inside]

CALCULATION REPORT

PH/DT-EO
EDMS NUMBER: 1511711

5.3. Heat transfer on the outside

5.3.1 Convection on the outside

The outside of the bottom plate of the box is considered as the lower surface of a cold plate, since it is definitely not warmer than surrounding temperature $T_{\infty 1}$.

$$\beta_{out.b} := \frac{1}{T_{f.out.b}} = 0.003 \ \frac{1}{K}$$

[Volumetric thermal expansion coefficient on the outside] {Eq 9.9}[1]

$$Ra_{out.b} := \frac{g \cdot \beta_{out.b} \cdot (T_{\infty 1} - T_{s1.b.ini}) \cdot \max(L_h, L_w)^3}{\nu_{out.b} \cdot \alpha_{out.b}} = 3.473 \cdot 10^9$$

[Rayleigh number on the outside] {Eq 9.25}[1]

$$Nu_{out.bot} := \begin{cases} \text{if } Ra_{out.b} < 10^7 \\ \quad 0.54 \cdot Ra_{out.b}^{0.25} \\ \text{else} \\ \quad 0.15 \cdot Ra_{out.b}^{\frac{1}{3}} \end{cases} = 227.159$$

[Nusselt number on the outside]

{Eq 9.30}[1]

{Eq 9.31}[1]

$$h_{conv.out.b} := \frac{k_{out.b} \cdot Nu_{out.bot}}{\max(L_h, L_w, L_l)} = 2.796 \ \frac{W}{m^2 \cdot K}$$

[Convection heat transfer coefficient on the outside] {Eq 9.24}[1]

5.3.2 Radiation on the outside

$$h_{rad.out.b} := \varepsilon_1 \cdot \sigma \cdot (T_{s1.b.ini} + T_{\infty 1}) \cdot \left(T_{s1.b.ini}^{\ 2} + T_{\infty 1}^{\ 2}\right) = 5.495 \ \frac{1}{m^2 \cdot K} \cdot W$$

[Radiation heat transfer coefficient on the outside]
{Eq 1.9}[1]

5.3.3 Combined radiation and convection on the inside

$$h_{comb.out.b} := h_{conv.out.b} + h_{rad.out.b} = 8.291 \ \frac{kg}{s^3 \cdot K}$$

[2]

CALCULATION REPORT

PH/DT-EO
EDMS NUMBER: 1511711

5.4. Heat transfer on the inside

5.4.1 Convection On the inside

The inside of the bottom plate of the box is considered as the upper surface of a hot plate, since it is definitely not colder than $T_{\infty 2}$.

$$\beta_{in.b} := \frac{1}{T_{f.out.b}} = 0.003 \ \frac{1}{K}$$

[Volumetric thermal expansion coefficient on the inside] {Eq 9.9}[1]

$$Ra_{in.b} := \frac{g \cdot \beta_{in.b} \cdot \left(T_{s4.b.ini} - T_{\infty 2}\right) \cdot \max\left(L_h, L_w\right)^3}{\nu_{in.b} \cdot \alpha_{in.b}} = 5.171 \cdot 10^9$$

[Rayleigh number on the inside] {Eq 9.25}[1]

$$Nu_{in.bot} := \begin{cases} \text{if } Ra_{in.b} < 10^7 \\ \quad 0.54 \cdot Ra_{in.b}^{0.25} \\ \text{else} \\ \quad 0.15 \cdot Ra_{in.b}^{\frac{1}{3}} \end{cases} = 259.383$$

[Nusselt number on the inside]

{Eq 9.30}[1]

{Eq 9.31}[1]

$$h_{conv.in.b} := \frac{k_{in.b} \cdot Nu_{in.bot}}{\max\left(L_h, L_w, L_l\right) - 2 \cdot l_{tot}} = 3.025 \ \frac{W}{m^2 \cdot K}$$

[Convection heat transfer coefficient on the inside] {Eq 9.24}[1]

5.4.2 Radiation on the inside

$$h_{rad.in.b} := \varepsilon_2 \cdot \sigma \cdot \left(T_{s4.b.ini} + T_{\infty 2}\right) \cdot \left(T_{s4.b.ini}^{\ 2} + T_{\infty 2}^{\ 2}\right) = 4.386 \ \frac{1}{m^2 \cdot K} \cdot W$$

[Radiation heat transfer coefficient on the inside] {Eq 1.9}[1]

5.4.3 Combined radiation and convection on the inside

$$h_{comb.in.b} := h_{conv.in.b} + h_{rad.in.b} = 7.411 \ \frac{kg}{s^3 \cdot K}$$

[2]

14

CALCULATION REPORT

PH/DT-EO
EDMS NUMBER: 1511711

5.5 Results at bottom

$$R''_{tot.bot} := \frac{1}{h_{comb.out.b}} + \frac{l_1}{k_1} + \frac{l_2}{k_2} + \frac{l_3}{k_3} + \frac{1}{h_{comb.in.b}} = 0.814 \; \frac{s^3 \cdot K}{kg}$$

[Thermal resistance over the bottom of the box] {Eq 3.6, 3.9, 3.13 & 3.19}[1]

$$q''_{bot} := \frac{(T_{\infty 1} - T_{\infty 2})}{R''_{tot.bot}} = 30.721 \; \frac{kg}{s^3}$$

[Heat flux through the bottom of the box] {Eq 3.19}[1]

$$q_{bot} := q''_{bot} \cdot L_w \cdot L_l = 27.477 \; W$$

[Heat flow through the bottom of the box]

$$T_{s1.bot} := T_{\infty 1} - q''_{bot} \cdot \left(\frac{1}{h_{comb.out.b}}\right) = 289.445 \; K$$

$$T_{s2.bot} := T_{s1.bot} - \frac{q''_{bot} \cdot l_1}{k_1} = 289.404 \; K$$

$$T_{s3.bot} := T_{s2.bot} - \frac{q''_{bot} \cdot l_2}{k_2} = 272.336 \; K$$

$$T_{s4.bot} := T_{s3.bot} - \frac{q''_{bot} \cdot l_3}{k_3} = 272.295 \; K$$

$$T_{inside.bot} := T_{s4.bot} - q''_{bot} \cdot \left(\frac{1}{h_{comb.in.b}}\right) = 268.15 \; K$$

[Temperatures on different surfaces/interfaces of the bottom] {Eq 1.2 & 1.3a}[1]

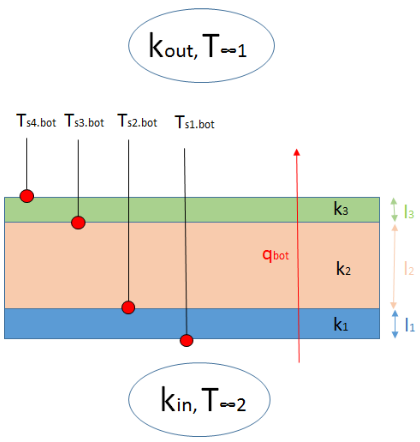

CALCULATION REPORT

PH/DT-EO
EDMS NUMBER: 1511711

6. Result summary

$q_v = 266.62\ W$ [Heat flow through the vertical walls of the box]
$q_{top} = 24.708\ W$ [Heat flow through the top of the box]
$q_{bot} = 27.477\ W$ [Heat flow through the bottom of the box]

[Total heat flow through the box]

$q_{tot} := q_v + q_{top} + q_{bot} = 318.805\ W$

[Temperatures on surfaces in contact with fluids.]

$T_{s1.v} = 15.697\ °C$ $T_{s1.top} = 15.627\ °C$ $T_{s1.bot} = 16.295\ °C$

$T_{s4.v} = 0.092\ °C$ $T_{s4.top} = 0.206\ °C$ $T_{s4.bot} = -0.855\ °C$

[Convection coefficients]

$h_{conv.out.v} = 1.018\ \frac{1}{m^2 \cdot K} \cdot W$ $h_{conv.out.t} = 0.841\ \frac{1}{m^2 \cdot K} \cdot W$ $h_{conv.out.b} = 2.796\ \frac{1}{m^2 \cdot K} \cdot W$

$h_{conv.in.v} = 1.08\ \frac{1}{m^2 \cdot K} \cdot W$ $h_{conv.in.t} = 0.894\ \frac{1}{m^2 \cdot K} \cdot W$ $h_{conv.in.b} = 3.025\ \frac{1}{m^2 \cdot K} \cdot W$

[Temperatures of inner and outer surfaces]

$T_{s4.v} = 0.092\ °C$ $T_{s4.top} = 0.206\ °C$ $T_{s4.bot} = -0.855\ °C$

$T_{s1.v} = 15.697\ °C$ $T_{s1.top} = 15.627\ °C$ $T_{s1.bot} = 16.295\ °C$

[Temperatures on the outermost surfaces. Compare to initial guess, and update T_{s1} and T_{s4} -assumptions if the difference is large]

$T_{s1.v} = 288.847\ K$
$T_{s1.v.ini} = 288.85\ K$
$\Delta T := T_{s1.v} - T_{s1.v.ini} = -0.003\ K$

$T_{s4.v} = 273.242\ K$
$T_{s4.v.ini} = 273.25\ K$
$\Delta T := T_{s4.v} - T_{s4.v.ini} = -0.008\ K$

$T_{s1.top} = 288.777\ K$
$T_{s1.t.ini} = 288.78\ K$
$\Delta T := T_{s1.top} - T_{s1.t.ini} = -0.003\ K$

$T_{s4.top} = 273.356\ K$
$T_{s4.t.ini} = 273.36\ K$
$\Delta T := T_{s4.top} - T_{s4.t.ini} = -0.004\ K$

$T_{s1.bot} = 289.445\ K$
$T_{s1.b.ini} = 289.45\ K$
$\Delta T := T_{s1.bot} - T_{s1.b.ini} = -0.005\ K$

$T_{s4.bot} = 272.295\ K$
$T_{s4.b.ini} = 272.3\ K$
$\Delta T := T_{s4.bot} - T_{s4.b.ini} = -0.005\ K$

7. References

[1] Fundamentals of heat and mass transfer, 6th Edition
Written by: *Theodore L. Bergman,*
Adrienne S. Lavine,
Frank P. Incropera,
David P. Dewitt.

[2] http://shop.iccsafe.org/media/wysiwyg/material/8950P203-sample.pdf
(14:29, 04/12/2015)

8. Appendices

8.1 Table A.4 (air and nitrogen properties) [1]

TABLE A.4 Thermophysical Properties of Gases at Atmospheric Pressure[a]

T (K)	ρ (kg/m^3)	c_p (kJ/kg · K)	$\mu \cdot 10^7$ (N · s/m^2)	$\nu \cdot 10^6$ (m^2/s)	$k \cdot 10^3$ (W/m · K)	$\alpha \cdot 10^6$ (m^2/s)	Pr
Air							
100	3.5562	1.032	71.1	2.00	9.34	2.54	0.786
150	2.3364	1.012	103.4	4.426	13.8	5.84	0.758
200	1.7458	1.007	132.5	7.590	18.1	10.3	0.737
250	1.3947	1.006	159.6	11.44	22.3	15.9	0.720
300	1.1614	1.007	184.6	15.89	26.3	22.5	0.707
350	0.9950	1.009	208.2	20.92	30.0	29.9	0.700
400	0.8711	1.014	230.1	26.41	33.8	38.3	0.690
450	0.7740	1.021	250.7	32.39	37.3	47.2	0.686
500	0.6964	1.030	270.1	38.79	40.7	56.7	0.684
550	0.6329	1.040	288.4	45.57	43.9	66.7	0.683
Nitrogen (N_2)							
100	3.4388	1.070	68.8	2.00	9.58	2.60	0.768
150	2.2594	1.050	100.6	4.45	13.9	5.86	0.759
200	1.6883	1.043	129.2	7.65	18.3	10.4	0.736
250	1.3488	1.042	154.9	11.48	22.2	15.8	0.727
300	1.1233	1.041	178.2	15.86	25.9	22.1	0.716
350	0.9625	1.042	200.0	20.78	29.3	29.2	0.711
400	0.8425	1.045	220.4	26.16	32.7	37.1	0.704
450	0.7485	1.050	239.6	32.01	35.8	45.6	0.703
500	0.6739	1.056	257.7	38.24	38.9	54.7	0.700
550	0.6124	1.065	274.7	44.86	41.7	63.9	0.702

CALCULATION REPORT

PH/DT-EO
EDMS NUMBER: 1511711

8.2 Equations used [1]

$$q''_x = k\frac{T_1 - T_2}{L} = k\frac{\Delta T}{L} \qquad (1.2)$$

$$q_x = q''_x \cdot A.$$

$$q'' = h(T_s - T_\infty) \qquad (1.3a)$$

$$h_r \equiv \varepsilon\sigma(T_s + T_{\text{sur}})(T_s^2 + T_{\text{sur}}^2) \qquad (1.9)$$

$$R_{t,\text{cond}} \equiv \frac{T_{s,1} - T_{s,2}}{q_x} = \frac{L}{kA} \qquad (3.6)$$

$$R_{t,\text{conv}} \equiv \frac{T_s - T_\infty}{q} = \frac{1}{hA} \qquad (3.9)$$

$$R_{t,\text{rad}} = \frac{T_s - T_{\text{sur}}}{q_{\text{rad}}} = \frac{1}{h_r A} \qquad (3.13)$$

$$R_{\text{tot}} = \sum R_t = \frac{\Delta T}{q} = \frac{1}{UA} \qquad (3.19)$$

$$T_f \equiv \frac{T_s + T_\infty}{2} \qquad (7.2)$$

$$\beta = -\frac{1}{\rho}\left(\frac{\partial\rho}{\partial T}\right)_p = \frac{1}{\rho}\frac{p}{RT^2} = \frac{1}{T} \qquad (9.9)$$

$$\overline{Nu}_L = \frac{\overline{h}L}{k} = C\,Ra_L^n \qquad (9.24)$$

$$Ra_L = Gr_L\,Pr = \frac{g\beta(T_s - T_\infty)L^3}{\nu\alpha} \qquad (9.25)$$

$$\overline{Nu}_L = \left\{0.825 + \frac{0.387\,Ra_L^{1/6}}{[1 + (0.492/Pr)^{9/16}]^{8/27}}\right\}^2 \qquad (9.26)$$

$$\overline{Nu}_L = 0.68 + \frac{0.670\,Ra_L^{1/4}}{[1 + (0.492/Pr)^{9/16}]^{4/9}} \qquad Ra_L \lesssim 10^9 \qquad (9.27)$$

Upper Surface of Hot Plate or Lower Surface of Cold Plate:

$$\overline{Nu}_L = 0.54\,Ra_L^{1/4} \quad (10^4 \lesssim Ra_L \lesssim 10^7) \qquad (9.30)$$

$$\overline{Nu}_L = 0.15\,Ra_L^{1/3} \quad (10^7 \lesssim Ra_L \lesssim 10^{11}) \qquad (9.31)$$

Lower Surface of Hot Plate or Upper Surface of Cold Plate:

$$\overline{Nu}_L = 0.27\,Ra_L^{1/4} \quad (10^5 \lesssim Ra_L \lesssim 10^{10}) \qquad (9.32)$$

B : Cavity convection analysis

CALCULATION REPORT

PH/DT-EO
EDMS NUMBER: 1541706

Prepared by: Kurt Oskar Edvin Martensson

Checked by: Joao Carlos Batista Lopes

Purpose: to check if convection can be neglected in an air volume enclosed by two parallell plates of different temperatures.

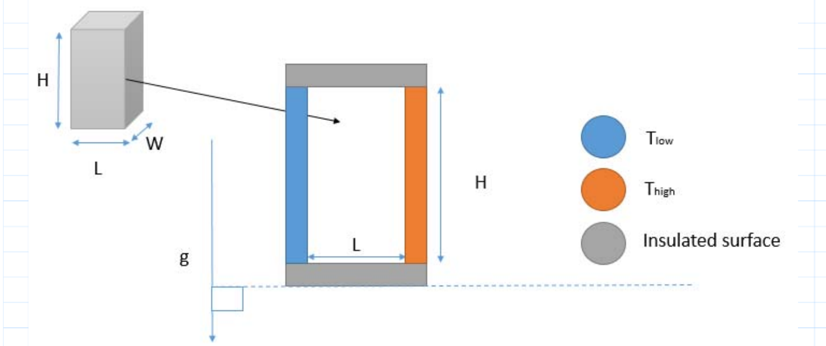

Assumptions made:

- Air inside.
- Atmospheric pressure.
- 250K< T_{high} , T_{low} <353.15K
- $1 < \frac{H}{L} < 10$
- $1 < \frac{w}{L}$

$T_{high} := 293.15\ K$

$T_{low} := 268.15\ K$

$L := 0.01\ m$

$g = 9.807\ \frac{m}{s^2}$

$T_f := \frac{(T_{low} + T_{high})}{2\ K} = 280.65$ [Film temperature]

Non-Commercial Use Only

CALCULATION REPORT

PH/DT-EO
EDMS NUMBER: 1541706

Linearly interpolated air properties.

$$\beta := \text{if } T_f < 273.15 \quad \left\| \left(4.51 - \frac{(4.51-3.67)}{50} \cdot (T_f - 223.15)\right) \cdot 10^{-3} \frac{1}{K} \right.$$
$$\text{else if } T_f < 293.15 \quad \left\| \left(3.67 - \frac{(3.67-3.43)}{20} \cdot (T_f - 273.15)\right) \cdot 10^{-3} \frac{1}{K} \right.$$
$$\text{else if } T_f < 313.15 \quad \left\| \left(3.43 - \frac{(3.43-3.2)}{20} \cdot (T_f - 293.15)\right) \cdot 10^{-3} \frac{1}{K} \right.$$
$$\text{else if } T_f < 333.15 \quad \left\| \left(3.2 - \frac{(3.2-3.0)}{20} \cdot (T_f - 313.15)\right) \cdot 10^{-3} \frac{1}{K} \right.$$
$$\text{else} \quad \left\| \left(3 - \frac{(3-2.83)}{20} \cdot (T_f - 333.15)\right) \cdot 10^{-3} \frac{1}{K} \right.$$
$$= 0.004 \ \frac{1}{K}$$

[Thermal expansion coefficient for air, from Table 1.]

$$\nu := \text{if } T_f < 300 \quad \left\| \left(11.44 + \frac{(15.89-11.44)}{50} \cdot (T_f - 250)\right) \cdot 10^{-6} \frac{m^2}{s} \right.$$
$$\text{else} \quad \left\| \left(15.89 + \frac{(20.92-15.89)}{50} \cdot (T_f - 300)\right) \cdot 10^{-6} \frac{m^2}{s} \right.$$
$$= \left(1.417 \cdot 10^{-5}\right) \frac{m^2}{s}$$

[Kinematic viscosity for air, from Table 2.]

$$\alpha := \text{if } T_f < 300 \quad \left\| \left(15.9 + \frac{(22.5-15.9)}{50} \cdot (T_f - 250)\right) \cdot 10^{-6} \frac{m^2}{s} \right.$$
$$\text{else} \quad \left\| \left(22.5 + \frac{(29.9-22.5)}{50} \cdot (T_f - 300)\right) \cdot 10^{-6} \frac{m^2}{s} \right.$$
$$= \left(1.995 \cdot 10^{-5}\right) \frac{m^2}{s}$$

[Thermal diffusivity for air, from Table 2.]

CALCULATION REPORT

PH/DT-EO
EDMS NUMBER: 1541706

If $Ra_L \le 10^3$, then free convection can be neglected and the air can instead be treated as a solid with the thermal conduction coefficient given below.

$$Ra_L := g \cdot \beta \cdot (T_{high} - T_{low}) \cdot \frac{L^3}{\nu \cdot \alpha} = 3.106 \cdot 10^3$$

[Rayleigh number.]

$$k := \text{if } T_f < 300 \; \left\| \left(22.3 + \frac{(26.3-22.3)}{50} \cdot (T_f - 250)\right) \cdot 10^{-3} \frac{W}{m \cdot K} \right. \; \text{else} \; \left\| \left(26.3 + \frac{(30-26.3)}{50} \cdot (T_f - 300)\right) \cdot 10^{-3} \frac{W}{m \cdot K} \right. = 0.025 \frac{kg \cdot m}{s^3 \cdot K}$$

[Thermal conduction coefficient for the eclosed air.]

$$L_{MAX} := \left(\frac{\nu \cdot \alpha \cdot 10^3}{(g \cdot \beta \cdot (T_{high} - T_{low}))}\right)^{\frac{1}{3}} = 6.854 \; mm$$

[Largest L that can be used if one desire to consider the air solid, given the temperatures of the walls.]

CALCULATION REPORT

PH/DT-EO
EDMS NUMBER: 1541706

Table 1. [1], page 941.

T (K)	ρ (kg/m^3)	c_p (kJ/kg · K)	$\mu \cdot 10^7$ (N · s/m^2)	$\nu \cdot 10^6$ (m^2/s)	$k \cdot 10^3$ (W/m · K)	$\alpha \cdot 10^6$ (m^2/s)	Pr
Air							
100	3.5562	1.032	71.1	2.00	9.34	2.54	0.786
150	2.3364	1.012	103.4	4.426	13.8	5.84	0.758
200	1.7458	1.007	132.5	7.590	18.1	10.3	0.737
250	1.3947	1.006	159.6	11.44	22.3	15.9	0.720
300	1.1614	1.007	184.6	15.89	26.3	22.5	0.707
350	0.9950	1.009	208.2	20.92	30.0	29.9	0.700

Table 2. [2], time: 15:10, Sep 8th-2015

Temperature - t - (^{o}C)	Density - ρ - (kg/m^3)	Specific Heat - c_p - (kJ/(kg K))	Thermal Conductivity - k - (W/(m K))	Kinematic Viscosity - ν - x 10^{-6} (m^2/s)	Expansion Coefficient - b - x 10^{-3} (1/K)	Prandtl's Number - P_r -
-150	2.793	1.026	0.0116	3.08	8.21	0.76
-100	1.980	1.009	0.0160	5.95	5.82	0.74
-50	1.534	1.005	0.0204	9.55	4.51	0.725
0	1.293	1.005	0.0243	13.30	3.67	0.715
20	1.205	1.005	0.0257	15.11	3.43	0.713
40	1.127	1.005	0.0271	16.97	3.20	0.711
60	1.067	1.009	0.0285	18.90	3.00	0.709
80	1.000	1.009	0.0299	20.94	2.83	0.708
100	0.946	1.009	0.0314	23.06	2.68	0.703
120	0.898	1.013	0.0328	25.23	2.55	0.70
140	0.854	1.013	0.0343	27.55	2.43	0.695
160	0.815	1.017	0.0358	29.85	2.32	0.69
180	0.779	1.022	0.0372	32.29	2.21	0.69
200	0.746	1.026	0.0386	34.63	2.11	0.685
250	0.675	1.034	0.0421	41.17	1.91	0.68
300	0.616	1.047	0.0454	47.85	1.75	0.68
350	0.566	1.055	0.0485	55.05	1.61	0.68
400	0.524	1.068	0.0515	62.53	1.49	0.68

References:

[1] Funamentals of heat and mass transfer, 6th Edition
Written by: *Theodore L. Bergman,*
Adrienne S. Lavine,
Frank P. Incropera,
David P. Dewitt.

[2] http://www.engineeringtoolbox.com/air-properties-d_156.html
Time: 15:10, 08/9/2015

C : Heat transfer comparison between two vertical plates

CALCULATION REPORT

PH/DT-EO
EDMS NUMBER: 1555107

Prepared by: **Kurt Oskar Edvin Martensson**

Purpose: to compare magnitudes of heat transfer through radiation, conduction and through natural convection, between two equal parallel plates with air in between. This tool is applicable in the temperature range 250K-350K.

$T_{hot} := 283.376\ K$ [Temperature of plate]

$T_{cold} := 279.2173\ K$ [Temperature of surrounding]

$H := 0.04\ m$ [Height of plate]

$S := 0.014\ m$ [Distance between plates]

$a := 0.95$ [Absorptivity of plate]

$\varepsilon := 0.95$ [Emissivity of plate]

$\sigma = \left(5.67 \cdot 10^{-8}\right) \dfrac{kg}{s^3 \cdot K^4}$ [Boltzmann constant]

$T_f := \dfrac{\left(T_{hot} + T_{cold}\right)}{2\ K} = 281.297$ [Film temperature]

$C_1 := 576$

$C_2 := 2.87$

[Constants from Table 4]

CALCULATION REPORT

PH/DT-EO
EDMS NUMBER: 1555107

Linearly interpolated air properties.

$$\beta := \begin{cases} \left(4.51 - \frac{(4.51-3.67)}{50} \cdot (T_f - 223.15)\right) \cdot 10^{-3} \frac{1}{K} & \text{if } T_f < 273.15 \\ \left(3.67 - \frac{(3.67-3.43)}{20} \cdot (T_f - 273.15)\right) \cdot 10^{-3} \frac{1}{K} & \text{else if } T_f < 293.15 \\ \left(3.43 - \frac{(3.43-3.2)}{20} \cdot (T_f - 293.15)\right) \cdot 10^{-3} \frac{1}{K} & \text{else if } T_f < 313.15 \\ \left(3.2 - \frac{(3.2-3.0)}{20} \cdot (T_f - 313.15)\right) \cdot 10^{-3} \frac{1}{K} & \text{else if } T_f < 333.15 \\ \left(3 - \frac{(3-2.83)}{20} \cdot (T_f - 333.15)\right) \cdot 10^{-3} \frac{1}{K} & \text{else} \end{cases} = 0.004 \frac{1}{K}$$

[Thermal expansion coefficient for air, from Table 2.]

$$\nu := \begin{cases} \left(11.44 + \frac{(15.89-11.44)}{50} \cdot (T_f - 250)\right) \cdot 10^{-6} \frac{m^2}{s} & \text{if } T_f < 300 \\ \left(15.89 + \frac{(20.92-15.89)}{50} \cdot (T_f - 300)\right) \cdot 10^{-6} \frac{m^2}{s} & \text{else} \end{cases} = \left(1.423 \cdot 10^{-5}\right) \frac{m^2}{s}$$

[Kinematic viscosity for air, from Table 1.]

$$\alpha := \begin{cases} \left(15.9 + \frac{(22.5-15.9)}{50} \cdot (T_f - 250)\right) \cdot 10^{-6} \frac{m^2}{s} & \text{if } T_f < 300 \\ \left(22.5 + \frac{(29.9-22.5)}{50} \cdot (T_f - 300)\right) \cdot 10^{-6} \frac{m^2}{s} & \text{else} \end{cases} = \left(2.003 \cdot 10^{-5}\right) \frac{m^2}{s}$$

[Thermal diffusivity for air, from Table 1.]

CALCULATION REPORT

PH/DT-EO
EDMS NUMBER: 1555107

$$k := \text{if } T_f < 300 \; \left\| \left(22.3 + \frac{(26.3-22.3)}{50} \cdot (T_f - 250)\right) \cdot 10^{-3} \frac{W}{m \cdot K} \right. \; \text{else} \; \left\| \left(26.3 + \frac{(30-26.3)}{50} \cdot (T_f - 300)\right) \cdot 10^{-3} \frac{W}{m \cdot K} \right. = 0.025 \frac{W}{m \cdot K}$$

[Thermal conductivity for air, from Table 1.]

Natural convection.

$$Ra_S := g \cdot \beta \cdot (T_{hot} - T_{cold}) \cdot \frac{S^3}{\nu \cdot \alpha} = 1.403 \cdot 10^3$$

[Rayleigh number.]
{Eq 9.38}[1]

$$Pr := \frac{\nu}{\alpha} = 0.71$$

[Prandtl number.]

$$Nu_H := \left(\frac{C_1}{\left(S \cdot \frac{Ra_S}{H}\right)^2} + \frac{C_2}{\left(S \cdot \frac{Ra_S}{H}\right)^{\frac{1}{2}}} \right)^{\frac{-1}{2}} = 2.753$$

[Nusselt number]
{Eq 9.45}[1]

$$h := \frac{k \cdot Nu_H}{H} = 1.707 \frac{W}{m^2 \cdot K}$$

[Convection heat transfer coefficient on the inside]
{Eq 9.24}[1]

$$q''_{conv} := (T_{hot} - T_{cold}) \cdot h = 7.1 \frac{W}{m^2}$$

{Eq 1.3a}[1]
[Net heat flux through convection]

CALCULATION REPORT

PH/DT-EO
EDMS NUMBER: 1555107

Radiation.

$$q''_{emiss} := \varepsilon \cdot \sigma \cdot \left| \left(T_{hot}^{\ 4} - T_{cold}^{\ 4} \right) \right| = 19.947 \ \frac{W}{m^2}$$

[Power emitted]
{Eq 1.7}[1]

$$F := \frac{\left(\left(4 \cdot \left(\frac{H}{S} \right)^2 + 4 \right)^{\frac{1}{2}} - 2 \right)}{2 \cdot \left(\frac{H}{S} \right)} = 0.709$$

[View factor]
{Table 13.1}[1]

$$F := 1$$

[View factor set to 1 in case of enclosed cavity]

$$G := q''_{emiss} \cdot F = 19.947 \ \frac{W}{m^2}$$

[Radiative power from each plate that reaches the other one]

$$q''_{rad} := q''_{emiss} - a \cdot G = 0.997 \ \frac{W}{m^2}$$

{Eq 1.7}[1]
[Net heat flux through radiation]

Conduction.

$$q''_{cond} := \frac{\left(T_{hot} - T_{cold} \right) \cdot k}{S} = 7.368 \ \frac{W}{m^2}$$

Result.

$$q''_{tot} := q''_{cond} + q''_{conv} + q''_{rad} = 15.466 \ \frac{W}{m^2}$$

$$q_{rad} := \frac{q''_{rad}}{q''_{tot}} = 0.064$$

$$q_{conv} := \frac{q''_{conv}}{q''_{tot}} = 0.459$$

$$q_{cond} := \frac{q''_{cond}}{q''_{tot}} = 0.476$$

CALCULATION REPORT

PH/DT-EO
EDMS NUMBER: 1555107

References.

[1] Funamentals of heat and mass transfer, 6th Edition
Written by: Theodore L. Bergman,
Adrienne S. Lavine,
Frank P. Incropera,
David P. Dewitt.

[2] http://www.engineeringtoolbox.com/air-properties-d_156.html
Time: 15:10, 08/9/2015

Tables.

Table 1. [1], page 941.

T (K)	ρ (kg/m^3)	c_p (kJ/kg·K)	$\mu \cdot 10^7$ (N·s/m^2)	$\nu \cdot 10^6$ (m^2/s)	$k \cdot 10^3$ (W/m·K)	$\alpha \cdot 10^6$ (m^2/s)	Pr
Air							
100	3.5562	1.032	71.1	2.00	9.34	2.54	0.786
150	2.3364	1.012	103.4	4.426	13.8	5.84	0.758
200	1.7458	1.007	132.5	7.590	18.1	10.3	0.737
250	1.3947	1.006	159.6	11.44	22.3	15.9	0.720
300	1.1614	1.007	184.6	15.89	26.3	22.5	0.707
350	0.9950	1.009	208.2	20.92	30.0	29.9	0.700

Table 2. [2], time: 15:10, Sep 8th-2015

Temperature - t - (^oC)	Density - ρ - (kg/m^3)	Specific Heat - c_p - (kJ/(kg K))	Thermal Conductivity - k - (W/(m K))	Kinematic Viscosity - ν - x 10^{-6} (m^2/s)	Expansion Coefficient - b - x 10^{-3} (1/K)	Prandtl's Number - P_r -
-150	2.793	1.026	0.0116	3.08	8.21	0.76
-100	1.980	1.009	0.0160	5.95	5.82	0.74
-50	1.534	1.005	0.0204	9.55	4.51	0.725
0	1.293	1.005	0.0243	13.30	3.67	0.715
20	1.205	1.005	0.0257	15.11	3.43	0.713
40	1.127	1.005	0.0271	16.97	3.20	0.711
60	1.067	1.009	0.0285	18.90	3.00	0.709
80	1.000	1.009	0.0299	20.94	2.83	0.708
100	0.946	1.009	0.0314	23.06	2.68	0.703
120	0.898	1.013	0.0328	25.23	2.55	0.70
140	0.854	1.013	0.0343	27.55	2.43	0.695
160	0.815	1.017	0.0358	29.85	2.32	0.69
180	0.779	1.022	0.0372	32.29	2.21	0.69
200	0.746	1.026	0.0386	34.63	2.11	0.685
250	0.675	1.034	0.0421	41.17	1.91	0.68
300	0.616	1.047	0.0454	47.85	1.75	0.68
350	0.566	1.055	0.0485	55.05	1.61	0.68
400	0.524	1.068	0.0515	62.53	1.49	0.68

Table 3. [1], page 815.

CALCULATION REPORT

PH/DT-EO
EDMS NUMBER: 1555107

TABLE 13.1 View Factors for Two-Dimensional Geometries [4]

Geometry	Relation
Parallel Plates with Midlines Connected by Perpendicular	$F_{ij} = \dfrac{[(W_i + W_j)^2 + 4]^{1/2} - [(W_j - W_i)^2 + 4]^{1/2}}{2W_i}$ $W_i = w_i/L,\ W_j = w_j/L$

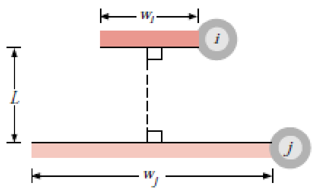

Table 5. [1], page 586.

TABLE 9.3 Heat transfer parameters for free convection between vertical parallel plates

Surface Condition	C_1	C_2	S_{opt}	S_{max}/S_{opt}
Symmetric isothermal plates ($T_{s,1} = T_{s,2}$)	576	2.87	$2.71(Ra_S/S^3L)^{-1/4}$	1.71
Symmetric isoflux plates ($q''_{s,1} = q''_{s,2}$)	48	2.51	$2.12(Ra^*_S/S^4L)^{-1/5}$	4.77
Isothermal/adiabatic plates ($T_{s,1}, q''_{s,2} = 0$)	144	2.87	$2.15(Ra_S/S^3L)^{-1/4}$	1.71
Isoflux/adiabatic plates ($q''_{s,1}, q''_{s,2} = 0$)	24	2.51	$1.69(Ra^*_S/S^4L)^{-1/5}$	4.77

D : Composite manufacturing report

1. INTRODUCTION

The new Upstream tracker (UT) detector in LHCb need to be insulated from the surrounding in terms of both heat, gas, light and other kinds of electromagnetic radiation. To ensure this, the UT is placed in an insulating box. This report presents the method and the specifications required to reproduce the composite parts that the UT-box will be made out of.

2. THE SANDWICH PANEL

2.1 CONSTRUCTION WITH PREPREG PLATES.

Pre-impregnated carbon fibre (also called prepreg) often comes as a roll of carbon fibre weave that is pre-impregnated with resin and then packed between two layers of a protective film so that it won't stick to itselft while rolled up. Usually those rolls needs to be stored at cold temperatures in order to keep the resin, and thereby the carbon fibre weave, soft. This particular prepreg has to be stored at -18°C.

The first step is to draw out the countours of the parts that should be produced, on the protective film of the prepreg. The cutting should be made with a cutter as sharp as possible, to minimize the risk of ugly edges on the weave.

To maximize the strength of the final product, it is preferable to have more than 2 orientations on the carbon fibres, since the carbon fibres strength is greater in the direction along the length of the fibre than in any other direction. Here two 300x200mm plates are made, with the following angular configuration;

[-45°;0°;45°;Cu;0°]

[-45°;0°;45°;0°]

Where 0° is the direction in which the fibres of the last carbon weave directed. The other numbers states the angle of each weave relative to the last one. The semicolon designates a new layer. The Cu-layer is a layer consisting of a copper net (Dexmet 2CU6-100FA) which will be the layer that will act as a Faraday cage once the box is ready. The cut out countors for this is shown in *Figure 1A* and the copper net can be seen in *Figure 6*. After the weave is cut, it is time to peel off the protective film, as shown in *Figure 1B.* When putting the sheets of weave together to the desired shape, start with only peeling of one of the protective sheets. Put the sheet were it should be attached and then peel of the second protective film. These layers of prepreg are put directly on a foam core as illustrated in *Figure 2.*

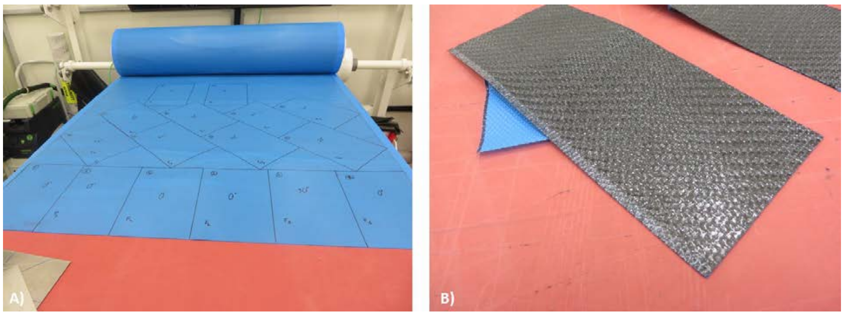

Figure 1: The roll of pre-impregnated carbon fiber weave, with cutting contours marked out (A) and a sheet of carbon fibre weave with one protective polymer sheet peeled of (B).

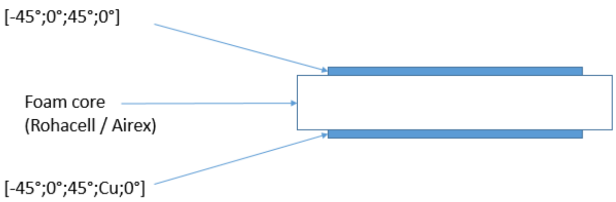

Figure 2: The composite sandwich.

For this panel Rohacell IG is used since it is cheaper than Airex, and the properties of Airex is not required for this particular study. After this, it is time to prepare for the cocuring of the sandwich. The vacuum configuration for the curing is shown in *Figure 3*. A breather material is used to create escape paths for the air and to absorb the excess of resin. A release film is put where there is risk for the resin to stick to something it is not supposed to stick to.

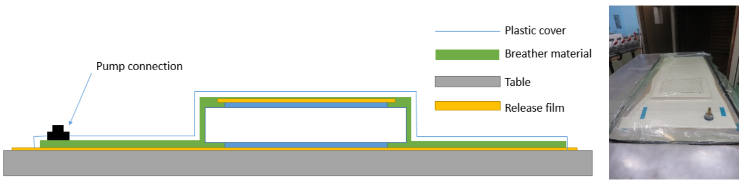

Figure 3: Foam core and carbon fiber panels set up for cocuring.

When the setup is ready it is sent into an oven to co-cure. The oven increases the temperature with a heating rate of 2°C/min until it reaches 120°C. The temperature stays at 120°C for two hours before it starts to cool down at a rate of 2°C/min until it reaches ambient temperature again. Since the oven contain a lot of heated air, the temperature will not have a change rate of -2°C/min at the lower temperatures where the natural heat exchange (between the oven ant its surroundings) implies a temperature change rate smaller than -2°C/min. Since the oven does not have a chiller, the temperature cannot be "forced" down. The curing cycle is shown in *Figure 4.* Ensure that all materials used as breather, release film and so on, can handle the temperature of the oven. When the sandwich has cured it is time to remove abundancies of the foam core. The uncut part can be seen in *Figure 5A,* and the final part in *Figure 5B.*

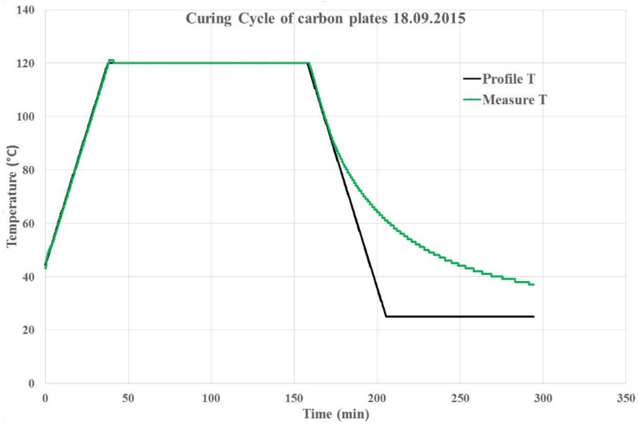

Figure 4: The curing cycle

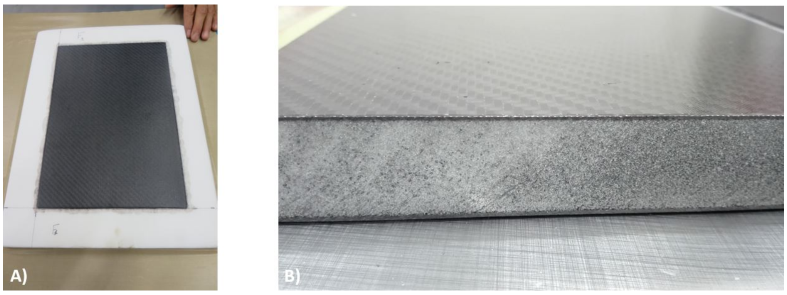

Figure 5: The cocured and uncut panel (A), and the finished panel (B).

The contact between the carbon plates and the Rohacell foam is very good. The resin from the prepreg have been absorbed by foam surface and there seems to be a very small risk for the carbon plates to come off from the foam core. The copper net is barely visible through the carbon, thus the outermost layer of carbon will probably have to be removed at the contact surfaces of the panel, in order for the copper nets to be able to connect to each other.

2.2 CONDUCTIVITY TEST

In order for the UT-box to works as a Faraday cage, all the panels copper net layers have to be connected to each other. In this part it is tested whether or not a sufficient good connection can be yielded by using joint pieces. I.e. if two panels of the box can be connected to each other through a third part that is not a panel. This is important to study due to contact surfaces impact on electric resistance.

The joint pieces will include a 90° angle since all panels are perpendicular to every panel that it is directly connected to. This joint piece is made of eight 80x190mm layers of prepreg (all layers aligned), and one layer of copper net. To get the 90° angle, those layers are all pressed around a square beam (with a release film on top and bottom) and sent into the oven for the same curing cycle as described in section 2.1. This process is shown in *Figure 6* and *Figure 7.*

Figure 6: Layers of carbon and copper attached to each other.

Figure 7: Applying pressure for shape.

Besides the joint piece, two plates illustrating the panels that should be connected, is produced. The two plates are made of 4 layers of prepreg, with the dimension 300x200mm, and one copper net. The angular config was the following;

[0° ; -45° ; 45° ; 0° ; Cu]

[-45 ; 0 ; 45 ; Cu ; 0]

The reason behind the different angular configurations was to be able to study whether the flatness of the plate is affected by this, or not (the conclusion was that there is no significant difference). When the pieces cure, the resin tends to be sucked up by the copper net and create an insulating layer of resin on top of the copper. This resin layer have to be removed in the areas where the plates and the joint piece should be in contact with each other, in order to get a proper connection. The resin layer at the top can be removed by gently polishing the area with sand paper. Be careful and do not polish too hard since this can cause the copper net to come off. The difference between the polished and unpolished surface can be seen in *Figure 8.* On each plate, 4cm is polished, as well as the whole joint piece.

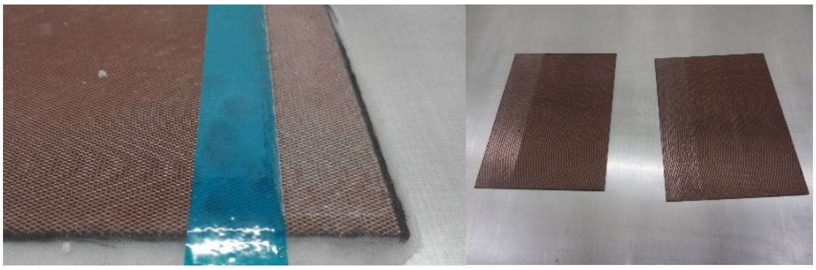

Figure 8: Polished contact areas.

When the contact areas are polished, they are put in contact with each other and fixed. The pieces were fixed by three M4-bolts, as shown in *Figure 9*, and the resistance were then measured as shown in *Figure 10*, with the difference the assembly was fixed by bolts and not wooden pieces. However, both fixation methods gave a resistance of 0.1Ω, which is good.

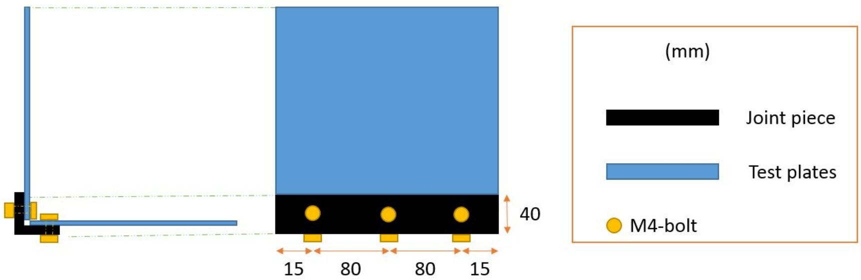

Figure 9: Sketch over the bolt fixed assembly.

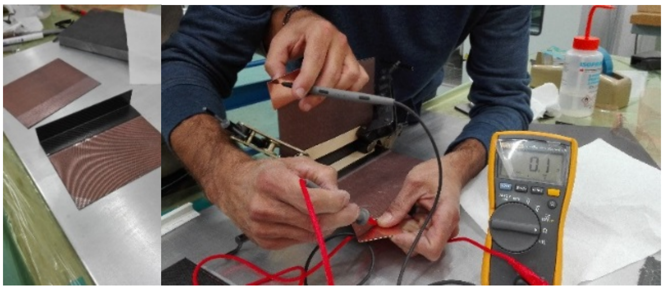

Figure 10: Resistance measurement over the three parts.

3. VACUUM RESIN INFUSION

Another way to make carbon fibre composite parts is to infuse the weave with resin by applying a pressure gradient over the weave. The setup for this is pretty similar to the setup described in *Figure* 3, but this setup also have an inlet connected to a resin reservoir. *Figure 11* shows an example where a flat panel is produced. More advanced shape can be produced by using the same method.

First of all, a Teflon sheet or any other release film should be used as a base, so that the part doesn't stick to the table. If you have a mould or such, which you want to shape the composite around, put this on the release film.

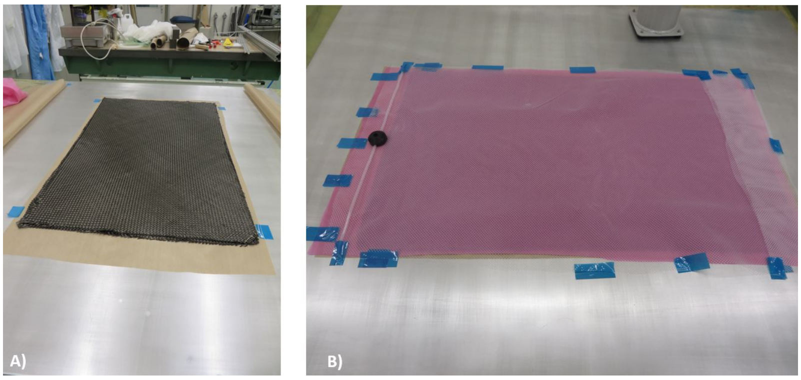

Figure 11: The "undressed" carbon fibre weave (A),

and the "dressed" carbon fibre weave (B).

After this it is time to "dress" the part in the carbon weave, a perforated peel ply and an infusion mesh, in that order. The undressed carbon fiber weave can be seen in *Figure 11A* and the dressed weave in *Figure 11B.*

Since this part is all flat, dressing this practically means to just put those layers on top. If the shape is more complex, it is important to have sufficient peel ply in places that is not along the shortest path between inlet and outlet. This will help the resin to get more evenly distributed.

After dressing the part, it is time to add an inlet and an outlet for the resin, and seal everything in a plastic bag. *Figure 12* shows a setup ready for infusion. One can also see in *Figure 12* that there is a perforated tube connected to both the inlet and the outlet. This is to apply a pressure gradient between the two edges, and not only between two points. This is done to ensure that the resin will spread all the way out to the corners.

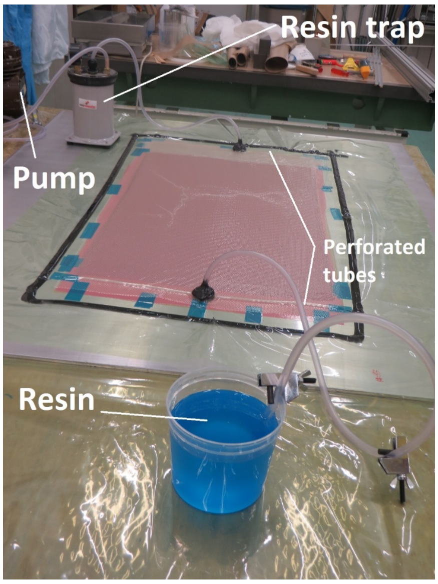

Figure 12: Setup ready for resin infusion.

A vacuum pump with a resin trap is then connected to the outlet, and a tube leading to a resin reservoir is connected to the inlet. This is shown in *Figure 12*. When the pump is started, the air inside the sealed volume will be extracted and thus creating an under pressure that will drag the resin from the inlet all the way to the outlet.

In *Figure 13A* you can see a picture taken during this process that shows the resin propagating towards the outlet edge. When the part is all covered in resin and all the air pockets are removed, it is time to seal the inlet ant the outlet. The part is then left in room temperature for about 24 hours to cure. When the composite have cured, remove all surrounding layers and the part is done. The cured part can be seen in *Figure 13B.*

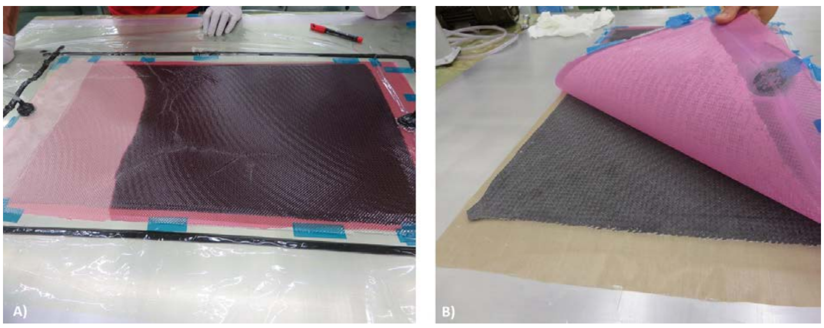

Figure 13: Resin being infused (A) and the finished part (B).

4. SUMMARY TABLE

Piece	Process used	Total curing time [h]	Curing max temperature [°C]	Flatness	Picture	Angular configuration.
Sandwich panel	Prepreg in vacuum bag	3.5	120	OK	5B	[-45° ; 0° ; 45° ; 0° ; Rohacell ; -45° ; 0° ; 45° ; Cu ; 0°]
Plate 1	Prepreg in vacuum bag	3.5	120	OK	8	[0° ; -45° ; 45° ; 0° ; Cu]
Plate 2	Prepreg in vacuum bag	3.5	120	OK	NA	[-45° ; 0° ; 45° ; Cu ; 0°]
Plate 3	Infusion in vacuum bag	24	25	OK	13B	[0° ; 45° ; 0° ; 45°]
Angle piece	Prepreg in mold	3.5	120	OK	6,7,10	[0° ; 0° ; 0° ; 0° ; 0° ; 0° ; 0° ; 0° ; Cu]

5. DATASHEET LINKS

Copper net: http://www.dexmet.com/1_pdf/Lightning%20Strike%20Brochure.pdf

Rohacell foam: http://www.rohacell.com/sites/lists/PP-HP/Documents/ROHACELL-IG-IG-F-mechanical-properties-EN.pdf

E : Polymer manufacturing report

1. INTRODUCTION

Creating a customized polymer part is not as straight forward as one might think. In this report the process behind is shown. The part created in this report is the polymer interface between the LHC beam pipe and the UT-box.

2. CREATING THE MOLD

First off, the shape that should be molded have to be etched in in some kind of solid. To make the extraction of the finished polymer part easier, it is very convenient to have a mold that you can easily split. The easiest way to do this depends on how complex the shape is. In this particular case, the shape is rather complex and thus we chosen to print two half molds with a high precision 3D-printer (Viper SI 2 3D system, with Accura 25 resin). Those 3D-printed parts can be seen in *Figure 1*.

Figure 1: The 3D-printed mold parts.

The first thing to do is to apply a release liquid (see section 5 for datasheet) on the mold parts so that the molded polymer part won't stick to the mold. This is easiest done with a soft brush. After it is made sure that all surfaces that will be in contact with the polymer, have been covered by release liquid, it is time to remove all abundant release liquid. Use regular drying paper and make sure that all abundant release liquid is removed, or else the polymer part will contain bubbles.

Figure 2: **Topmounted plastic tubes (A),**

The nozzle and the splice sealing silicone added (B).

Next step is to assembly the mold parts in to usable mold. The two halfs of the mold are attached to each other by bolts. External support plates (the grey plates in *Figure 2*) are used so that the mold won't buckle out in the middle where there is no bolt. There are two outlets on top of the mold and an inlet on the bottom. A nozzle is attached to the inlet and plastic tubes are attached to the outlet. This is shown in *Figure 2A* and *Figure 2B.* The plastic tubes will prevent polymer from spilling if the mold gets over filled. After this the the splices are sealed with silicone, so that the polymer won't pour out from the mold.

3. PREPARATION OF THE POLYMER

The polymer is mixed with the hardener and stirred properly.

The mixing relations vary with desired stiffness of the polymer. The polymer is then sent in to a pressure chamber. When the pressure around the polymer gets very low, the gas bounded to the polymer will start to expand and the polymer will start to bubble. When the bubbles bursts the expanded gas is released and then sucked out of the chamber. This procedure will reduce the risk of obtaining undesired gas bubbles in the final product. When the bubbling have stopped you can turn of the pressure chamber and then take out the polymer. The pressure chamber can be seen in *Figure 3A* and the bubbling polymer mix can be seen in *Figure 3B*.

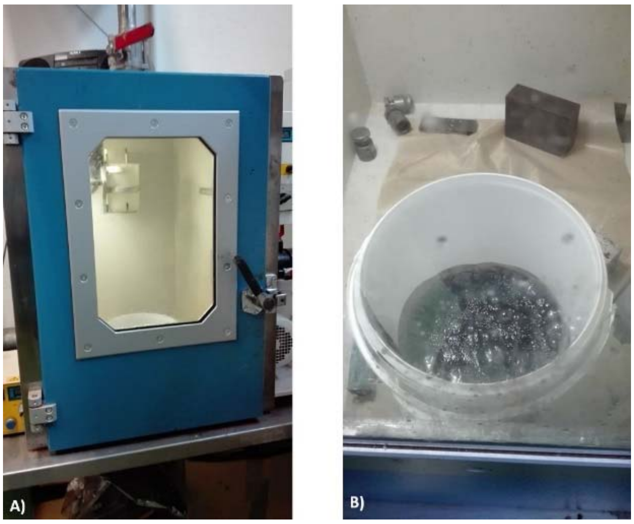

Figure 3: **The pressure chamber (A) and the bubbling polymer(B).**

4. FILLING THE MOLD WITH POLYMER

When the polymer mix is ready it is time fill the mold with it.

This is done by filling a syringe (*Figure 4A*) with the polymer. This syringe is driven by pressurized air that is pumped in through the endcap (*Figure 4B*). The air the pushes the polymer out of the syringe and in to the mold. When the mold is filled the polymer will come up through the outlets on the top and start to fill the plastic tubes. This can be seen in *Figure 5B*. *Figure* 5A shows the connection between the nozzle and the syringe. Stop the filling and let the polymer sink back in to the mold. Put in some more polymer and repeat this until the polymer in the plastic tubes stops to sink away. When the polymer does not sink, the mold should be completely filled. When the mold is filled it is time to seal the nozzle at the bottom so that the polymer stays in place. In *Figure 6* one way to do this is shown.

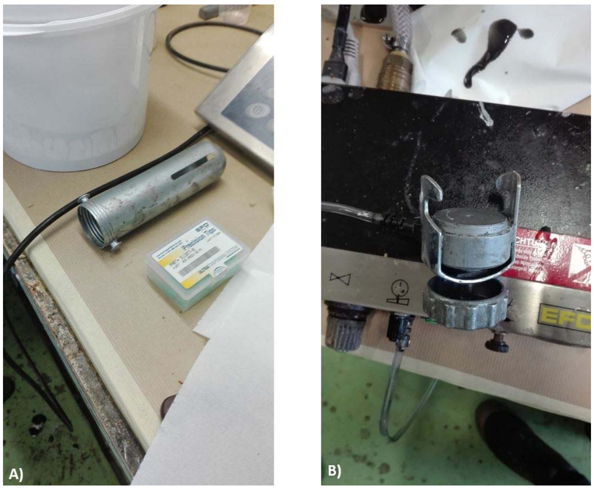

Figure 4: **The syringe (A) and the endcap (B).**

Figure 5: **Filling of the mold. Top view (A) and bottom view (B).**

Figure 6: **Sealing of the nozzle after filling the mold.**

When the mold is sealed, the part is ready for curing. It is cured for 15 hours at 60°C.

5. DATASHEET LINKS

3D-printer:
http://www.3dsystems.com/products/datafiles/viper/datasheets/International/viper_si2_uk.qxd.pdf

Resin:
http://www.quickparts.com/UserFiles/File/Accura__25.pdf

Release liquid:
http://www.chemcenters.com/images/suppliers/169257/Araldite%20QZ%2013.pdf

Polymer (and hardener):
http://www.axson-decoline.de/Datenblatt/re11501A--94--re1020-de.pdf

F : Conceptual design report, UT PLUG – INTERFACE BETWEEN UT AND LHCB BEAM PIPE

Joao Carlos Batista Lopes
Olivier Jamet

03 July 2015

1. INTRODUCTION

This report provides preliminary calculations necessary to validate the shape of the polymer plug that will be used as an interface between the UT box and the LHCb beam pipe.

2. GEOMETRY

The figures below provide the geometry and sizes of the UT plug.

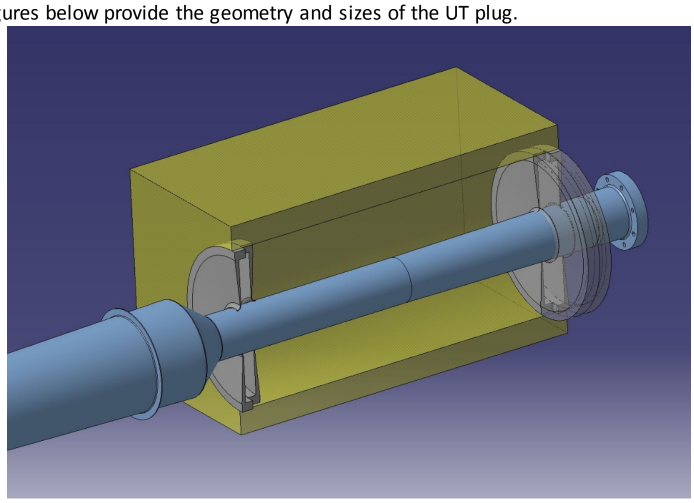

Figure 1 - UT plug

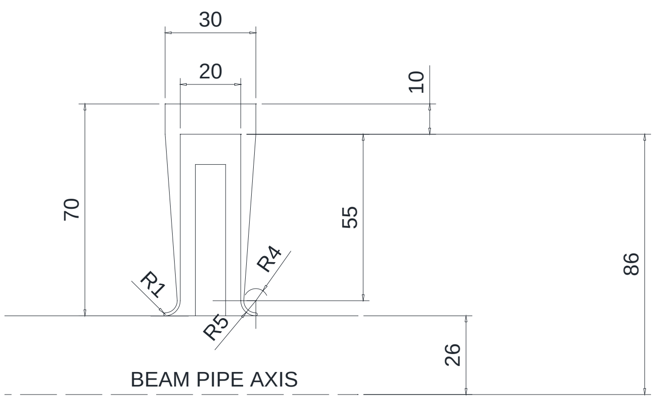

Figure 2 - plug cross section

Joao Carlos Batista Lopes
Olivier Jamet

03 July 2015

3. MATERIAL PROPERTIES

3.1 RADIATION HARDNESS

The figures below provide the radiation the radiation hardness of polymer materials that can be used as interface between the beam pipe and the UT box.

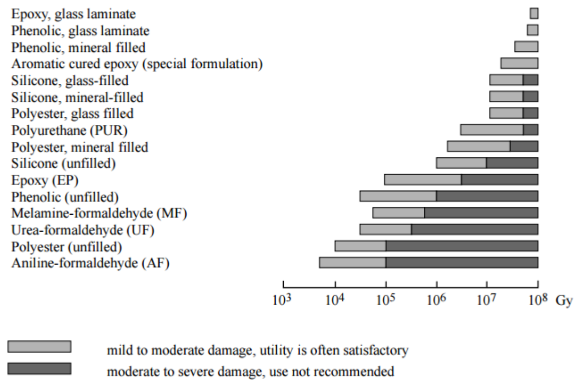

Figure 3 - PUR radiation resistance [https://cds.cern.ch/record/357576/files/CERN-98-01.pdf]

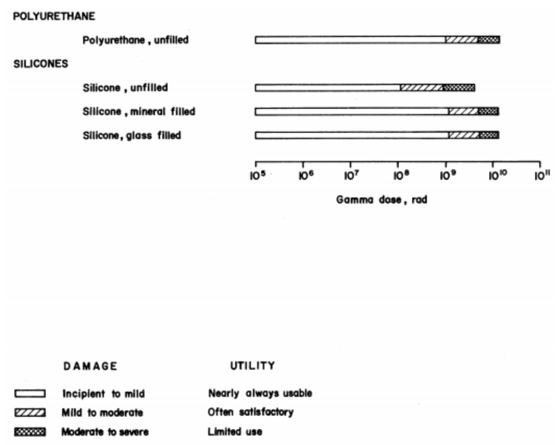

Figure 4 - PUR radiation resistance [https://cds.cern.ch/record/186329/files/CERN-72-07.pdf]

Joao Carlos Batista Lopes
Olivier Jamet

03 July 2015

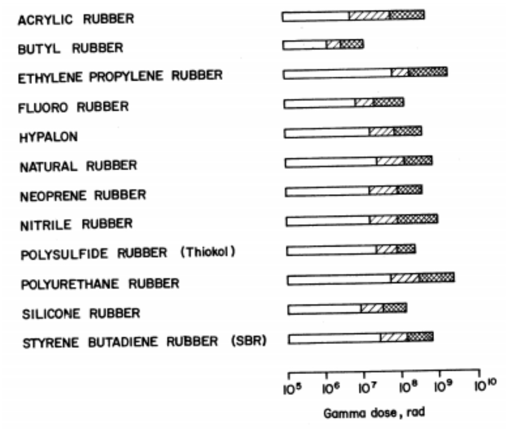

Figure 5 - Elastomers radiation resistance [https://cds.cern.ch/record/186329/files/CERN-72-07.pdf]

3.2 MECHANICAL PROPERTIES

The table below provides a list of materials that can be used to manufacture the UT plug. Yhese materials were selected based on the results of the radiation hardness test as well as on the mechanical properties of the materials.

Table 1 - Potential materials to be used in the fabrication of the UT plug

Material	Hardness	Tensile strength	Temperature
Ethylene propylene rubber	Shore A 30-95	7-21 MPa	-50 to 160^{0}C
Polyurethane rubber	Shore A 20-90	2-15 MPa	
Silicone rubber	Shore A 10-90	11 MPa	-120 to 300^{0}C

The UT plug shall be light tight and therefore as to be in contact with the beam pipe. In order to reduce the force that the plug may transmit to the beam pipe, the plug shall be made with a soft/medium soft material. For the purpose of this preliminary assessment it was considered that a hardness shore A 40.

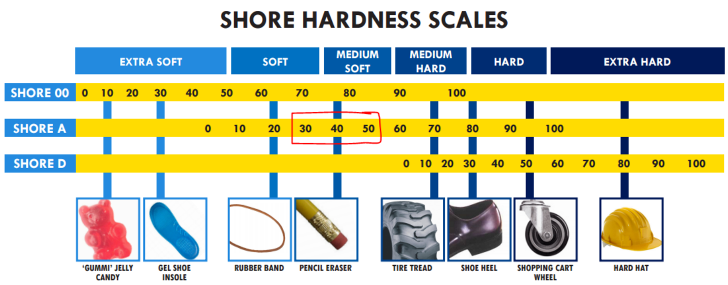

Figure 6 - Hardness scale

Joao Carlos Batista Lopes
Olivier Jamet

03 July 2015

3.3 MATERIAL PROPERTIES USED IN THE SIMULATION

The figures below show the analytical calculations used to determine the rubber mechanical properties. These calculations are only for reference, material testing is required in order to assess the real material properties. The Mooney- Rivlin model was the constitutive model used simulate the behaviour of the material.

Material hardness $H := 40$

Initial elasticity modulus $E_0 := \left(11.427 \cdot H - 0.4445 \cdot H^2 + 0.0071 \cdot H^3\right) \cdot psi = \left(1.381 \cdot 10^6\right) Pa$

Mooney coefficients $C_{10} := 0.1333 \cdot E_0 = \left(1.841 \cdot 10^5\right) Pa$

$C_{01} := 0.0333 \cdot E_0 = \left(4.598 \cdot 10^4\right) Pa$

Initial shear modulus $G_0 := 2 \cdot \left(C_{10} + C_{01}\right) = \left(4.601 \cdot 10^5\right) Pa$

Poisson ratio $\nu := \dfrac{E_0}{2 \cdot G_0} - 1 = 0.501$

If the Poisson ration is >0.5 means that there is no GLOBAL volume change under loads (of course there is local change under the loads). eg: rubber.

Material incompressibility parameters

$$D_1 := \begin{cases} 0\ MPa & \text{if } \nu \geq 0.5 \\ \dfrac{1 - 2 \cdot \nu}{C_{10} + C_{01}} & \text{else} \end{cases} = 0\ Pa$$

Initial bulk modulus

$$k_0 := \begin{cases} 9999999999999999\ MPa^{-1} & \text{if } D_1 = 0 \\ \dfrac{2}{D_1} & \text{else} \end{cases} = \left(1 \cdot 10^{10}\right) Pa^{-1}$$

Figure 7 – Mooney-Rivlin coefficients for expected material hardness

Joao Carlos Batista Lopes
Olivier Jamet

03 July 2015

4. FINITE ELEMENT ANALYSIS

4.1 BOUNDARY CONDTIONS

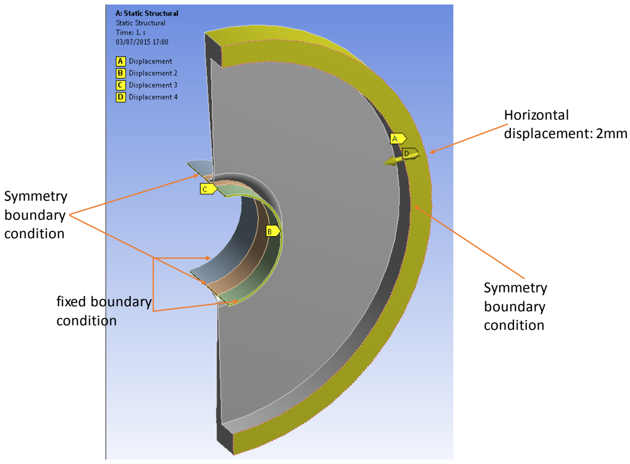

Figure 8 – Horizontal displacement applied to the plug

4.2 RESULTS– FRICTIONLESS CONTACT BETWEEN PLUG & BEAM PIPE

For the first simulation we considered that the contact between the beam pipe and the plug is frictionless.

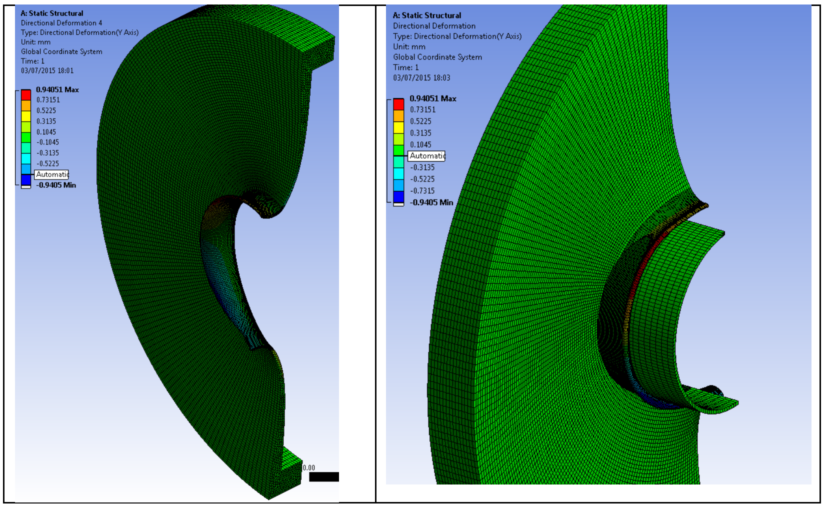

Figure 9 - Vertical displacement (perpendicular to beam pipe)

Joao Carlos Batista Lopes
Olivier Jamet

03 July 2015

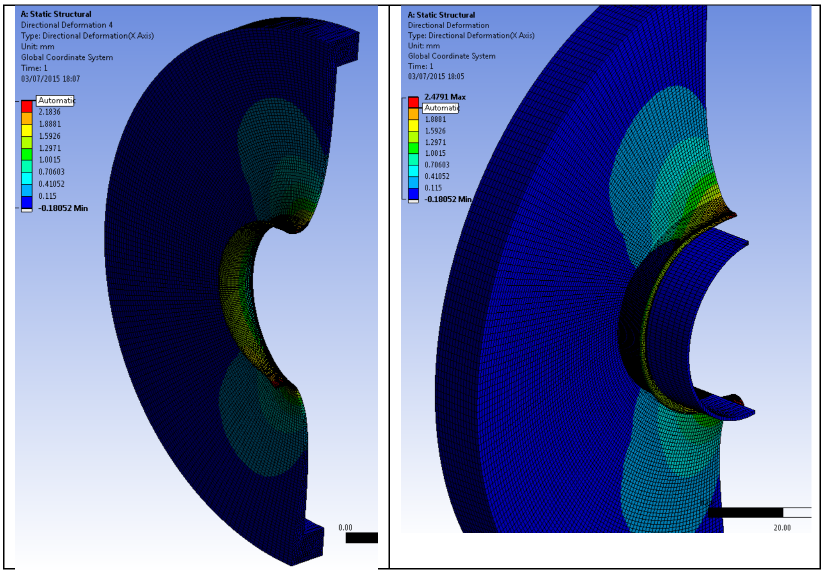

Figure 10 – Horizontal displacement (beam pipe direction)

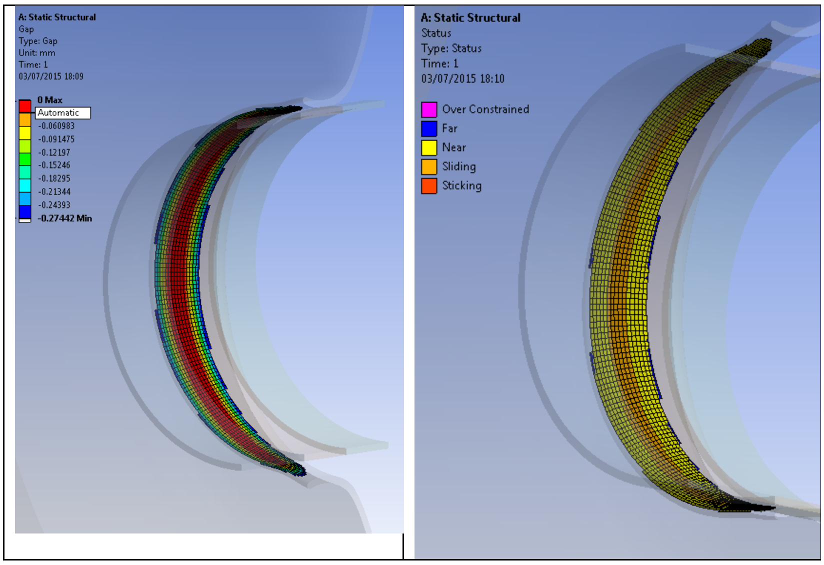

Figure 11 - Contact gap and status

Joao Carlos Batista Lopes
Olivier Jamet

03 July 2015

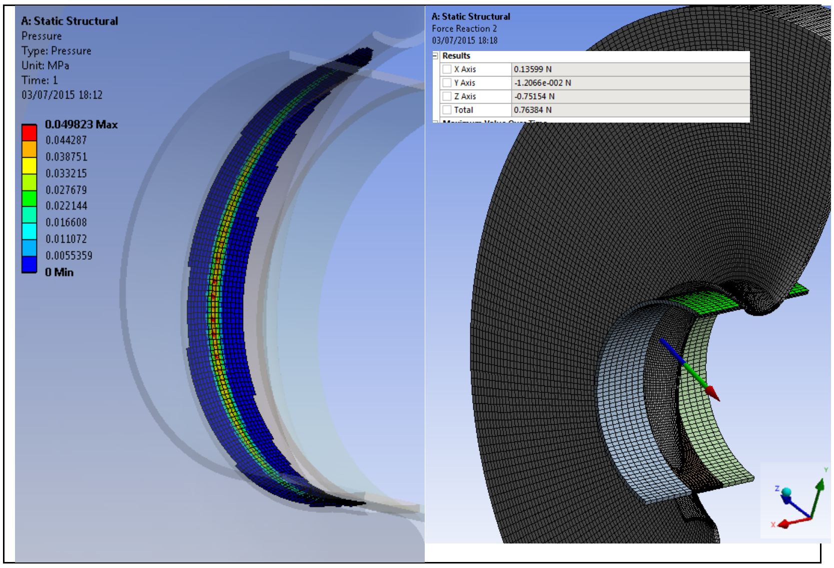

Figure 12 - Contact pressure and force

4.3 RESULTS– FRICTIONAL CONTACT BETWEEN PLUG & BEAM PIPE

For the first simulation we considered that a frictional contact between the beam pipe and the plug. The friction coefficient used in the computation was 0.25.

Joao Carlos Batista Lopes
Olivier Jamet

03 July 2015

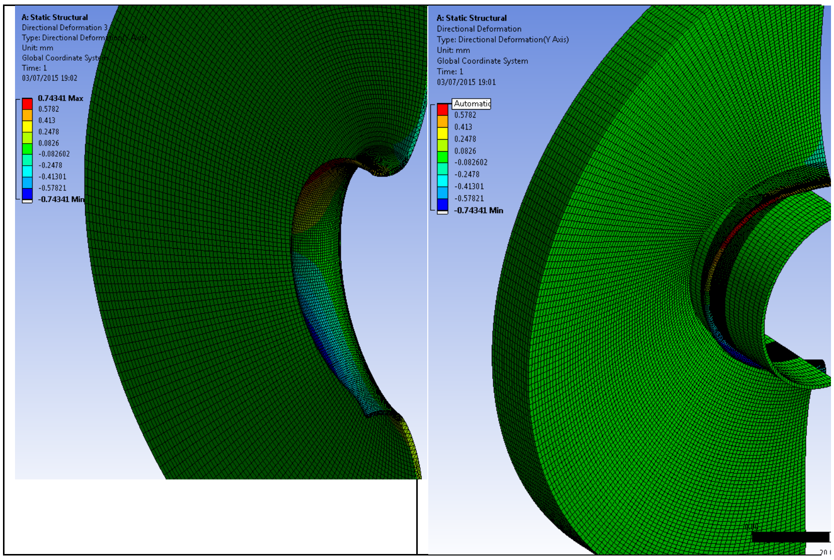

Figure 13 - Vertical displacement (perpendicular to beam pipe)

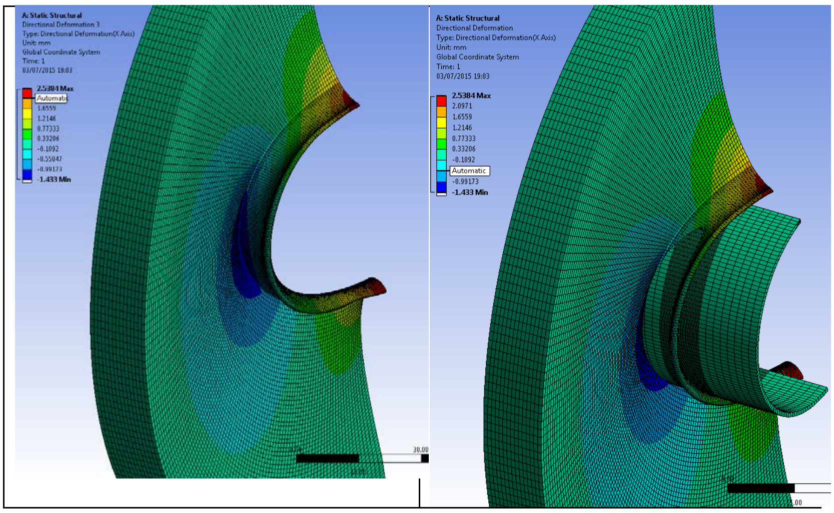

Figure 14 – Horizontal displacement (beam pipe direction)

Joao Carlos Batista Lopes
Olivier Jamet

03 July 2015

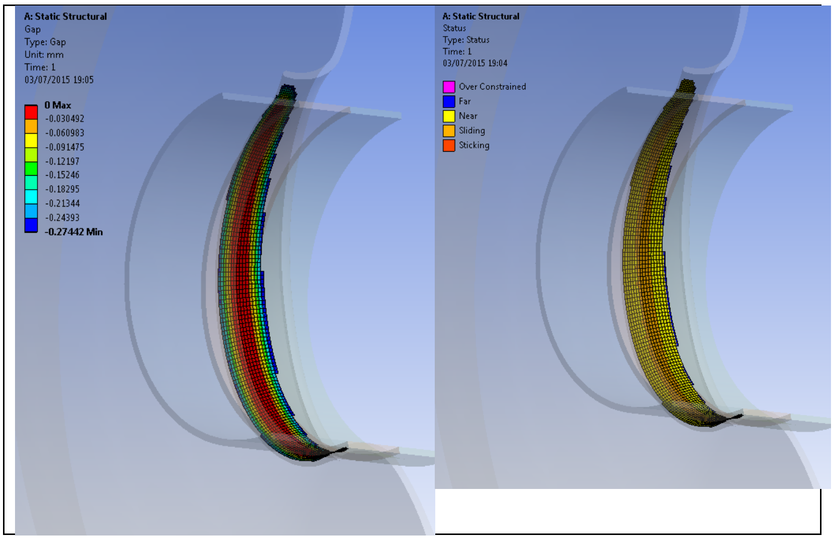

Figure 15 - Contact gap and status

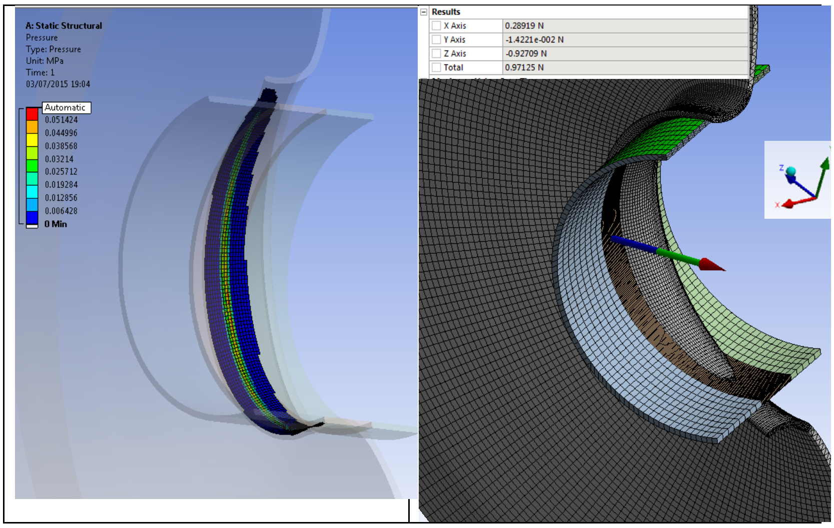

Figure 16 - Contact pressure and force

Joao Carlos Batista Lopes
Olivier Jamet

03 July 2015

5. ANNEX 1 – CANDIDATE MATERIAL FOR UT PLUG

The figure below provide the material properties of a polymer that was used as a plug in the ATLAS experiment.

Axson TECHNOLOGIES

RE 12800 POLYOL
RE 1020 ISOCYANATE

ELECTRICAL POLYURETHANE RESIN
TWO-COMPONENT - COLD CURING
RIGID

DESCRIPTION

Casting resin for mechanical and numerous electrical applications especially for low or medium voltage.
Example: potting electronic cards, transformers, capacitors and components.

PROPERTIES

- *Two-component liquid polyurethane resin*
- *Solvent free*
- *Very good dielectric properties*
- *Rigid*
- *Good impact resistance*

PHYSICAL PROPERTIES				
		RE 12800	**RE 1020**	**MIXED**
Composition		**POLYOL**	**ISOCYANATE**	
Mix ratio by weight Mix ratio by volume at 25°C		100 100	28 32	
Aspect		liquid	liquid	liquid
Colour **RE 12800 POLYOL** **-(37)** **-(97)**		red black	dark-amber	red black
Viscosity at 25°C (mPa.s)	BROOKFIELD LVT	2,700	120	1,200
Specific gravity liquid component at 25°C Specific gravity cured product at 23°C (g/cm³)	ISO 1675 : 1985 ISO 2781 : 1996	1.40 -	1.22 -	- 1.38
Gel Time at 25°C (200 gr) (min.) **RE 12800 POLYOL** **-(37)** **-(97)**	Gel Timer TECAM			65
Curing time at 25°C (200gr)	Hours			12 - 24
Final hardness at 25°C (200gr)	Days			7

MECHANICAL PROPERTIES at 23°C (1)			
Hardness	ISO 868 : 2003	Shore D1 / D15	80 / 74
Tensile strength	ISO 527 : 1993	MPa	20
Elongation at break	ISO 527 : 1993	%	15
Flexural modulus	ISO 178 : 2001	MPa	900
Impact strength (Un notched specimens)	ISO 179/1eU :1993	kJ/m²	25

(1): *Average values obtained on standard specimens / Hardening 16 hours at 80°C.*

PROCESSING

Before use it is necessary to mix the POLYOL part until both colour and aspect become homogeneous. POLYOL and ISOCYANATE have to be mixed at a temperature higher than 18°C according to the mix ratio indicated on the technical data sheet. Before casting check that parts or moulds are free of any trace of moisture.

Joao Carlos Batista Lopes
Olivier Jamet

03 July 2015

RE 12800 POLYOL
RE 1020 ISOCYANATE

ELECTRICAL POLYURETHANE RESIN
TWO-COMPONENT - COLD CURING
RIGID

THERMAL AND SPECIFIC PROPERTIES (1)			
Working temperature	-	°C	-40 / +120
Thermal conductivity	ISO 2582 : 1978	W/m.K	0.35
Glass transition temperature (Tg)	ISO 11359 : 2002	°C	35
Coefficient of thermal expansion (CTE) (-25°C to +20°C) (+55°C to +130°C)	ISO 11359 : 1999	10^{-6} K^{-1}	70 170
Water absorption (23°C – 24 Hours)	ISO 62 :1999	%	0.2
Directive 2002/95/CE (ROHS) (2)	-	-	conform

(1) Average values obtained on standard specimens / Hardening 16 hours at 80°C.
(2) European directive on the restriction of the use of certain hazardous substances electrical and electronic equipment.

DIELECTRIC AND INSULATING PROPERTIES at 23°C (1)			
Dielectric strength (50 Hz - 1 mm)	CEI 60243-1 E2 : 1998	kV/mm	27
Dielectric constant ε (100 Hz)	CEI 60250 : 1969	-	4.5
Dissipation factor tan δ (100 Hz)	CEI 60250 : 1969	-	0.03
Volume resistivity (1000 V)	CEI 60093 E2 : 1980	Ω.cm	1.10^{16}

HANDLING PRECAUTIONS

Normal health and safety precautions should be observed when handling these products :

- *ensure good ventilation,*
- *wear gloves, glasses and protective clothes.*

For further information, please consult the product safety data sheet.

STORAGE CONDITIONS

Shelf life is 12 months for POLYOL and ISOCYANATE in a dry place and in their original unopened containers at a temperature between 15 to 25°C.
Any open can must be tightly closed under dry inert gas (dry air, nitrogen, etc.).

Joao Carlos Batista Lopes
Olivier Jamet

03 July 2015

6. ANNEX 2- FORMULAS USED TO DETERMIN THE MATERIAL PROPERTIES

E (psi) = 11.427*A -0.4445*A^2 + 0.0071*A^3 Lindemann (XANSYS)

From E. F. Gobel, Rubber Springs Design, John Wiley, New York, 1978.

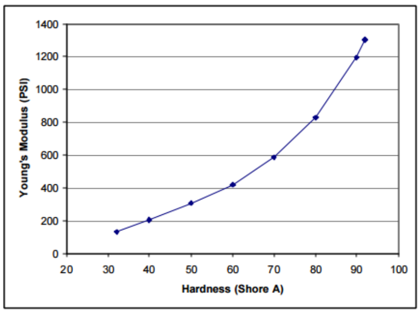

Figure 17 - Mooney-Rivlin model and material elastic modulus

E

Shore-A	E	C10	C01
[°]	psi	psi	psi
35	176.61	23.49	5.945
36	177.045	23.635	5.945
37	179.22	23.925	5.945
38	183.135	24.36	6.09
39	189.225	25.23	6.38
40	196.62	26.245	6.525
41	205.755	27.405	6.815
42	215.76	28.71	7.25
43	227.505	30.305	7.54
44	239.685	31.9	7.975
45	252.735	33.64	8.41
46	266.655	35.525	8.845
47	281.445	37.555	9.425
48	296.67	39.585	9.86
49	312.33	41.615	10.44
50	328.425	43.79	11.02
51	344.955	45.965	11.455
52	361.92	48.285	12.035
53	379.32	50.605	12.615
54	397.59	53.07	13.195
55	415.86	55.39	13.92
56	434.565	58	14.5
57	453.705	60.465	15.08
58	473.715	63.22	15.805
59	494.16	65.83	16.53
60	515.475	68.73	17.11
61	537.66	71.63	17.98
62	560.715	74.82	18.705
63	585.075	78.01	19.575
64	610.305	81.345	20.3
65	637.275	84.97	21.315
66	665.985	88.74	22.185
67	696	92.8	23.2
68	728.625	97.15	24.36
69	762.99	101.79	25.375
70	799.965	106.72	26.68

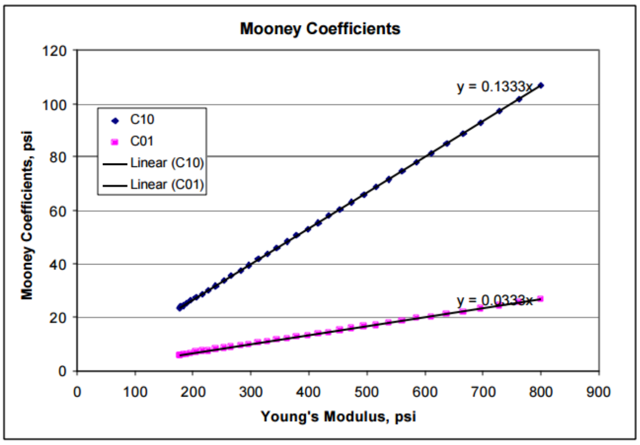

From Waltz (XANSYS)

Figure 18 - Mooney-Rivlin model and material shore hardness